SALP/Lot 2.c
CLS.DOS/NT/04.289
Issue : 1rev1 **Ramonville, 22 December 2004**
Nomenclature : SALP-RP-MA-EA-21234-CLS

Envisat RA2/MWR ocean data validation and cross-calibration activities. Yearly report. Contract N° 03/CNES/1340/00-DSO310

		COMPANY	DATE	INITIALS
PREPARED BY	Y. FAUGERE F. MERTZ J. DORANDEU	CLS		
QUALITY VISA	M. DESTOUESSE	CLS		
ACCEPTED BY	J. DORANDEU	CLS		
APPROVED BY	N. PICOT	CNES		

CLS 8-10 Rue Hermès - Parc Technologique du Canal - 31526 Ramonville St-Agne - FRANCE
Telephone 33 5 61 39 47 00 Fax 33 5 61 75 10 14

DOCUMENT STATUS SHEET

Project Control Initials	ISSUE	DATE	REASON FOR CHANGE

D :page deleted I :Page Inserted M :Page modified

LIST OF ACRONYMS

TBC	To be confirmed
TBD	To be defined
AD	Document Applicable
DR	Document de Référence

List of tables and figures

List of tables :

Liste of figures :

CONTENTS

1. INTRODUCTION

This report is an overview of Envisat validation and cross calibration studies carried out at CLS during the year 2004. This work was performed under SALP contract (N° 03/CNES/1340/00-DSO310 Lot 2C) supported by CNES at the CLS Space Oceanography Division. It is divided into two parts:

- CAL/VAL Envisat activities
- Envisat/ERS-2 and Envisat/Jason-1 cross calibration activities

Some of the results described here were presented at the QWG meetings (Toulouse, March and November 2004), ERS/Envisat Symposium meeting (Saltsburg, September 2003)

Since the beginning of the mission, Envisat data have been analysed and monitored in order to assess the quality of Envisat GDR products for ocean applications.

A statistical evaluation of Envisat altimeter data has been carried out to produce a global calibration of this mission. All relevant parameters from altimeter measurements (Ocean 1 retracking) and geophysical corrections are evaluated and tested. Moreover, Sea Surface Height (SSH) crossovers and along-track analyses have also been performed.

Cross-calibration methods have been developed and applied to assess the consistency of Envisat data with the ERS-2 and Jason-1 missions.

2. DATA

2.1. QUALITY OVERVIEW

The Envisat altimetric data have a good general quality over ocean. The availability has improved: less than 5% of data are missing on recent cycles. The MWR availability has also improved. Moreover, some modifications have been performed by ESA to decrease the duration of the S-Band anomaly events. Statistics and performances of altimeter and radiometer parameters are consistent with expected values. Finally the Envisat is quite consistent with Jason-1 and Ers-2.

2.2. AVAILABLE CYCLES

16 GDR cycles have been produced this year: cycles 19 to 30 as part as the current processing and cycles 14 to 11 as part at the reprocessing activities. As shown by the chart below, two different IPF processing chains have been used.

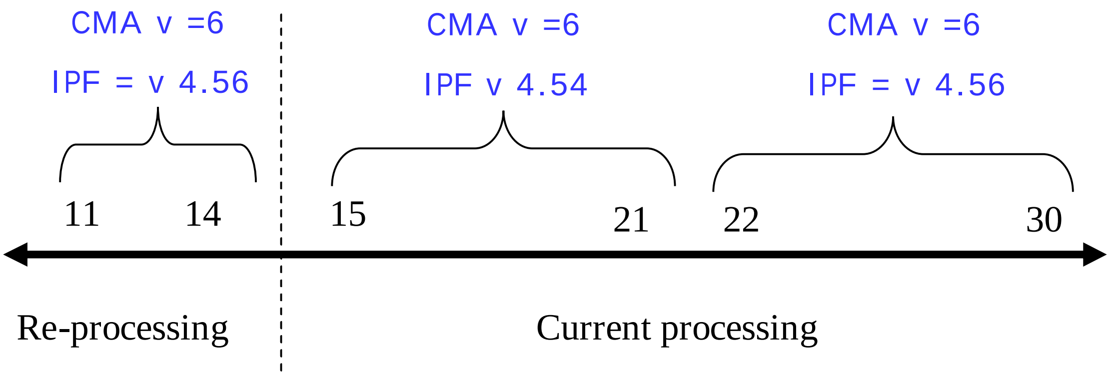

GDR products of cycles 15 to 17 have been produced by the CMA software using Level 1B directly supplied by the two Payload Data Handling Stations (PDHS) in Kiruna and Frascati. From cycle 18 onwards there is a new step in the Level 1B generation loop: the Low Rate Reference Archive Center (LRAC) receives Level 1 B from PDHS and produces a consolidated Level 1B. The CMA uses now this consolidated Level 1B to produce GDRs.

A quality assessment report has been carried out for each cycle and is available on http://www.aviso.oceanobs.com/html/donnees/calval/validation_report/en/welcome_uk.html. The purpose of this document is to report the main features of the data quality from the Envisat mission.

2.3. ALGORITHMS

In order to assess the product quality some updates were necessary:

- Ice flag: The same method as in the ERS-2 OPR quality assessment (e.g. Mertz et al., 2003) has been used for ENVISAT (see 4.2.1.2)

- S-Band anomaly flag: see 4.2.1.3

- Model ionosphere correction: There is no model available in the product. Thus the JPL GIM ionosphere correction is computed to assess the dual frequency and Doris corrections. The GIM model has been computed thanks to the procedures kindly provided by Remko Scharroo to the CCVT (Scharroo, 2002).

- Filtered dual frequency ionosphere correction: A 300-km low pass filter is applied along track on the dual frequency ionosphere correction to reduce the noise of the correction.

3. INSTRUMENT AND PLATEFORM STATUS

The instrument and platform events are detailed here for each cycle.

3.1. ACRONYMS

The main acronyms used to described the events are explained below.

CTI tables: Configuration Table Interface. They Contain the setting of the instruments and are uploaded on board after a switch off, a reset

HTR Refuse: Heater Refuse

ICU: Instrument Control Unit, a part of the distributed command and control function implemented on ESA spacecraft. The unit receives, decodes and executes high-level commands for its instrument, and autonomously performs health-checking and parameter monitoring. In the event of anomalies it takes autonomous recovery actions.

MCMD: Macrocommand

OCM: Orbit Controle Mode/maneuvre

P/L SOL: Payload Switch Off Line

SEU: Single Event Upset

SM-SOL by PMC: SM Switch Off Line by Payload Main Computer

SW: Software

TM: Telemetry

3.2. CYCLE 011

– Ra2 switch-down - Planned SM-SOL by PMC1 (2002/11/18 04 :38 :00 to 2002/11/19 19:19:21, Pass 382-429)
– DORIS Navigator switch-down - Planned SM-SOL by PMC1 (2002/11/18 04 :38 :02 to 2002/11/22 12 :40 :00, Pass 382-505)
– MWR switch-down - Planned SM-SOL by PMC1 (2002/11/18 04 :37 :59 to 2002/11/20 12 :20 :06, Pass 382-448)
– Orbit Maintenance Maneuver (2002/11/07 18 :15 :51 to 2002/11/07 21 :06 :17,Pass 83-85)
– Orbit Maintenance Maneuver (2002/11/29 03 :35 :30 to 2002/11/29 06 :25 :57,Pass 696-698)

3.3. CYCLE 012

– RA-2 went to HTR-0 Refuse (2002/12/21 04 :31 :26 to 2002/12/21 12 :52 :00, Pass 325-333)

– Orbit Inclination Maneuver (2002/12/18 04 :28 :18 to 2002/12/18 06 :36 :46, Pass 238-240)
– Orbit Maintenance Maneuver (2002/12/18 22 :17 :22 to 2002/12/19 00 :17 :34, Pass 259-261)

3.4. CYCLE 013

– RA-2 went to HTR-0 Refuse (2003-01-16 01 :52 :36 to 2003-01-17 17 :00 :35)
– RA-2 went to suspend mode (2003-01-25 23 :56 :36 to 2003-01-27 19 :54 :02)
– Orbit Maintenance Maneuver (2003/01/14 00 :55 :17 to 2003/01/14 03 :45 :42 TAI)
– Orbit Maintenance Maneuver (2003/02/11 23 :04 :49 to 2003/02/12 01 :04 :57 TAI)

3.5. CYCLE 014

– SEU's caused a Software Anomaly (2003/03/02 02 :46 :44 to 2003/03/03 16 :46 :35).
– Subsystems unavailable - Autonomous P/L switch-off (2003/03/15 04 :21 :08 to 2003/03/17 19:00:13)
– RA2 in HTR0/Refuse due to HPA primery bus undercurrent (2003/03/17 21 :09 :32 to 2003/03/18 18 :50 :40)
– Orbit Inclination Maneuver (2003/02/21 03 :42 :57 to 2003/02/21 05 :53 :24)
– Orbit Maintenance Maneuver (2003/03/03 23 :51 :14 to 2003/03/04 01 :51 :22)

3.6. CYCLE 015

– Wrong setting of Ra2 parameters (no CTI tables have been up-loaded on-board) from 18 Mar 2003 18 :50 :40 to 9 Apr 2003 17 :12 :24, Pass 1 to 452
– RA-2 unavailability (Format Header Error forcing ICU to RS/WT/INI) from 8 Apr 2003 15:08:57.000 to 9 Apr 2003 17 :12 :24.000, Pass 437 to 452
– RA-2 unavailability (Format Header Error forcing ICU to RS/WT/INI) from 8 Apr 2003 15:08:57.000 to 9 Apr 2003 17 :12 :24.000, Pass 613 to 624
– RA-2 unavailability : Multiple SEU caused ICU switchdown, Pass 879 to 901

3.7. CYCLE 016

– RA2 unavailability (known SEU failure) (from 5 May 2003 12 :30 :17.000 to 6 May 2003 10 :01 :10.000, Pass 191 to 215)
– RA-2 unavailability (ICU in SUSPEND due to TM FMT Error when a Reduced FMT was requested) (from 11 May 2003 11 :06 :33.000 to 12 May 2003 10 :14 :35.726, Pass 361 to 387)
– Orbit Maintenance Maneuver (from 2003/05/14 22 :40 :13 to 2003/05/15 00 :40 :19 TAI, Pass 460 to 462)
– RA-2 unavailability (Switch-down for PMC SW upgrade and OCM) from 18 May 2003 06 :25 :17.000 to 19 May 2003 15 :59 :28.000, Pass 548 to 602)
– MWR unavailability (Switch-down for PMC SW upgrade and OCM) from 18 May 2003 06 :25 :24.000 to 19 May 2003 14 :45 :40.000, Pass 548 to 602)
– DORIS unavailability (Switch-down for PMC SW upgrade and OCM) from 18 May 2003 06 :25 :25.000 to 19 May 2003 13 :21 :28.000, Pass 548 to 602)

– Orbit Inclination Maneuver (from 2003/05/20 04 :11 :53 to 2003/05/20 06 :23 :31 TAI, Pass 610 to 612)
– RA-2 unavailability (ICU went to RS/WT/INI) from 1 Jun 2003 14 :36 :40.000 to 2 Jun 2003 09 :20 :35.000, Pass967 to 987

3.8. CYCLE 017

Orbit Maintenance Maneuver (from 2003/06/07 01 :08 :16 to 2003/06/07 03 :08 :23 TAI, Pass 119 to 122)

3.9. CYCLE 018

– Orbit Maintenance Maneuver (from 2003/07/11 0 :58 :45 to 2003/07/11 03 :49 :08 TAI, Pass 90 to 94)
– RA2 unavailability (RA-2 in STBY/REF due to MCMD timeout) (from 26 Jul 2003 15 :28 :11 to 26 Jul 2003 17 :25 :35, Pass 538)
– RA2 unavailability (RA-2 picked up Mission Planning schedule) (from 31 Jul 2003 16 :11 :02 to 31 Jul 2003 18 :06 :30, Pass 682)
– Orbit Maintenance Maneuver (from 2003/07/11 0 :58 :45 to 2003/07/11 03 :49 :08 TAI), Pass 91 to 94)

3.10. CYCLE 019

– Orbit Maintenance Maneuver (from 2003/08/15 1 :31 :29 to 2003/08/15 03 :31 :35 TAI, Pass 91 to 93)
– RA-2 went to STBY/Refuse due to Individual EchoesMCMD Timeout (from 2003-08-15 16 :40 :21 to 2003-08-15 18 :35 :35, Pass 110)
– RA-2 went to STBY/Refuse due to Individual EchoesMCMD Timeout (from 2003-08-30 15 :28 :00 to 2003-08-30 20 :47 :35, Pass 538 to 543)
– PLSOL . Instrument Switch OFF/ON (from 2003-09-04 22 :52 :52 to 2003-09-06 16 :41 :09, Pass 689 to 738)

3.11. CYCLE 020

– RA-2 in STANDBY / REFUSE MODE (from 2003-09-21 15 :36 :40 to 2003-09-21 17 :33 :30, Pass 166 to 167)
– RA-2 is in RS/WT/INT mode (from 2003-09-27 00 :28 :08 to 2003-09-27 12 :52 :00, Pass 320 to 333)
– Wrong setting of Ra2 parameters (no CTI tables have been up-loaded on-board) (from 2003-09-27 12 :52 :00 to 2003-09-30 12 :45 :00, Pass 334 to 407)
– Orbit Maintenance Maneuver (2003/09/30 00 :40 :53 to 2003/09/30 02 :41 :00 TAI, Pass 405 to 407)

3.12. CYCLE 021

– Orbit Inclination Maneuver (2003/10/28 04 :56 :18 to 2003/10/28 07 :09 :44 TAI, Pass 210 to 212)
– RA-2 is in RS/WT/INT mode. 29 Oct 2003 06 :47 :04 to 29 Oct 2003 12 :58 :35, Pass 242 to 247)
– Orbit Maintenance Maneuver (2003/10/31 01 :13 :10 to 2003/10/31 03 :13 :25 TAI, Pass 291 to 293)
– RA-2 is in RS/WT/INT mode. TM format header error (02 Nov 2003 15 :16 :56 to 03 Nov 2003 12 :08 :35, Pass 366 to 389)
– Orbit Maintenance Maneuver (2003/11/18 23 :02 :30 to 2003/11/19 01 :52 :55 TAI, Pass 833 to 835)

3.13. CYCLE 022

– RA-2 is in RS/WT/INT mode (2003-11-26 13 :31 :20 to 2003-11-26 19 :39 :35, Pass 49 to 54)
– RA-2 PLSOL . Instrument Switch OFF/ON (2003-12-03 07 :18 :43 to 2003-12-05 16 :35 :05, Pass 241 to 308)
– MWR PLSOL . Instrument Switch OFF/ON (2003-12-03 07 :18 :43 to 2003-12-04 18 :45 :41)
– RA-2 is in RS/WT/INT mode. (2003-12-06 15 :55 :52 to 2003-12-10 19 :16 :36, Pass 338 to 455)
– Orbit Maintenance Maneuver (2003/12/15 21 :02 :28 to 2003/12/15 23 :02 :36, Pass 601 to 603)
– Orbit Maintenance Maneuver (2003/12/26 21 :03 :30 to 2003/12/26 23 :03 :34, Pass 916 to 918)

3.14. CYCLE 023

– Orbit Maintenance Maneuver (2004/01/21 23 :54 :27 to 2004/01/22 01 :54 :37)
– Orbit Maintenance Maneuver (2004/01/26 22 :26 :07 to 2004/01/27 00 :26 :11)

3.15. CYCLE 024

– Orbit Inclination Maneuver (2004/02/04 04 :46 :39 to 2004/02/04 06 :58 :05)
– Orbit Maintenance Maneuver (2004/02/05 11 :17 :21 to 2004/02/05 13 :17 :23)
– Orbit Maintenance Maneuver (2004/02/24 11 :48 :39 to 2004/02/24 13 :48 :45)

3.16. CYCLE 025

– Orbit Maintenance Maneuver (2004/04/07 20 :05 :30 to 2004/04/07 22 :05 :34)

3.17. CYCLE 026

– RA-2 in STANDBY/REF DUE TO MCMD H202 FAILURE (2004-22-04 15 :15 :36 2004-22-04 17 :07 :05)
– RA-2 Switch down to RESET/WAIT due to too many SEU's reported. (2004-05-10 02 :06 :31 2004-05-10 11 :27 :30)
– Orbit Inclination Maneuver (2004/04/14 04 :43 :02 2004/04/14 06 :55 :00)

– Orbit Maintenance Maneuver (2004/05/07 01 :08 :56 2004/05/07 03 :09 :04)

3.18. CYCLE 027

– RA2 went to suspend owing to repeated type 10 entries in report format (2004/05/31 02 :45 :27 to 2004/05/31 12 :01 :50)
– No DORIS data from 2004/06/06 13 :00 :00 to 2004/06/14 14 :52 :00. Following an onboard incident, Doris instrument has been switched to the redundant chain. Doris data are unavailable from June, 6th to June, 14th. To allow GDR production, POE with laser only data have been produced during this period.
– RA2 in SUSPEND Mode (2004/06/21 14 :47 :51 to 2004/06/21 19 :24 :30, Pass 995 to 999)

3.19. CYCLE 028

– RA2 in ICU rs/wt/ini (2004/07/18 13 :47 :03 to 2004/07/18 19 :59 :00, Pass 765 to 771)
– Orbit Maintenance Maneuver (2004/06/30 08 :08 :29 to 2004/06/30 10 :08 :35, Pass 242 to 244)

3.20. CYCLE 029

– RA2 in ICU RS/WT/INI. (SDU problem in RAM) (2004/08/10 15 :00 :39 to 2004/08/11 10 :59 :30, Pass 423 to 445)
– Orbit Maintenance Maneuver (2004/08/17 02 :04 :20 to 2004/08/17 04 :04 :26, Pass 607 to 609)

3.21. CYCLE 030

– RA2 in ICU RS/WT/INI. (SDU problem in RAM) (2004/09/26 13 :39 :50 to 2004/09/27 16 :23 :30, Pass 765-795)
– Abnormal behaviour of the RA-2 sensor (2004/09/27 16 :23 :30 to 2004-09-29 10 :21 :07, Pass 796-846)
– Collision avoidance Maneuver (2004/09/01 22 :52 :27 to 2004/09/02 00 :52 :37, Pass 60-62)
– Collision avoidance Maneuver (2004/09/02 23 :44 :27 to 2004/09/03 01 :44 :37, Pass 89-91)
–Orbit Inclination Maneuver (2004/09/21 04 :14 :37 to 2004/09/21 06 :29 :19, Pass 610-612)
– Orbit Maintenance Maneuver (2004/09/24 03 :53 :38 to 2004/09/24 05 :53 :46, Pass 695-697)

4. MISSING AND EDITED MEASUREMENTS

4.1. MISSING MEASUREMENTS

The cycle by cycle percentage of missing measurements over ocean has been plotted on Figure 1. Half of the processed cycles has more than 5% of unavailability. Cycles 13, 14, 15, 16, 17, 22 have an unavailability over 10%. Passes 1 to 452 of cycle 15 have not been delivered because of a wrong setting of Ra2. This explains the high ratio of missing measurements for this cycle. Several long Ra2 events occurred during cycles 13, 14, 16, 17, 22 which implied a lot of missing passes. Apart from the instrumental and platform events, 1 to 30 passes can be missing because of either to LRAC_PDHSs data generation to level1 problems or occasionally ingestion problems on F-PAC side. Notice however that the situation has been largely improved with a mean data of availability of 97% in 2004 (cycle 23 onwards)

4.2. EDITED MEASUREMENTS

Data editing is necessary to remove altimeter measurements having lower accuracy. There are 4 steps in the editing procedure. The first step is based on flags. Then, measurements are edited using thresholds on several parameters. The third step uses cubic splines adjustments to the ENVISAT Sea Surface Height (SSH) to detect remaining spurious measurements. The last step consists in removing an entire pass where SSH-MSS mean and standard deviation have unexpected values.

The steps 1, 2 and 4 are detailed below.

4.2.1. Editing by flags

Three flags are used on Envisat data: the land/sea radiometer flag, the ice flag and the S-Band anomaly flag. The first flag is given in the products whereas the two others are not.

4.2.1.1. Land/sea radiometer flag

When this flag is ON over ocean, it means that the radiometer data is missing in level 1B delivered to FPAC, or in coastal area. The percentage of missing measurements over ocean has been plotted on Figure 2. It is computed as following:

Ratio=Number of [land/sea radiometer is ON and land/sea altimeter flag is OFF] / Number of [land/sea altimeter flag is OFF]

The mean value is around 4% but the radiometer unavailability is not constant. It is greater than 5% for cycles 14 to 19 but lower than 3% from cycle 21 onwards.

On cycle 30 there is no missing MWR data. However, the computed ratio is about 1% because of the coastal areas (the visibility circle of the radiometer is larger than the visibility circle of the altimeter).

4.2.1.2. Computed ice flag

No ice flag is available in Envisat product. However, as Envisat operates between ±82° of latitude, sea ice is an important issue for oceanic applications. A study has been performed during the validation phase (Faugere et al, 2003) and an empirical algorithm has been chosen for quality assessment. A measurement is set to ice if:

|latitude| >50 deg And	**N_{20Hz} criterion**: the number of 20Hz valid data < 17 Or **MWR criterion**: |MWR–ECMWF| > 10cm Or **Peakiness criterion**: Peakiness>2

Figure 3 shows the cycle by cycle percentage of edited points by the sea ice flag over ocean. The observed trend is due to the annual cycle as clearly depicted by the red and blue curves.

4.2.1.3. Computed S-Band anomaly flag

An anomaly occasionally occurs on the S-Band. The S-Band waveforms are not meaningful qnd so all S-Band parameters. This anomaly concerns the "summation of the S-Band power echoes". Consequently the Dual Frequency ionosphere correction is not reliable during these periods. A measurement is set if:

|Sigma0(Ku)–Sigma0(S)| > 5dB

The ratio of flagged measurements over ocean is plotted on Figure 4. The mean value is around 4%. There have been, on average, 3 S-Band anomaly events by cycle since cycle 11. Recently, some modification have been performed by ESA to decrease the duration of these events.

4.2.2. Editing by thresholds

The thresholds are expected to remain constant throughout the ENVISAT mission, so that monitoring the number of edited measurements allows a survey of data quality. Table 1 gives for each tested parameter, the minimum and maximum thresholds used in the routine quality assessment. These thresholds have been derived from the Topex experience. However, the variability relative to MSS and the standard deviation of 18Hz range have been refined specifically for Envisat data.

Parameter	Min threshold	Max threshold
Sea surface height (m)	-130	100
Variability relative to MSS (m)	-2	2
Number of 18Hz valid points	10	-
Std. deviation of 18Hz range (m)	0	0.25
Off nadir angle from waveform (deg2)	-0.200	0.160
Dry tropospheric correction (m)	-2.500	-1.900
Invert barometer correction (m)	-2.000	2.000
MWR wet tropospheric correction (m)	-0.500	0.001
Dual Ionospheric correction (m)	-0.200	-0.001
Significant wave height (m)	0.0	11.0
Sea state Bias (m)	-0.5	0
Backscatter coefficient (dB)	7	30
Ocean tide height (m)	-5	5
Long period tide height (m)	-0.500	0.500
Earth tide (m)	-1.000	1.000
Pole tide (m)	-5.000	5.000
RA2 wind speed (m/s)	0.000	30.000

Table 1 : Editing thresholds

The wind, pole tide, earth tide, dry troposphere correction and Inverted Barometer criteria have never been active over the period. Figure 5 shows the cycle by cycle percentage of points edited on the other criteria. The main editing criteria are the Rms of Ku range, the off nadir angle and SSH-MSS. The other ratios are lower than 0.2%. These ratios are stable except SSH-MSS on cycle 30. This is linked to the abnormal behaviour of the Ra2 sensor during 50 passes.

These ratios are strongly lower than those observed on other altimeters like Jason or Topex. Figure 6 shows a comparison of the editing ratio between Envisat and Jason. Figure 7 and Figure 8 show the measurements edited respectively on Envisat and Jason. The edited measurement density on Envisat is strongly lower than on Jason, especially in wet areas.

4.2.3. Editing on SLA statistic over the passes

The last editing step consists in testing the mean and standard deviation of the SSH-MSS over the entire pass. If one of the two statistics is abnormally high, then the entire pass is edited. This step can be very useful to detect data degraded by orbit error for example.

A specific study has been performed to determine how to compute the statistics, and which thresholds should be applied. The statistics have to be computed on very stable areas. The selection criteria are:

- The latitude: the range value can be degraded near the ice, despite the use of the ice flag. Moreover, the MSS is less accurate over 66°.
- The oceanic variability: the standard deviation of SLA can be very high because of the mesoscale variability. Areas with high oceanic variability have to be removed to detect the abnormally high standard deviation.
- The bathymetry and distance from the coast: A lot of corrections (tides for example) are less accurate in low bathymetry areas and near the coast (Japan sea).
- The sample: The statistic have to be computed on a significant number of points

All those criteria have been tested and combined. The conclusion is that two criteria are needed:

1st criterion: for small portions of pass (less than 200 points) the sample is not big enough to compute reliable statistics. The selection must not be severe:

Selected areas: latitude<66°, variability<30cm, bathymetry<-1000m, distance>100km

Threshold: 30 cm on mean and standard deviation

2nd criterion: for other passes

Selected areas: latitude<66°, variability<10cm, bathymetry<-1000m, distance>100km

Threshold: 15 cm on mean and standard deviation

Figure 9 shows the cycle by cycle percentage of points edited. On cycles 11, 12, 21 and 26, several entire passes have been edited because of a bad orbit quality related to inclination manoeuvre or lack of Doris data (cycle 11).

4.2.4. Rain flag

The rain flag is set if both:

- the expected Ku-band backscatter coefficient, determined by linear interpolation in an input table as a function of the S-band backscatter coefficient, and the measured Ku-band backscatter coefficient exceeds a value

- the integrated liquid water content from the radiometer exceed some given threshold

The rain flag is not used in the editing process. Figure 10 shows the cycle per cycle number of additional points which would be eliminated if it was used. It is quite stable, around 13000, that is to say about 1%. We can notice that apparently the rain flag has not been impacted by the S-band Sigma0 jump associated with the IPF change on cycles 22 and 14.

Figure 11 shows the map of rain flagged points on cycle 30. We can compare it to Figure 5. Wet areas signature is visible on both maps but the density is higher on the first one. Moreover some regions, like mid latitude in Atlantic Ocean, are almost exclusively edited by the rain flag. At mid and high latitudes more than fifty consecutive points can be rain flagged. Figure 12 and Figure 13 show 2 examples of SSH-MSS on Envisat and ERS-2 on pass segments where the rain flag is set on. In the first case, the rain flag seems to be efficient: between -23 and -29 deg of latitude, the altimetric signal is disturbed on both satellites. In the second case, Envisat is rain flagged between 49 and 55 deg of latitude whereas the 2 SLA seem consistent.

4.2.5. Anomalous measurements after Ra2 recovery

When the Ra2 recovers from a special event, the fist data delivered have sometimes wrong SSH-MSS values. It happens on:

- Cycle 16 / Pass 216
- Cycle 16 / Pass 388
- Cycle 20 / Pass 334
- Cycle 26 / Pass 790
- Cycle 27 / Pass 390

Figure 14 shows cycle 20 / pass 334. The first data delivered have SSH-MSS>2m using the range in Ku band and after few minutes, the SSH-MSS decreases gradually to reach normal values (~43cm). Note that on the S-Band, the same behaviour is observed.

An investigation has been performed on the recovery cases on the period May-September 2004. The SLA has been plotted after 6 recovery cases. The results of this study are summarized on Figure 15.

For cycle 26 / Pass 790 and Cycle 27 / Pass 390, the behaviour is the same: 1’07 s after the end of the Ra2 event, the first data delivered have SLA around 5 m. After a few seconds, the SLA decreases as in the Cycle 20 / Pass 334 case. Obviously, something occurred on board to allow this change of regime.

On the 3 next cases (27/1000, 28/772, 29/446), the first delivered data seem normal. So we can say that this behaviour is not systematic. Moreover this behaviour doesn't seem to be connected to a specific event.

Finally, in the last case (30/796) the first delivered data have SLA around 5 meters. However, the SLA doesn't decrease after a few seconds. It remains with this value during several days.

We have checked the behaviour of the USO clock period. ESA provided to the users the files containing the range error due to the USO clock variability. (http://earth.esa.int/pcs/envisat/ra2/auxdata/). The USO correction has been plotted in the 3 first cases on Figure 16. The origin of the X-axis is exactly the date of the first ocean measurement delivered after each recovery. For cycle 26 / Pass 790 and Cycle 27 / Pass 390, the behaviour is the same: The USO correction rises from about 24 mm to 29 mm and then flattens out after approximately 150s. For 27/1000, the USO correction is flat. So the USO is indeed sensitive to the Ra2 event but don't explain the big effect on the range

5. STATISTICAL MONITORING

Both mean and standard deviation of Envisat data main parameters have been monitored since the beginning of the mission. In particular, it is important to analyze the differences between corrections of the same type as a function of time. Only valid points (according to editing criteria) are used to analyze the behavior of these parameters over a long time series.

5.1. ALTIMETER PARAMETER

5.1.1.1. Number and RMS of Ku and S-band elementary measurements

The mean number of Ku and S 18Hz elementary data is plotted on Figure 17. The mean values are about 19.97 and 19.90 respectively for Ku and S band. These values are very high compared to other altimeters. The two drops on the Ku-band on cycles 14 and 20 are due to a wrong setting of the Ra2. On these two cycles, just after a recovery of Ra2, no CTI tables were uploaded onboard.

Histograms of RMS of Ku and S-band Range are plotted on Figure 18. The cycle by cycle mean RMS of Ku and S 20Hz elementary data are plotted on Figure 19. These parameters are quite stable. The mean values are respectively 9.0 and 31.1 cm. In Ku Band, it corresponds to about 2 cm at 1Hz, assuming uncorrelated 20Hz measurements. It is consistent with the expected values.

5.1.1.2. Ku and S-band SWH

Histograms of Ku and S-band SWH are plotted on Figure 20. The Ku SWH histogram has a good shape. The new retracking has improved the low waves (0-1m) but a zero class has appeared. The cycle by cycle mean Ku and S-band SWH are plotted on Figure 21. The curve reflects sea state variations. The mean values are respectively 2.7 and 2.6 cm. No anomalies have been detected.

5.1.1.3. Ku and S-band Sigma0

Histograms of Ku and S-band Sigma0 are plotted on Figure 22. Notice that 3.5 dB have been subtracted to the Ku Sigma0 to be compliant with the wind speed model (Witter and Chelton, 1991). The mean Ku and S-band Sigma0 are plotted on Figure 23. The mean values in Ku band are stable, around 11.1 dB. Two 0.66 dB jumps are visible on the S-Band on cycles 14 and 22. They are due to a correction of the AGC evaluation. This modification has been included in IPF version 4.56, used since cycle 22 for the current processing and for all the reprocessed cycles. On Figure 24 we can see jumps in the Ku-S Sigma0 difference between cycle 21 / pass 778 and cycle 22 / pass 39. During this period, there is a mixing of IPF version: those passes have been produced either with IPF version 4.54 or 4.56.

5.1.1.4. Squared mispointing

The histogram of the squared mispointing is plotted on Figure 25. It has a good shape but it has a strong bias of 0.026 deg^2 which corresponds to 0.16 degrees. Investigations are on-going at algorithm level to deal with the bias issue. The mean squared mispointing is plotted on Figure 26. The 0.005 deg^2 jump between cycle 21 and 22 is due to the upgrade of new IF mask filter auxiliary data file. A slight rising trend is observed on the parts of the curve. That could be due to the aging of the onboard filter. However, no impact have been detected on the data quality.

5.1.1.5. Ionosphere correction

Comparisons have been made between the Dual Frequency (DF) ionosphere correction, the Doris one, and JPL GIM model. The mean and standard deviations are plotted on Figure 27 and Figure 28. The mean GIM-Dual is very stable, around -0.7 cm bias. The standard deviation of GIM-Dual is around 1cm. The decrease is due to an inter-annual decrease of ionosphere activity.

5.1.1.6. USO drift

A drift has been detected on the USO clock period. ESA provided to the users the files containing the range error due to the USO clock variability. (http://earth.esa.int/pcs/envisat/ra2/auxdata/).

Figure 29 and Figure 30 show respectively the number and the mean per day of range error estimations. Before cycle 15, a lot of estimations are missing. After cycle 15 there are some gaps lasting several hours but, there are enough values to compute a mean value per day. The mean has a clear decreasing trend from 01/06/2003. A linear approximation has been computed from that date. It is plotted on Figure 31. The trend is -4.1 mm/year over the period. This correction has to be added to the range.

5.2. WET TROPOSPHERE CORRECTION

Mean and standard deviation cycle by cycle of MWR-ECMWF model difference are plotted on Figure 32 and Figure 33. There are a slight rising trend on the mean. There is a known drift on the 36.5 GHz brightness temperature. However no link has been established between the TB drift and the MWR trend.

The standard deviation drops down by 2 mm from cycle 13. This is due to a change in the ECMWF model on the 14th January 2003. The impact of these changes has been found to be meteorologically positive, and it is confirmed by the improved consistency with the MWR

(see http://www.ecmwf.int/products/data/operational_system/evolution/evolution_2003.html)

The scatter plot of MWR correction according to ECMWF model for cycle 30 is given on Figure 34.

A complete monitoring of all the radiometer parameters is available in the cyclic Envisat Microwave Radiometer Assessment Report (http://earth.esa.int/pcs/envisat/mwr/reports/).

5.3. CROSSOVER ANALYSIS

Crossover differences are systematically analysed to estimate data quality and SSH performances. The standard SSH calculation for Envisat is defined below.

SSH=Orbit –Range

+ Inverse dry troposphere correction (Cartesian grids)

+ Inverse barometer correction (Cartesian grids)

+Radiometer Wet troposphere correction

+Dual Frequency correction (filter 300km)

+Non parametric SSB

+GOT00V2

+Earth tide correction

+Pole tide correction

5.3.1.1. Mean of SSH differences

The number and mean crossover differences using 3 selections are respectively plotted on Figure 35 and Figure 36. On the black curve, no selection is applied. On the red curve, areas with shallow waters have been removed (bathy<-1000m). On the greblueen curve, areas with shallow waters (1000 m), of high ocean variability (> 20 cm) and high latitudes (> |50| degrees) have been removed. Using, this selection, the remaining areas are very stable and allow an accurate monitoring of the data quality.

There is a strong annual signal on the 3 curves. This signal is not centered around zero and has an amplitude of 1-2 cm. The mean difference is in average positive which means that:

SSH on descending tracks > SSH on ascending tracks

Figure 37 shows the mean crossover differences in 5 areas. The signal in South Pacific and South Atlantic is larger than in the other part of the globe (2-3 cm). This behaviour, still under study, might be connected with the orbit error.

Figure 38 shows the impact of using another SSH formula on the mean and the standard deviation crossover differences (Bathy<-1000). For this analysis a long wave length error has been computed. The long wave length error estimation is performed by a global minimization of crossover differences using a (1 and 2 cycles/revolution) sinusoidal model. The mean difference drops to zero using this orbit error.

The map of mean crossover from cycles 11 to 30 is on Figure 39. It shows systematic differences between ascending and descending passes in some areas. The mean locally overtakes 4 cm (in South Pacific and South Atlantic), which is probably due to the gravity model used (see chapter 6)

5.3.1.2. Standard deviation of SSH differences

Figure 40 shows the standard deviation of SSH differences at crossover. The standard deviation is between 9 and 12 cm when no selection is applied. The last selection allows us to monitor the Envisat performance. In that case the standard deviation is between 7.5 and 8.5 cm. Most of the cycles have a standard deviation between 7.5 and 7.7cm. But there are some variations that can be explained:

- Cycle 15 is strongly different because of the low number of crossover points. There are less than 10000 crossovers only whereas on other cycles there are more than 20000
- Cycles 12, 16, 21, 26 have higher values >8cm because of out of plane manoeuvres
- Cycle 21 has a strong value (8.5) because of the combine effect of 2 manoeuvres, an intense solar activity between these 2 manoeuvres, and a lack of laser measurements between these two manoeuvres
- Cycle 11 has a relative high value because of a lack of Doris data

Figure 41 shows the impact of using another SSH formula the standard deviation (Bathy<-1000). The long wave length correction strongly improves the performances (4 cm rms). The use of FES02 model instead of GOT00V2 slightly improves the performances except for a few cycles. However, note that when the full data set (no selection) is used better results are obtained with Got00V2. Got00V2 uses local model for coastal areas which improves the SSH performance in these regions. The use of GIM ionosphere correction instead of the dual slightly degrades the performances.

The map of standard deviation crossover differences on Figure 42 shows usual results with high variability areas linked to ocean variability.

5.3.1.3. Pseudo Time tag bias

Mean of pseudo time tag bias is plotted on Figure 43. The mean value is 0.14 ms which is a good performance. An annual signal, similar to the one seen on the crossover mean differences is observed. The amplitude of this signal is about 0.4 ms.

5.4. SEA LEVEL ANOMALY

5.4.1.1. Mean Sea level Estimation

Figure 44 shows the cycle by cycle mean of SSH–MSS CLS01V1. In black, the SSH is computed without the USO drift. In red, the SSH is computed using the drift estimated in 5.1.1.6 :

$$Range_{corrected}=Range-4.1 \text{ mm/year} \Rightarrow SSH_{corrected}=SSH+4.1 \text{ mm/year}$$

There is a sinusoidal signal due to the seasonal effect. The mean over the period is around 44 cm. This signal is strongly reduced on Figure 45 when the high latitude, the low bathymetry and the high variability areas are removed. When applying the USO drift, SSH-MSS has an increasing trend. A comparison between the MSL estimations of Envisat, Jason-1, T/P and GFO has been performed. The results of this study are available in Appendix A.

5.4.1.2. SLA variability

Figure 46 shows the standard deviation of SSH–MSS. When high latitude, low bathymetry and high variability areas are removed SSH –MSS standard deviation is between 9 and 10 cm.

6. COMPARISON GDR/DELFT ORBIT

The Delft university computes routinely a precise orbit for Envisat. The Eigen-Grace01S orbits are available at `http://www.deos.tudelft.nl/ers/precorbs/orbits/` (Doornbos et al, 2004). The main details of the processing of these orbits are:

- `Software: GEODYN-II (GSFC)`
- `Gravity: EIGEN-GRACE01S (GFZ-Potsdam)`
- `Tides: PGS7751E (GSFC)`
- `Non-gravitational forces: ANGARA (TU Delft, ESOC, HTG)`
- `Thermospheric density: MSIS-86`
- `Earth-orientation parameters: from IERS EOP-C04`
- `DORIS data sigma: 0.50 mm/s`
- `SLR data sigma: 4 cm + 1-20 cm depending on station`
- `Arc length: 5.5 days, new arc every 3.5 days, 2 days overlap`
- `Drag estimation sub-arc length: 1/4 orbit (25.1496 minutes)`
- `cpr along/cross-track sub-arc length: 12 hours`

The Delft orbit has been updated in our database for cycles 13-25 allowing us to compare it to the GDR orbit.

6.1. ORBIT DIFFERENCES

Figure 47 and Figure 48 show the differences along track for each cycle between 13 and 24. Higher differences are visible on several cycles especially on cycle 21. Figure 49 shows the mean differences over the period 13-25. The differences are less than 3 cm in most areas. However they can overtake this value in few areas. In the tropical Atlantic for example, the delft orbit has sensitively lower values than the GDR orbit. On the contrary in North-West Pacific, the delft orbit has sensitively higher values than the GDR orbit. Figure 50 shows the same differences but separating ascending and descending passes. Similar features are visible. However some additional geographically correlated differences are visible. Around Galapagos islands for example, the difference is negative on descending passes, positive on ascending passes and consequently around zero using both. On Figure 52 we can see that the global bias between the two orbits is about 7.4 mm. It is quite stable over the period.

Figure 51 shows the variance differences. Several passes have high differences. They correspond to passes near an event impacting the orbit quality. There are also high difference in small areas, West Chile and South India. The global variance of the difference is 5.1 cm^2.

6.2. PERFORMANCES COMPARISON AT CROSSOVERS

Figure 53 shows the mean SSH differences at crossovers using the GDR orbit and the Delft orbit. The geographically correlated signals described in 5.3.1.1 are reduced largely with the Delft orbit. That is probably due to the use of the Grace Gravity Model.

Figure 54 shows the cycle by cycle mean and standard deviation SSH differences at crossovers. The two curves have the same sinusoidal signal, but with 3 mm bias. The Delft orbit is slightly more centred than the GDR one. The standard deviations at crossovers are very close.

Figure 55 shows the difference:

Variance[SSH_{Delft} differences at crossovers] - Variance[SSH_{GDR} differences at crossovers]

In red, we can see the passes where the Delft orbits have lower performances, certainly a few passes of cycle 21. On the contrary, in the blue areas, the Delft orbit performs better, about 3 cm^2. Figure 56 shows that, in average, the gain is about 1-2 cm^2 except for cycle 21.

7. CROSS CALIBRATION

Comparisons with ERS-2 and Jason-1 have been performed by computing, on the one hand, along track residuals between ERS-2 and ENVISAT and, on the other hand, crossovers between Jason and ENVISAT. Indeed, ENVISAT and ERS-2 have the same ground track and the time difference between both satellites is about 28 minutes.

7.1. CROSS CALIBRATION WITH JASON-1

Jason-1 GDR cycles 34 to 101 have been used for this analysis and compared to Envisat GDR cycle 12 to 30. Three types of cross-calibration methods have been performed. First, Envisat and Jason-1 are compared using dual crossovers. Then an orbit error computation allows us to qualify the big wave length differences. Finally performances of Envisat and Jason-1 are compared on the same space/time sampling.

7.1.1. [Envisat - Jason-1] dual-crossovers

Dual crossovers are computed with a 1 and 3 hour time lag for altimeter and radiometer parameters, and a 10-day time lag for SSH differences in order to reduce geophysical variability.

Figure 57 shows the number of crossover points for cycles 12 to 30. The variation can be due to, the sea ice coverage seasonal cycle and the availability of the two satellites.

Moreover the number and the location of dual crossovers vary with a 120-day period. Indeed Envisat is helio-synchronous contrary to Jason-1. Running mean over 120-day periods are computed on 1 hour crossover time lag to correct from this effect. The results of this analysis, plotted according Jason cycle, covers the following period: Envisat cycle 14 to 28.

7.1.1.1. SWH and SIGMA0 comparisons

Figure 58 shows the [Envisat – Jason-1] Ku SWH differences at 1H/3H crossovers. There is a good consistency between the 2 satellites. The global SWH mean value is around 15.7/15.7 cm, Envisat being higher than Jason. A very slight trend is visible on the running mean curve. The standard deviation is 21.2/27.0 cm.

Figure 59 shows the [Envisat – Jason-1] Ku Sima0 differences at 1H/3H crossovers. There is a good consistency between the 2 satellites. The global mean value is -2.9/-2.9 dB and the standard deviation is 0.2/0.4 dB. Jason-1 Ku-band sigma0 is strongly higher than Envisat. Envisat Ku-band sigma0 has been aligned on ERS-2 to satisfy the MWC wind model. Notice that Jason-1 Ku-band sigma0 is 2.3 dB higher than TOPEX. This difference is described in (Vincent et al., 2003).

7.1.1.2. Troposphere comparisons

Figure 60 shows the [Envisat radiometer – ECMWF model] and [Jason-1 radiometer – ECMWF model] differences at latitude lower than 66°. A 1 cm jump occurs just after the safehold mode of the Jason-1 platform on cycle 69 Jason-1 (Dorandeu et al, 2004). It is visible on cycle Envisat 22 on the J1 mean curve. The standard deviation of the Jason radiometer-model is lower than Envisat one mainly thanks to the third additional channel (18.7 GHz) in the JMR.

7.1.1.3. SSH comparisons

SSH comparisons have been computed on dual-crossover differences with a 10-day time lag. The following table summarises the corrections used on the two satellites for SSH computation in the initial configuration:

initial configuration	**ENVISAT**	**JASON**
Orbit	CNES (product)	CNES (product)
Range	product	product
Inverse barometer	time varying pressure (product)	time varying pressure (product)
Dry troposphere	product	Product
Wet troposphere	ECMWF (product)	ECMWF (product)
Ionosphere	Dual Frequency (product)	Dual Frequency (product)
SSB	Non parametric (product)	Non parametric (product)
Ocean tide	GOT99 (updated)	GOT99 (product)
Earth tide	product	product
Pole tide	product	product

Table 2 : Parameters used to compute SSH for ENVISAT and Jason.

Figure 61 shows the [Envisat – Jason-1] mean and standard deviation SSH differences. Envisat measures 26.5 to 27.5 cm higher than Jason-1 depending on the cycle. The standard deviation is between 7 and 8 cm.

The maps of mean and standard deviation [Envisat-Jason-1] SSH differences at crossover from cycles 12 to 30 are on Figure 62. There are systematic differences which locally overtakes 4 cm. They are probably due to gravity model differences. The map of standard deviation crossover differences shows the high variability areas linked to ocean variability.

7.1.2. Long wave length differences

The Envisat/Jason-1 long wave length differences have been computed by global minimization of 10-day (EN-J1) SSH differences. The method is described in (Le Traon et al., 1998).

The mean and standard deviation of the long wave length differences have been computed for cycles 12 to 30. The maps are plotted on Figure 63. The geographical patterns of the mean are consistent with the [Envisat-Jason-1] SSH mean differences. The long wave length error variability ranges from 2 cm to 5 cm in South East Pacific.

7.1.3. Performance comparisons on same time/space sampling

It is interesting to compute statistics from the same geographic area and from the same time period, since both satellites should give comparable general results. A selection on latitude, bathymetry and variability is applied on Jason-1 and Envisat. The time periods are the periods corresponding to Envisat cycles.

7.1.3.1. Crossover

The objective is to compare the long term monitoring of Envisat and Jason-1 crossover performances. In order to compare performances, SSH crossovers have been interpolated with a spline tension equal to 0. Therefore the SSH is not filtered along track. Areas with shallow waters have been removed (bathy<-1000m).

Performances at crossovers are compared, for the two satellites on Figure 64. The number of Jason crossover points is strongly greater than the Envisat one between cycles 13 and 19 and cycle 22. Indeed a lot of Envisat passes are missing on those cycles. The mean of Envisat/Envisat and Jason-1/Jason-1 SSH differences at crossovers is respectively 0.8 cm and 0.2 cm. There is a sinusoidal signal on Jason-1 but it is not annual, as on Envisat. The standard deviation of Envisat/Envisat and Jason-1/Jason-1 SSH difference at crossovers are respectively 6.6 cm and 6.7 cm. Performances are slightly better on Envisat except for cycles 12, 16, 21 and 26.

7.1.3.2. SLA

Figure 65 shows the [Envisat – Jason-1] number of points, mean and standard deviation of along track Sea Level Anomaly relative to MSS. There are systematically more measurements for Jason-1, because of a better availability and lower inclination of the orbit. The mean curves are obtained removing 43.7 and 16.4 cm respectively on Envisat and Jason-1. The standard deviation of Envisat and Jason-1 are very close, respectively 9.4 cm and 9.5 cm.

Figure 66 shows the Mean Sea Level estimation of Envisat, Jason-1, T/P. 10-day statistics have been computed for Envisat. The 3 satellites show a consistent annual signal and rising trend. Figure 67 shows firstly the Envisat MSL trend over cycle 11 to 30 and secondly the J1-EN MSL trend differences over the Envisat period. The Envisat and Jason MSL trend are quite consistent. However there are some slight differences for example around the Bengal Gulf, where Envisat MSL trend is about 2cm greater than Jason MSL trend.

A more complete study on the comparison between the MSL estimations of Envisat, Jason-1, T/P and GFO has been performed. The results of this study are available in Appendix A.

7.2. CROSS CALIBRATION WITH ERS-2

To perform the comparisons with ERS-2, OPR cycles (version 6.4) from CERSAT centre have been used. Each ERS-2 cycle (from 80 to 97) has been processed as described in the ERS-2 Quality assessment reports (Mertz et al., 2004). All the necessary updates were performed on ERS-2 data to be homogeneous with the Envisat data set. Envisat and ERS-2 data are collocated by repeat track analysis in order to compare the main relevant parameters. As the on-board register of ERS-2 failed in June 2003 (cycle 85), from Envisat cycle 18 onwards, the cross calibration is done only for data in a restricted area (in the visibility of ESA ground stations over Europe, North Atlantic, the Arctic and western North America). In order to obtain a continuous long-term monitoring for the whole period of Envisat, the statistics are calculated over the restricted area for cycles 12 to 29.

7.2.1. Computation of a restricted mean track

To lead to a homogeneous pattern of the statistics between ERS-2 and Envisat for the whole Envisat mission, a restricted mean track has been computed over cycles 86 to 91 ERS-2. An example of ERS-2 valid data is given in Figure 68. Several cycles where needed to obtain a pattern as complete as possible. Then, statistical (ERS-2 – Envisat) differences have been re-computed for all the cycles before June 2003.

7.2.2. SWH and SIGMA0 comparison

The [ERS-2 - Envisat] global mean difference of significant wave height is -21.7 cm and the standard deviation is 26.7 cm. ERS-2 measures lower SWH than Envisat. For each cycle, the scatter plot shows a good consistency between the two parameters, nevertheless, the differences are higher in strong SWH geographical areas (Figure 69 and Figure 70). This explains the larger variability during winter on the cycle by cycle statistics (Figure 71).

The mean difference of backscatter coefficient is 0.04 dB and the standard deviation is 0.3 dB (Figure 72). Note that the ERS-2 SIGMA0 has been corrected for a +0.25 dB bias as described in Dorandeu, 2000. A bias has also been applied (-3.5 dB) on Envisat in order to be compliant with the wind speed model (Witter and Chelton, 1991). From the cyclic mean and standard deviation differences, no special behaviour can be detected.

7.2.3. Radiometer parameters comparison

Brightness temperatures differences have also been monitored (Figure 73 and Figure 74). The 23.8 and 36.5 GHz mean differences are around -3.3K and -3.4K respectively. The seasonal signal in the 23.8 GHz TB is clearly evidenced from individual daily means (Figure 75 top), with interannual variations stronger in summer 2003 likely to be the reason of the drop down to -4K during summer 2003 (cycles 16 to 19) in the difference.

From the daily 36.5 GHz individual TBs (Figure 75 bottom), the seasonal signal is less pronounced but remains. It is not evident to decorrelate the seasonal and interannual signals of the two satellites from the drift present in Envisat 36.5 GHz TB. The combination of those effects certainly impacts the behaviour of the difference values shown in Figure 74.

Many leads can be taken into account and clarified before concluding about the TBs:

- the drift in the Envisat 36.5 GHz channel is not clearly identified, and decorrelated from the seasonal and interannual signals
- the drift applied on ERS-2 23.8 GHz channel (Eymard et al., 2003) is shown to be updated as described in the ERS-2 annual report (Mertz et al., 2005), where a new correction provided by Scharroo et al., 2004 is tested
- the calibration between the two satellites may introduce an artificial seasonal signal. Indeed, the estimations of biases are different for small values of TBs and strong values of TBs, leading to an overestimation of one satellite in strong values areas and an underestimation in weak areas.
- the long-term monitoring is done on the ERS-2 restricted area and this may induce more variability in the estimations.

The algorithm present in the Envisat GDR products is the neural one proposed by Labroue and Obligis, 2003. This algorithm has been validated and adapted to correct ERS-2 radiometer corrections (Tran and Obligis, 2003). ERS-2 data set has then been updated with this algorithm. Previously, the drift correction of the 23.8 GHz brightness temperature was applied on ERS-2 (Eymard et al., 2003). As described in Labroue 2003, the neural algorithm used to compute the radiometer wet troposphere correction better retrieves the dry troposphere areas than the parametrical algorithm. An example of the improvement of this new computation is given in Figure 76 and in Figure 77: the drier values are much better consistent between the two satellites. However, a trend is still visible in the scatter plot, Envisat having a slightly drier correction in dry areas and a wetter correction in wet areas. This certainly impacts the mean and standard deviation of the neural radiometer wet tropo correction difference (Figure 78). In this case also, a seasonal signal is noticeable. Note that the neural algorithm applied on ERS-2 from Tran and Obligis, 2003, is an adaptation of the Envisat algorithm with biases applied. This is another source of inconsistency between the two satellites and may be refined.

7.2.4. SSH comparison

In order to compare the SSH estimations from the two missions, Envisat and ERS-2 data sets have been updated with similar algorithms and corrections, as described in Table 3.

initial configuration	ENVISAT	ERS-2
Orbit	CNES (product)	Cycles 12 to 17: DGME-04 Cycle 18 to 29: DPAF
Range	product	SPTR+USO provided by ESA, +time tag bias applied
Inverse barometer	time varying pressure (product)	time varying pressure
Dry troposphere	ECMWF (product)	ECMWF rectangular grid
Wet troposphere	ECMWF rectangular grid	ECMWF rectangular grid
Ionosphere	GIM model	GIM model
SSB	Non parametric (product)	BM3 (Gaspar and Ogor, 1996)
Ocean tide	GOT00 (product)	GOT00
Earth tide	product	product
Pole tide	product	Computed

Table 3 : List of parameters used to perform SSH comparisons between Envisat and ERS-2 along track residuals. In yellow, the parameters are in the product.

DGME-04 orbits (Scharoo and Visser 1998) have been updated on ERS-2 products until cycle 85 (cycle 17 Envisat). The mean and standard deviation of [ERS-2 - Envisat] SSH difference are plotted on Figure 79. The SLA difference is stable until cycle 20, about -34.5 cm. From cycle 21 onwards it is more variable, between -37 and -33cm. This variability can be explained by several reasons:

- the use of a less reliable orbit (DPAF)
- the use of temporary SPTR corrections at the end of the period
- the variability of the coverage from one cycle to another

8. CONCLUSION

20 GDR cycles have been produced since the beginning of the Envisat mission: cycle 11 to 30. The availability has improved: Less than 5% of data are missing on recent cycles. Among the available data, 4% have no MWR correction and 4% are impacted by the S-Band anomaly.

The ENVISAT Ra-2 and MWR data show good general results. Statistics and performances of altimeter and radiometer parameters are consistent with expected values:

- Editing ratios are stable
- Mean of RMS of 20Hz: ~9cm
- The MWR neural algorithm is very consistent with the ECMWF model
- Standard deviation of SSH difference at crossovers is less than 8 cm when high latitude, low bathymetry and high variability areas are removed
- The SSH-MSS standard deviation is about 9-10 cm and the mean is around 44 cm when high latitude, low bathymetry and high variability areas are removed

However some anomalies are currently under investigation:

- The S-band anomaly needs to be solved or at least flagged in the product
- The USO drift has to be monitored and corrected
- The annual cycle (1.5 cm amplitude) of mean Envisat/Envisat SSH difference at crossover has to be understood

Cross calibration with Jason-1 confirms these good results. The Envisat and Jason-1 altimeter and radiometer parameters have a good consistency. Performances at crossover and along track on a same time/space sampling are very close. The SSH bias between the two missions is 26.9cm.

Cross calibration with ERS-2 has been performed on cycles 12 to 17 on the whole ocean and on cycles 18 to 29 over a restricted area. SWH and SIGMA0 show good consistency between the two satellites. The neural algorithm has been updated on ERS-2 to be homogeneous with Envisat and better results are obtained on dry areas. The SSH bias is around -35 cm over the restricted area.

GDR cycles 9 and 10 will be soon reprocessed in the last version of IPF/CMA. So, in early 2005, more than two years of homogeneous Envisat data will be available. This will allow a better quality assessment and more accurate long-term monitoring.

9. REFERENCES

Dedieu M., Eymard L., Marimont C., Obligis E., Tran N., Envisat Microwave Radiometer assessment reports (cyclic). http://earth.esa.int/pcs/envisat/mwr/reports/

Dorandeu J., F. Mertz and J. Stum 2000: Note on ERS-2 Sigma0 variations since January 2000. August 2000. CLS/DOS/NT/00.286. http://www.ifremer.fr/cersat.

Dorandeu J., M. Ablain, Y. Faugère, F. Mertz, B. Soussi, Jason-1 global statistical evaluation and performance assessment. Calibration and cross-calibration results, Marine Geodesy Special issue on Jason-1 Calibration/Validation Part III,2004

Doornbos E., R. Scharro, Improved ERS and Envisat Precise Orbit determination, Presentation in ERS/Envisat Symposium Saltzburg 2004

EOP-GOQ and ESRIN PCF team, Envisat Cyclic Altimetry Reports http://earth.esa.int/pcs/envisat/ra2/reports/pcs_cyclic/

Eymard L., E. Obligis and N. Tran, 2003: "ERS-2/MWR drift evaluation and correction", CLS/DOS/NT/03.688

Faugere Y., Mertz F., Dorandeu J., Envisat GDR quality assessement report (cyclic), 2003 http://www.aviso.oceanobs.com/html/donnees/calval/validation_report/

Faugere Y., Mertz F., Dorandeu J., Envisat validation and cross calibration activities during the verification phase. Synthesis report. ESTEC contract N°16243/02/NL/FF WP6, May 16 2003

Labroue S. and E. Obligis, January 2003, Neural network retrieval algorithms for the ENVISAT/MWR, Technical note CLS.DOS/NT/03.848

Le Traon P. Y., F. Ogor, 1998: "ERS-1/2 orbit improvement using TOPEX/POSEIDON: the 2 cm challenge." *J. G. Res.*, VOL 103, p 8045-8057, April 15, 1998.

Martini A. and P. Féménias, 2000: The ERS SPTR2000 Altimetric Range Correction: Results and Validation. ERE-TN-ADQ-GSO-6001. 23 November 2000.

Mertz F., Faugere Y., Dorandeu J., Envisat GDR cross calibration report (cyclic).

Mertz, F., Y. Faugere and J. Dorandeu, Validation of ERS-2 OPR cycle 083-086. CLS.OC.NT/03.702 issue 083-086. April 17, 2003.

Pontonnier G., M. Ablain, B. Soussi, P. Thibeau, Jason-1 GDR quality assessement report (cyclic), http://www.aviso.oceanobs.com/html/donnees/calval/validation_report/

R. Scharroo and P. N. A. M. Visser : “Precise orbit determination and gravity field improvement for the ERS satellites”, *J. Geophys. Res.*, 103, C4, 8113-8127, 1998

Scharroo R., Routines for iono corrections, internet communication to the CCVT community, December 12, 2002

Tran N. and E. Obligis, December 2003, Validation of the use of ENVISAT neural algorithm on ERS-2. CLS-DOS-NT-03.901.

10. FIGURES

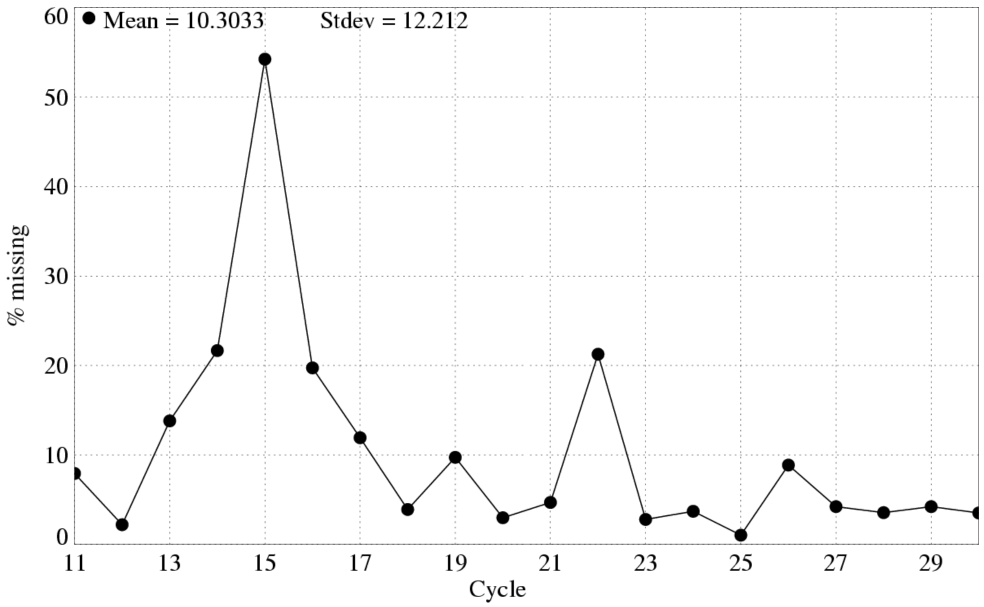

Figure 1 : % of missing measurements relative to a nominal track over ocean

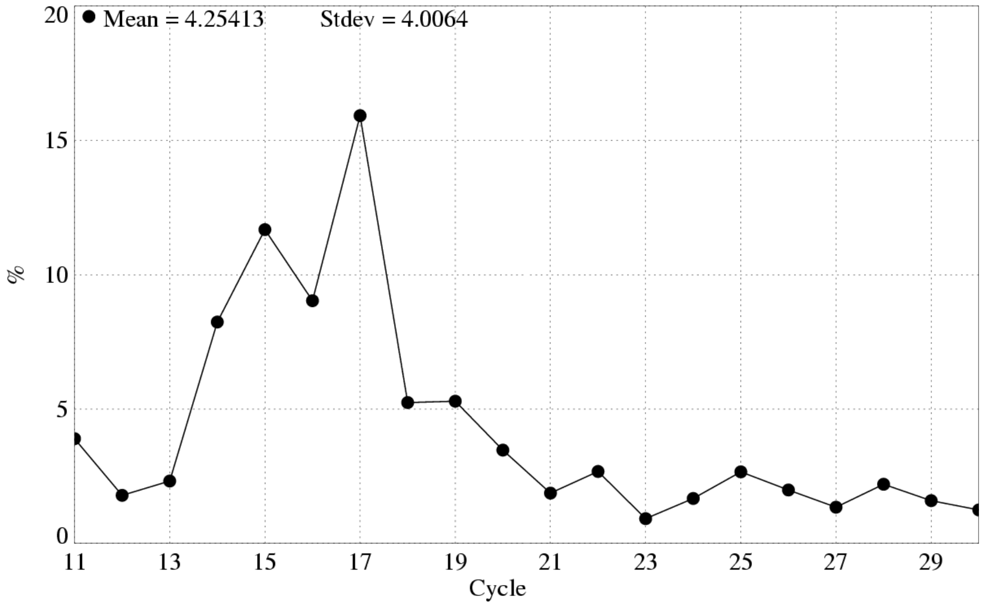

Figure 2 : % of measurements edited by the land/ocean radiometer flag over ocean

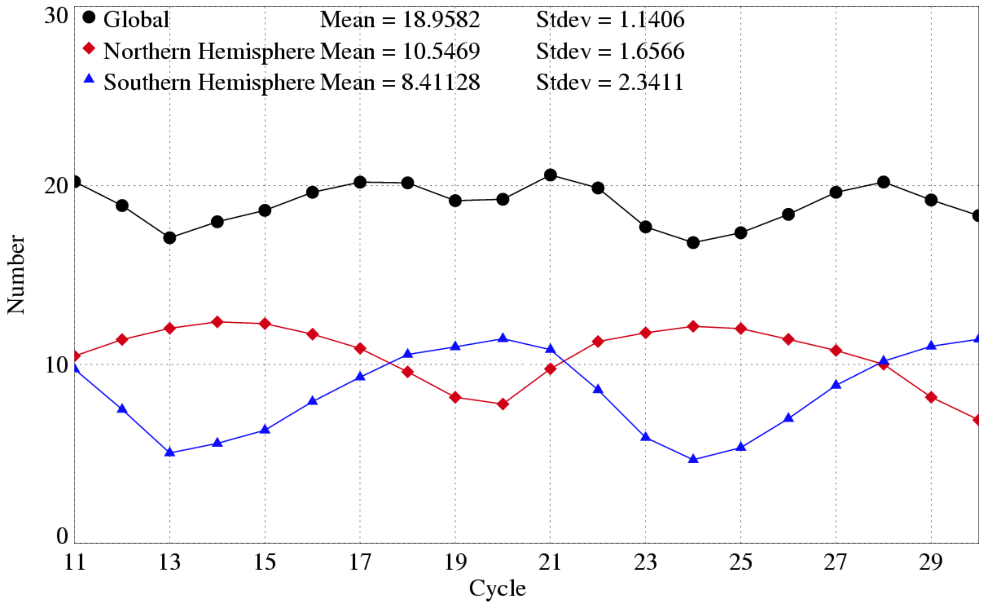

Figure 3 : % of edited points by sea ice flag over ocean, Northern Hemisphere (left), Southern Hemisphere (right)

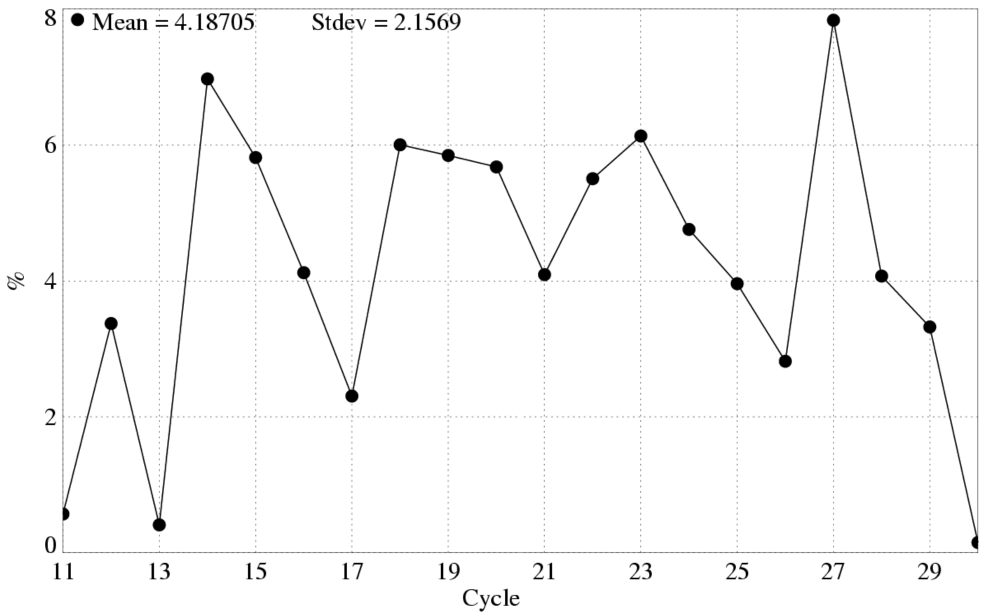

Figure 4 : % of measurements edited because of the S-Band anomaly over ocean

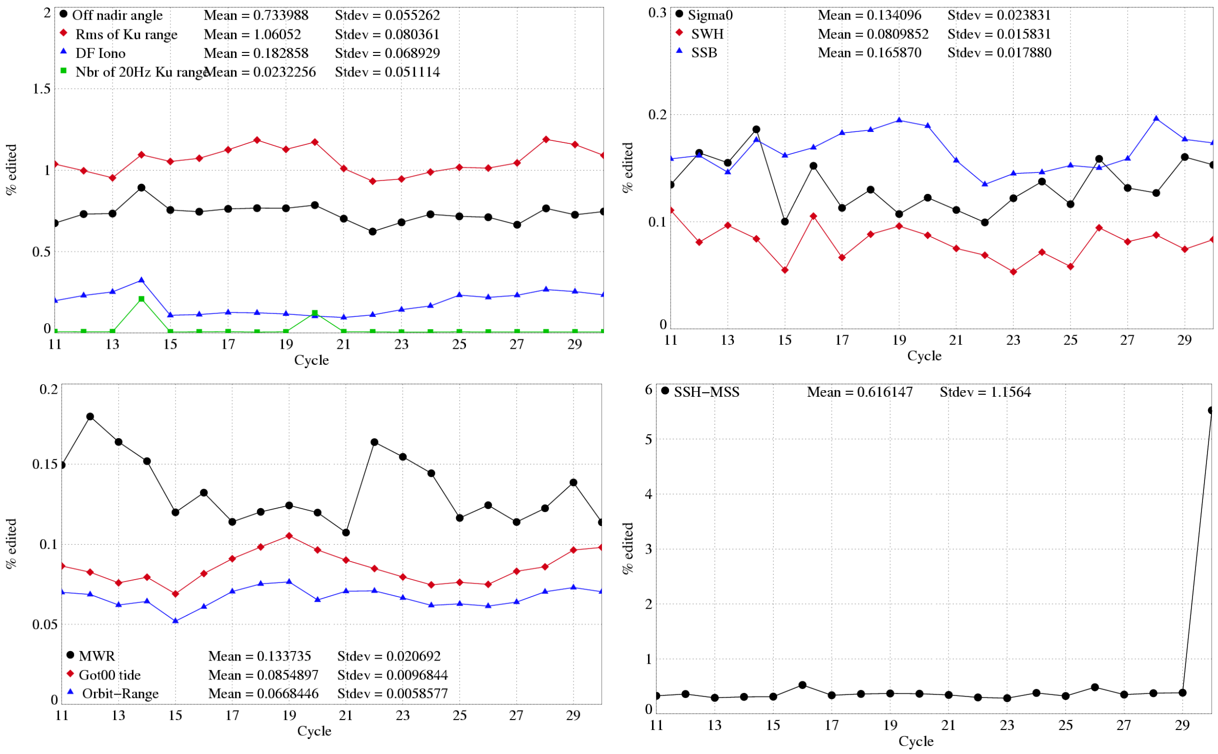

Figure 5 % of edited points by threshold

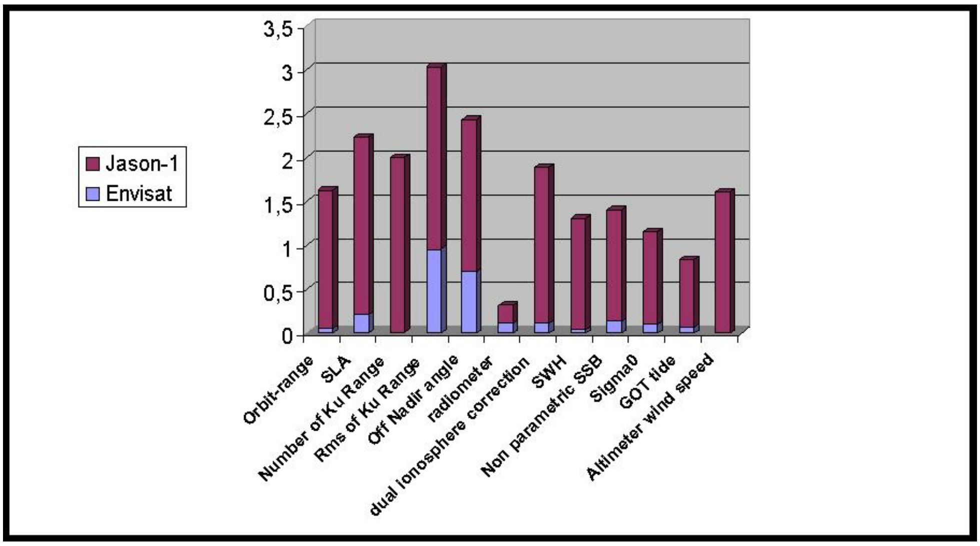

Figure 6 : % of edited measurements on a 10 day period

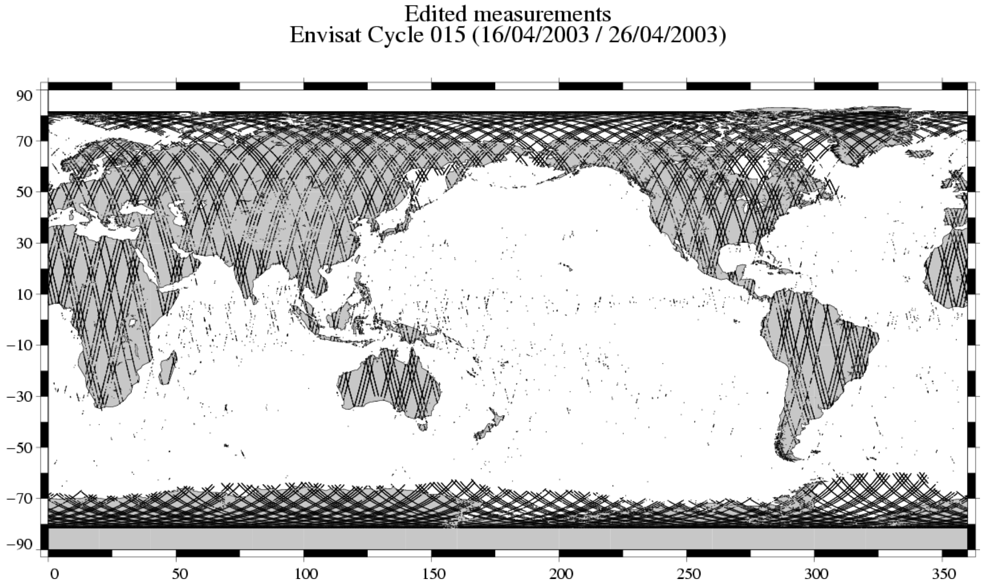

Figure 7 : Map of Envisat edited measurements on a 10 day period

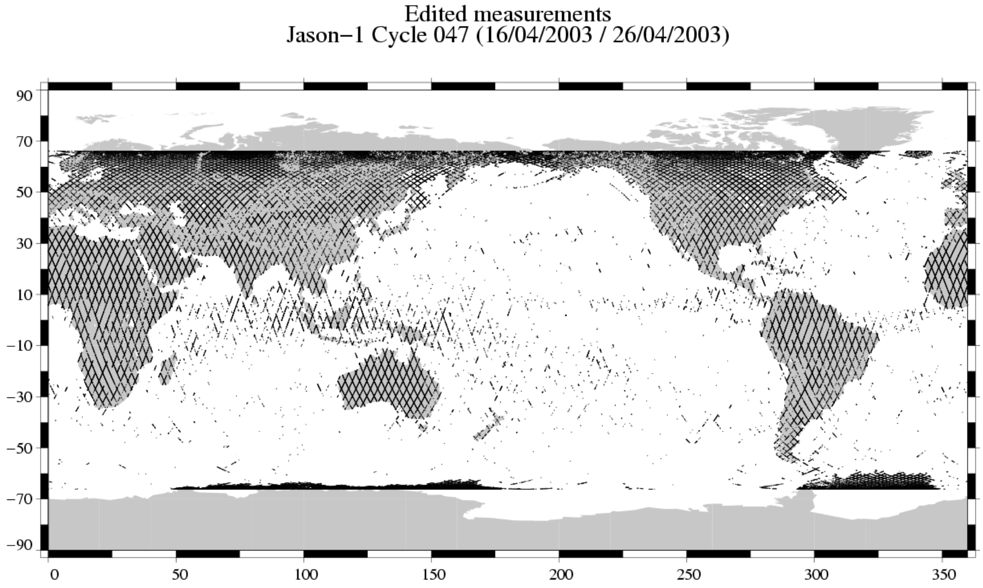

Figure 8 : Map of Jason-1 edited measurements on a 10 day period

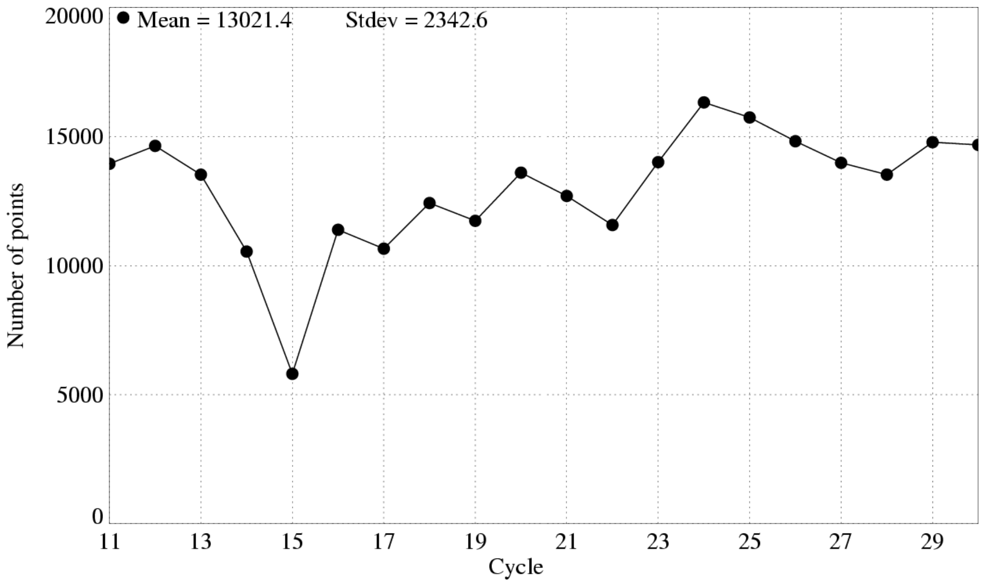

Figure 9 % of edited points by SLA statistics over the pass

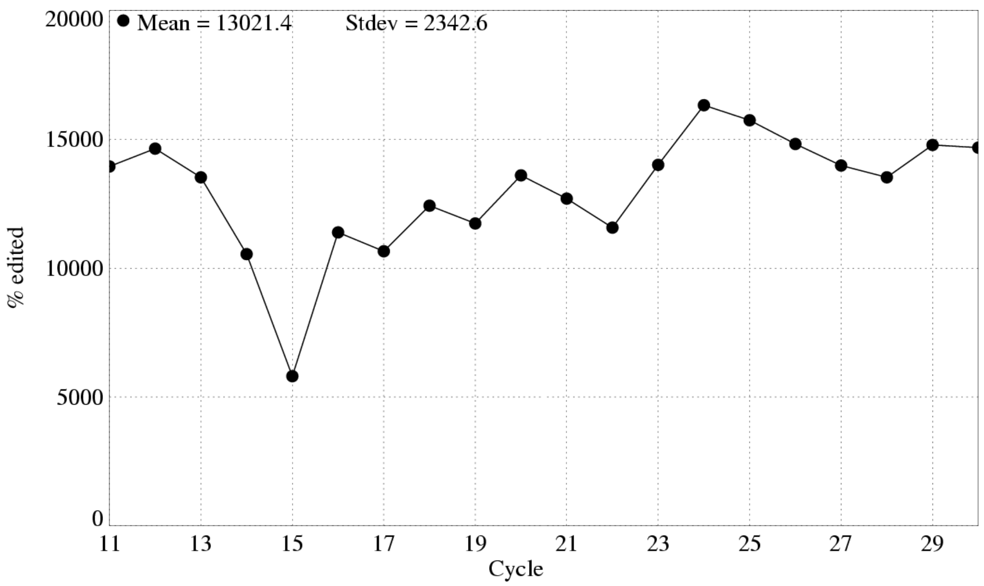

Figure 10 Additional edited point using the rain flag

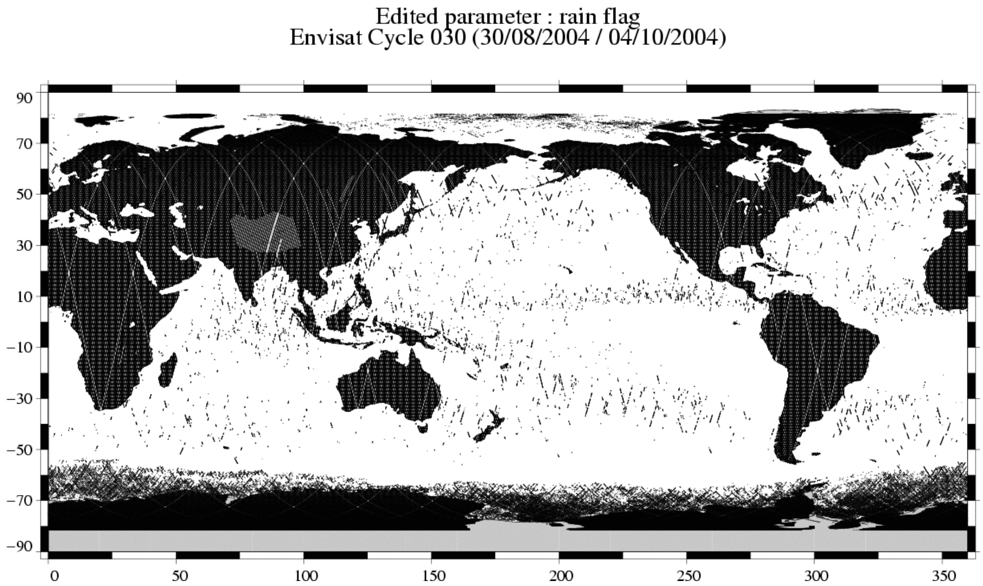

Figure 11 Data where the rain flag is ON data on cycle 18 (July 2003)

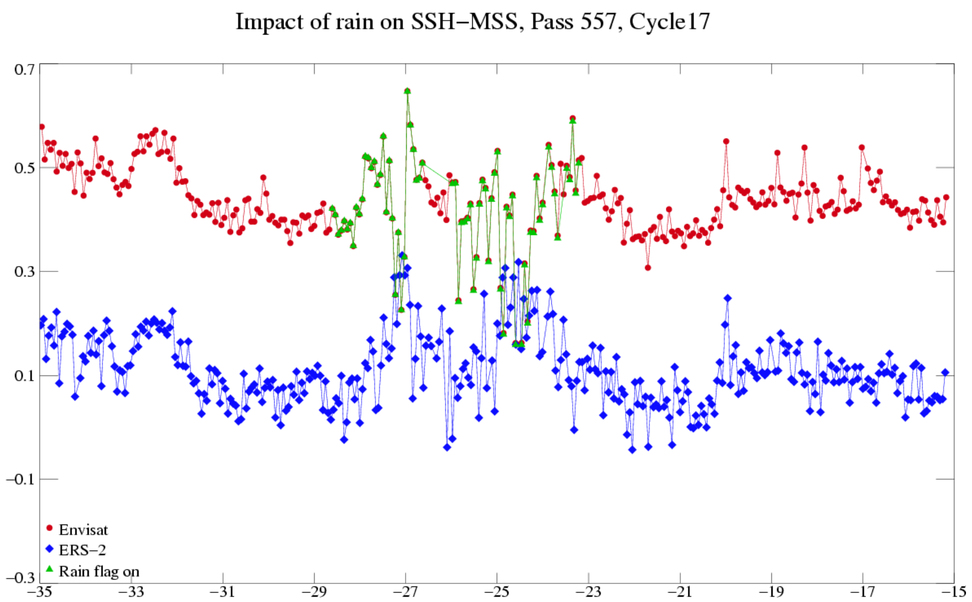

Figure 12 : Impact of rain on SSH-MSS, Pass 557, Cycle 17

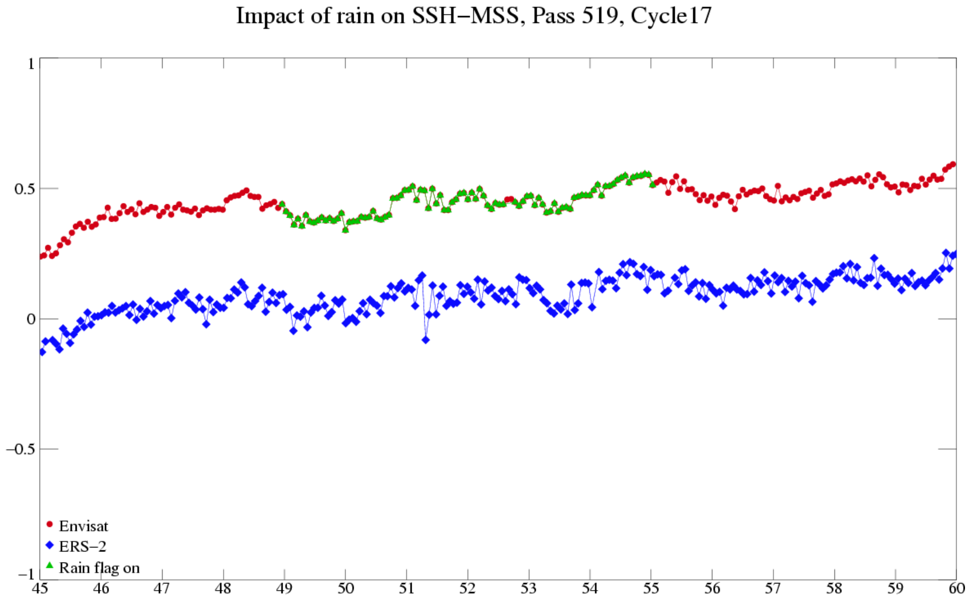

Figure 13 : Impact of rain on SSH-MSS, Pass 519, Cycle 17

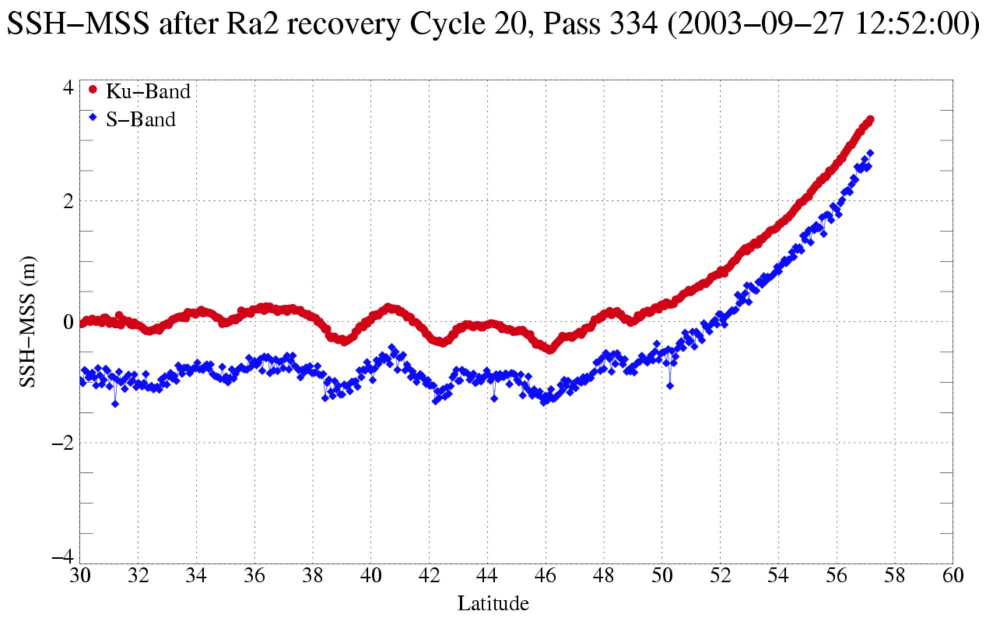

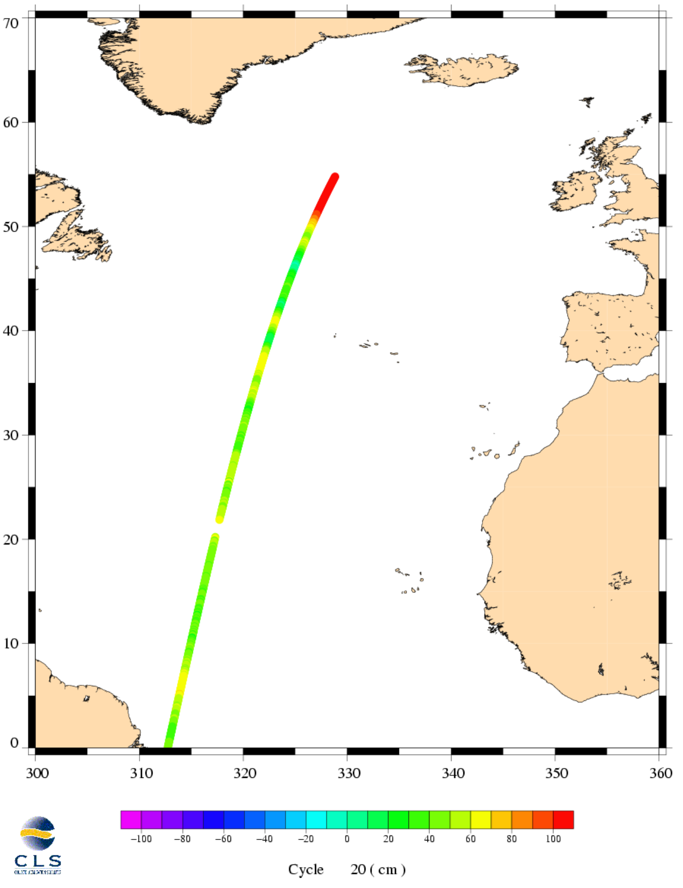

Figure 14 SSH-MSS on cycle 20 / pass 334

Date Start/End	Event	First ocean data delivered Cycle / Pass/ Date	SSH-MSS over ocean
2004-05-10 02:06:31 / 2004-05-10 11:27:30	RESET/WAIT due to too many SEU's reported	26 / 790 / 2004-05-10 11:28:37	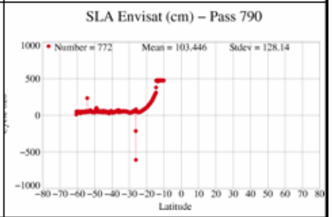
2004/05/31 02:45:27 / 2004/05/31 12:01:50	Suspend owing to repeated type 10 entries in report format	27 /390/ 2004-05-31 12:02:57	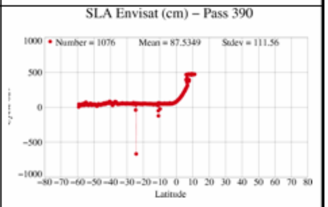
2004/06/21 14:47:51 / 2004/06/21 19:24:30	SUSPEND Mode	27/ 1000 / 2004-06-21 19:25:37	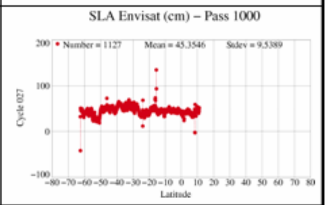

Date Start/End	Event	First ocean data delivered Cycle / Pass/ Date	SSH-MSS over ocean
2004/07/18 13:47:03 / 2004/07/18 19:59:00	in ICU rs/wt/ini	28 / 772 / 2004-07-18 20:00:06	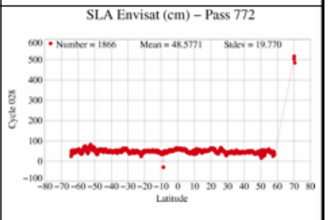
2004/08/10 15:00:39 / 2004/08/11 10:59:30	in ICU RS/WT/INI	29 / 446/ 2004-08-11 11:00:37	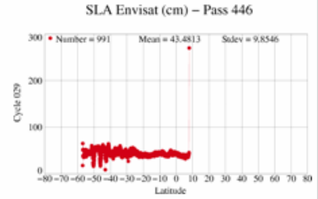
2004/09/26 13:39:50 / 2004/09/27 16:23:30	SUSPEND mode owing to a SEU INTERRUPT	30/ 796 / 2004-09-27 16:24:37	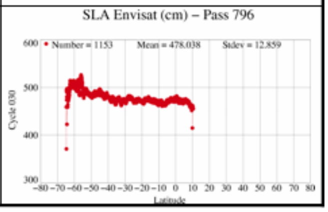

Figure 15 SLA on the first data delivered after recovery (May-septembre 2004)

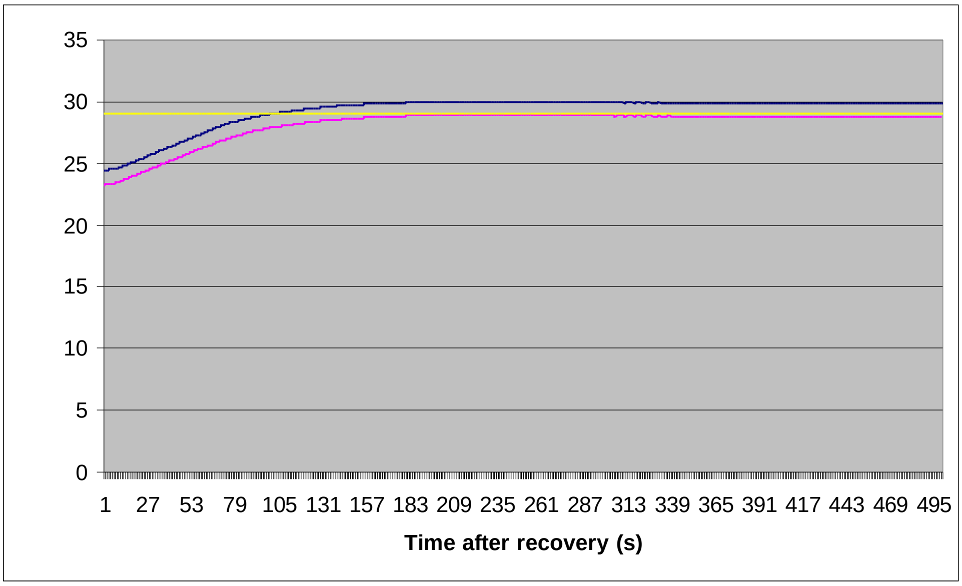

Figure 16 USO correction after recovery (blue: 2004-05-10, purple: 2004-31-05, yellow: 2004-21-06)

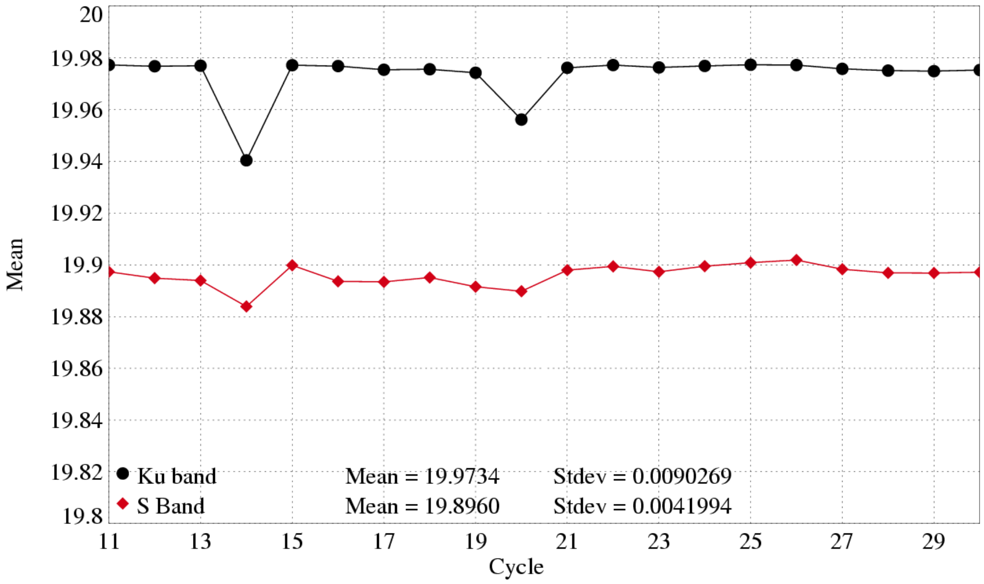

Figure 17 Mean of Number of Ku and S elementary range

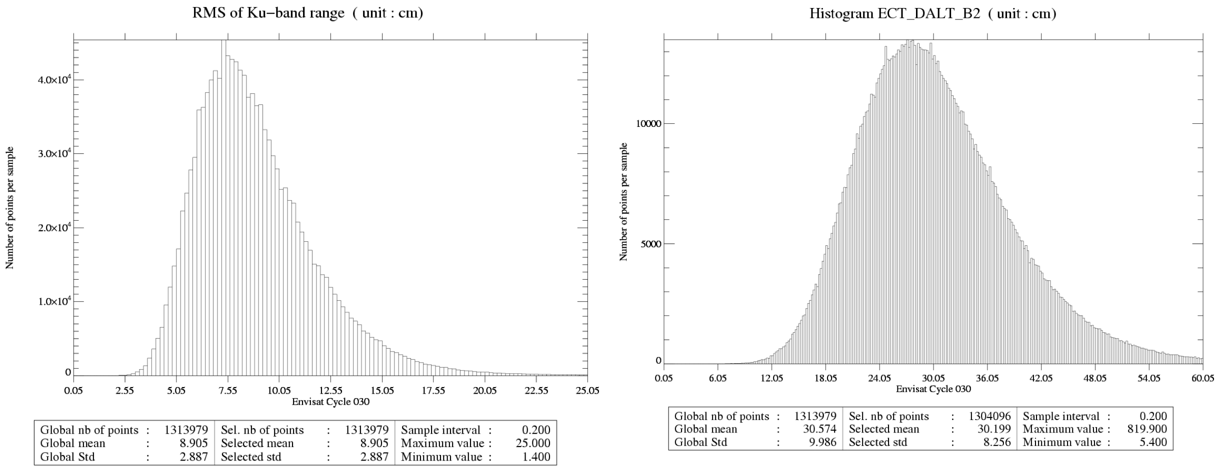

Figure 18 Histogram of RMS of Ku and S–band range (cm)

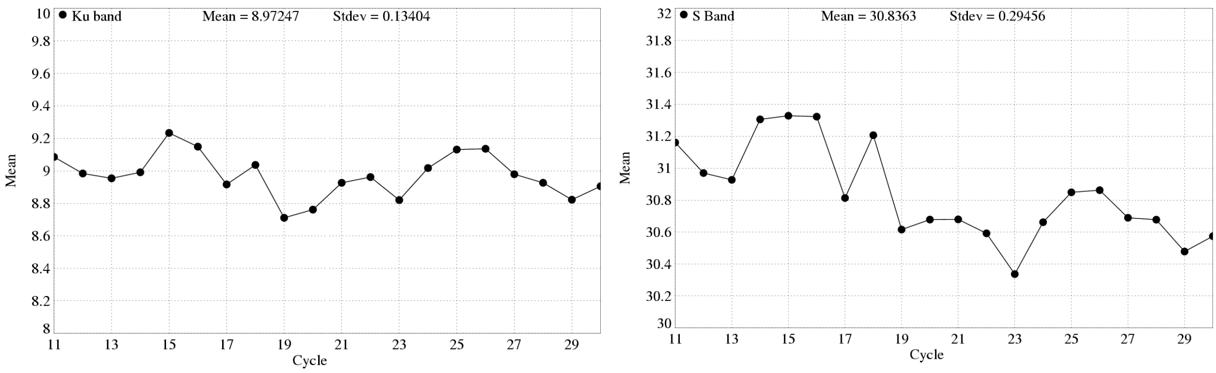

Figure 19 : Mean of RMS of Ku and S-band range (cm)

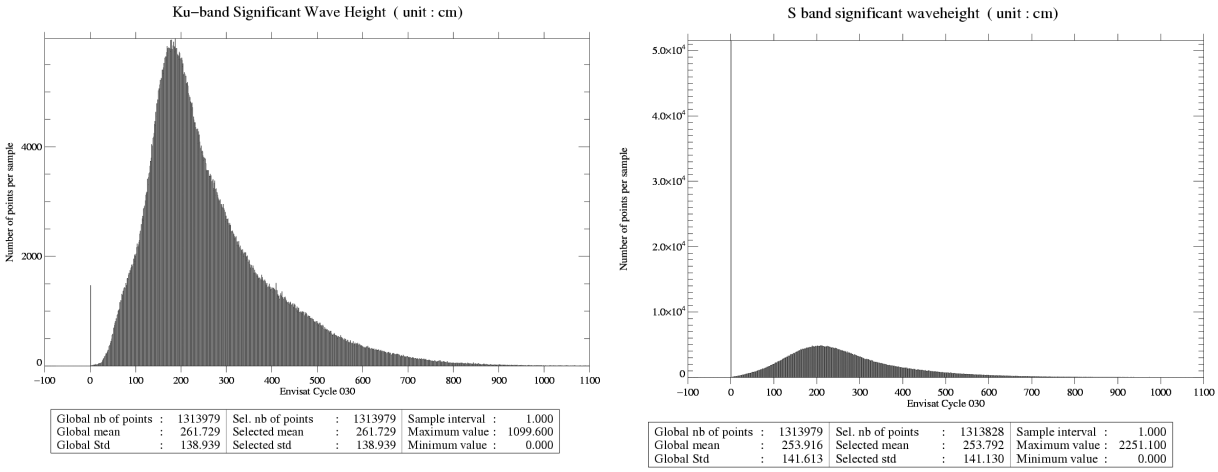

Figure 20 Histogram of Ku and S SWH (m)

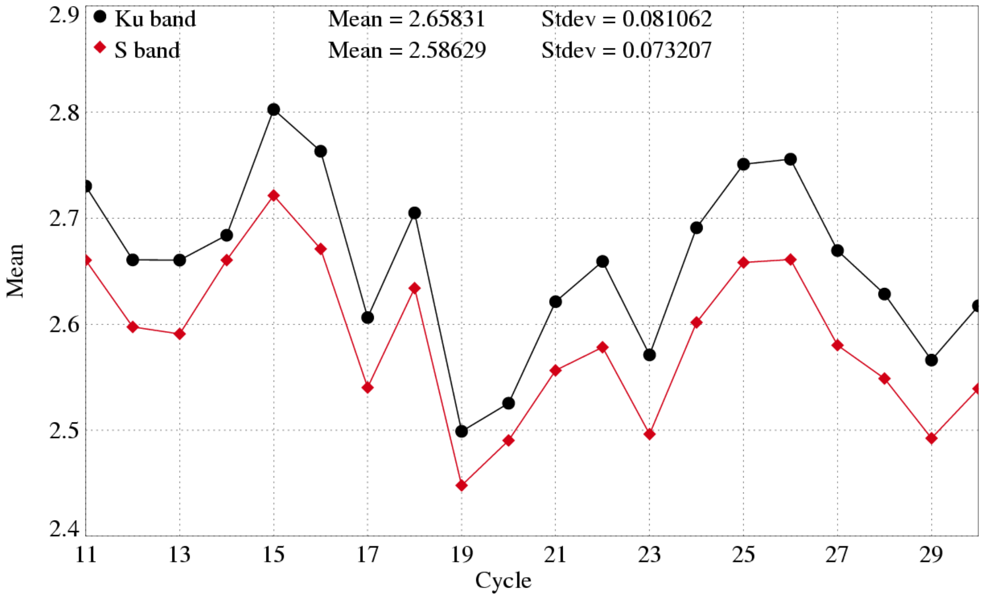

Figure 21 : Mean of Ku and S SWH (m)

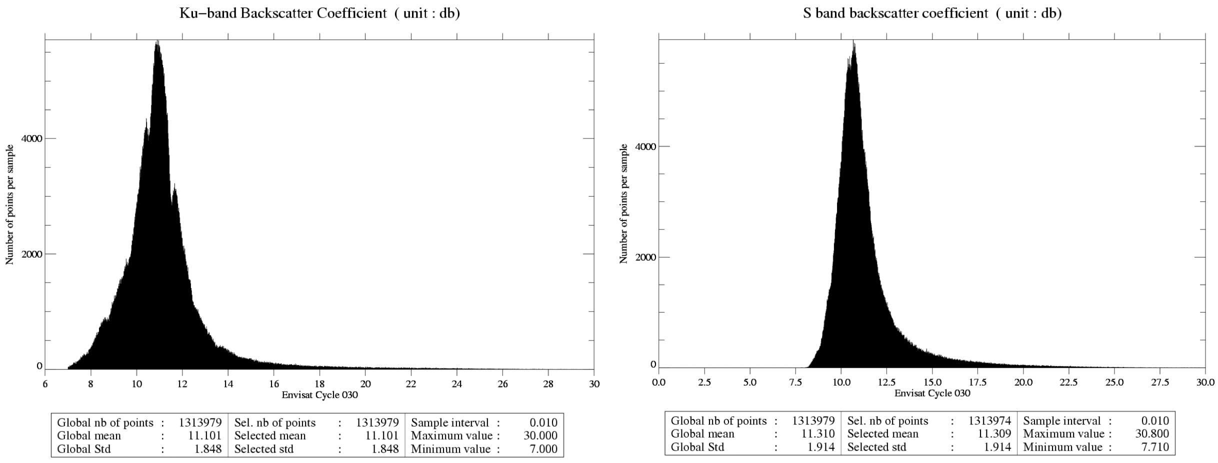

Figure 22 Histogram of Ku and S Sigma0 (dB)

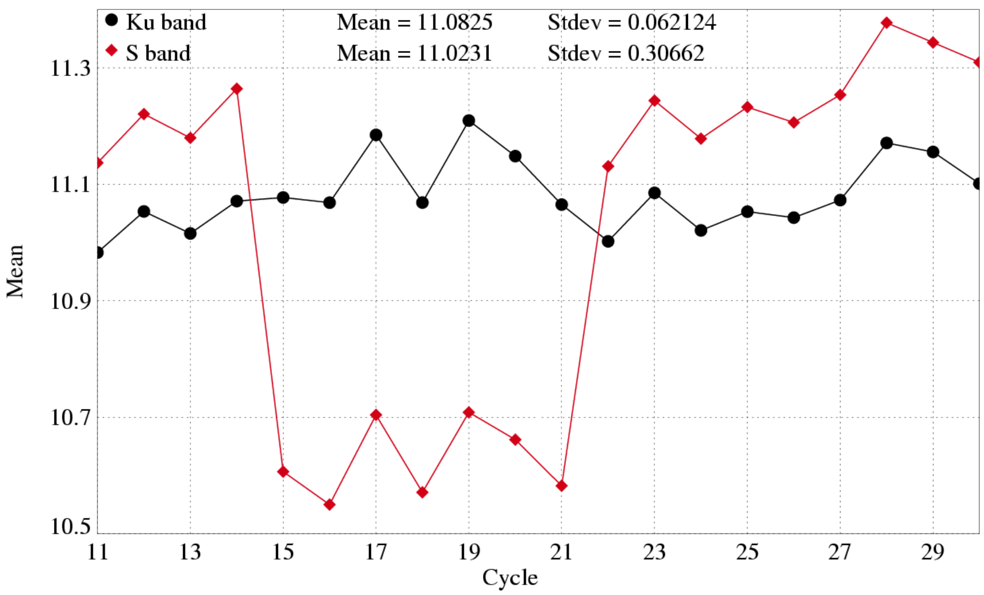

Figure 23 : Mean of Ku and S Sigma0 (dB)

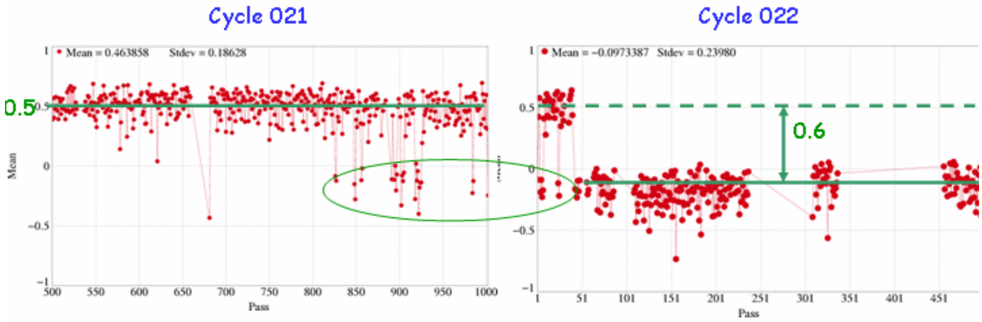

Figure 24 Mean per pass of [Sigma0(Ku)-Sigma0(S)] on cycle 21 and 22

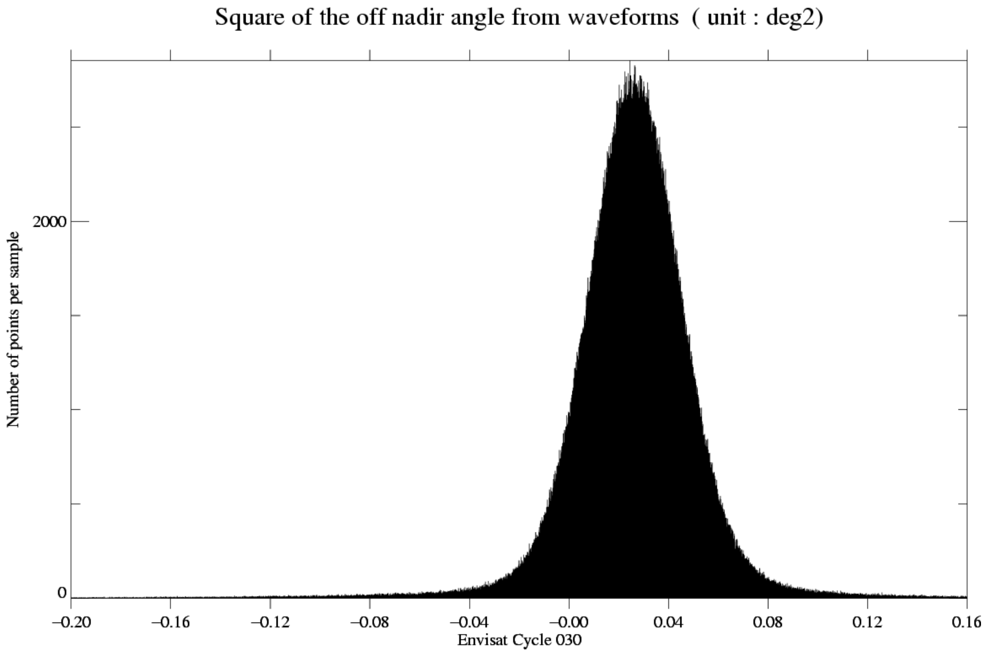

Global nb of points	:	1313979	Sel. nb of points	:	1313974	Sample interval	:	0.000
Global mean	:	0.026	Selected mean	:	0.026	Maximum value	:	0.160
Global Std	:	0.025	Selected std	:	0.025	Minimum value	:	−0.200

Figure 25 Histogram of off-nadir angle from waveforms (deg2)

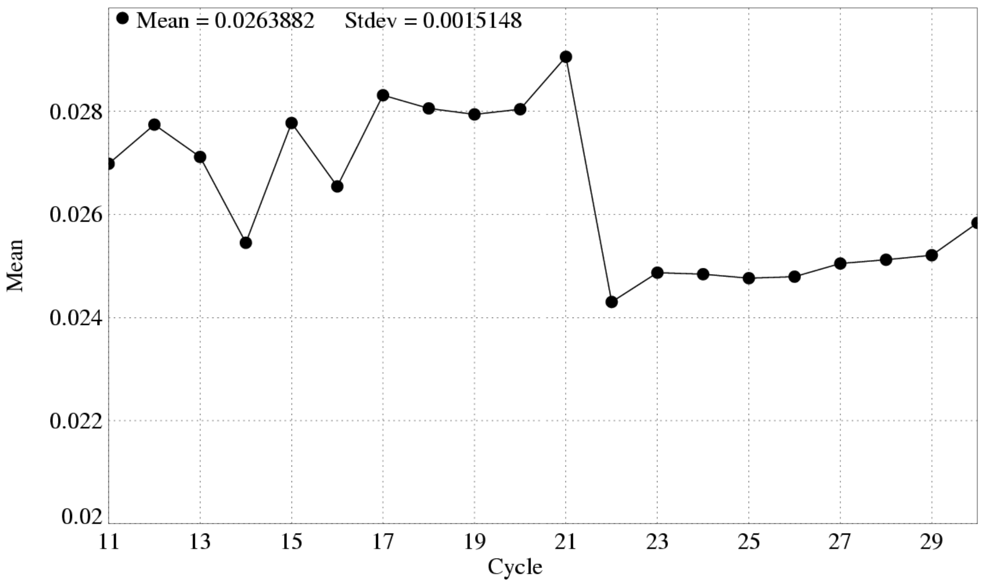

Figure 26 : Mean of off-nadir angle from waveforms (deg2)

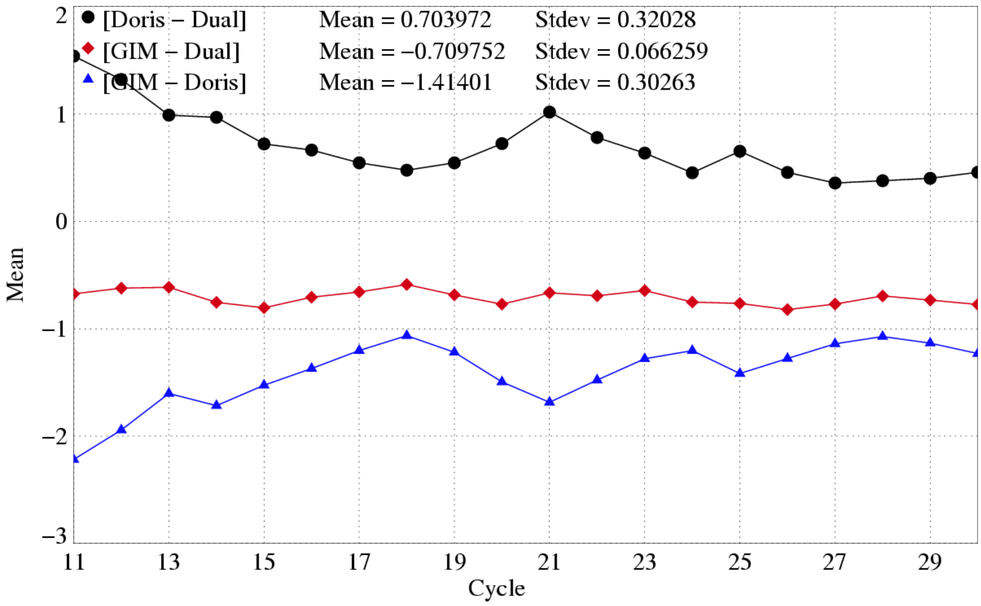

Figure 27 : Mean of [Doris-Dual], [GIM – Dual] and [GIM-Doris] ionospheric correction (cm)

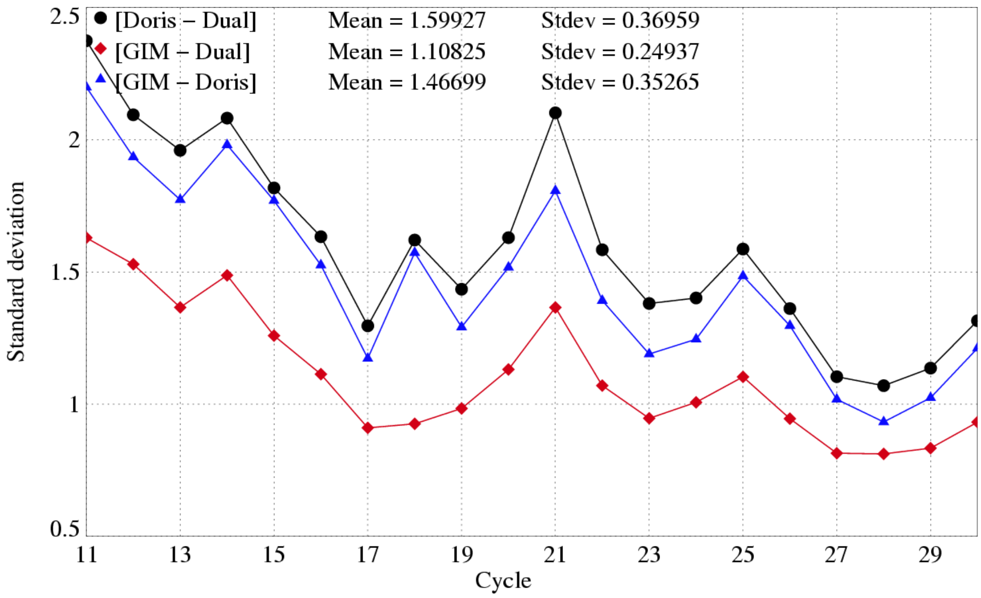

Figure 28 : Standard deviation of [Doris-Dual], [GIM – Dual] and [GIM-Doris] ionospheric correction (cm)

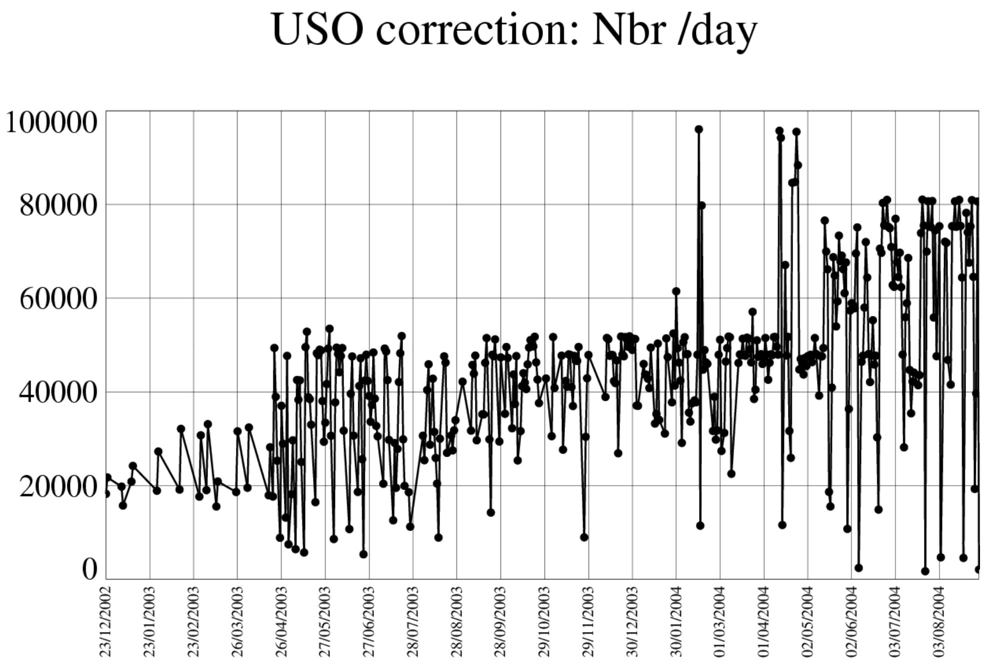

Figure 29 Number of range error estimations

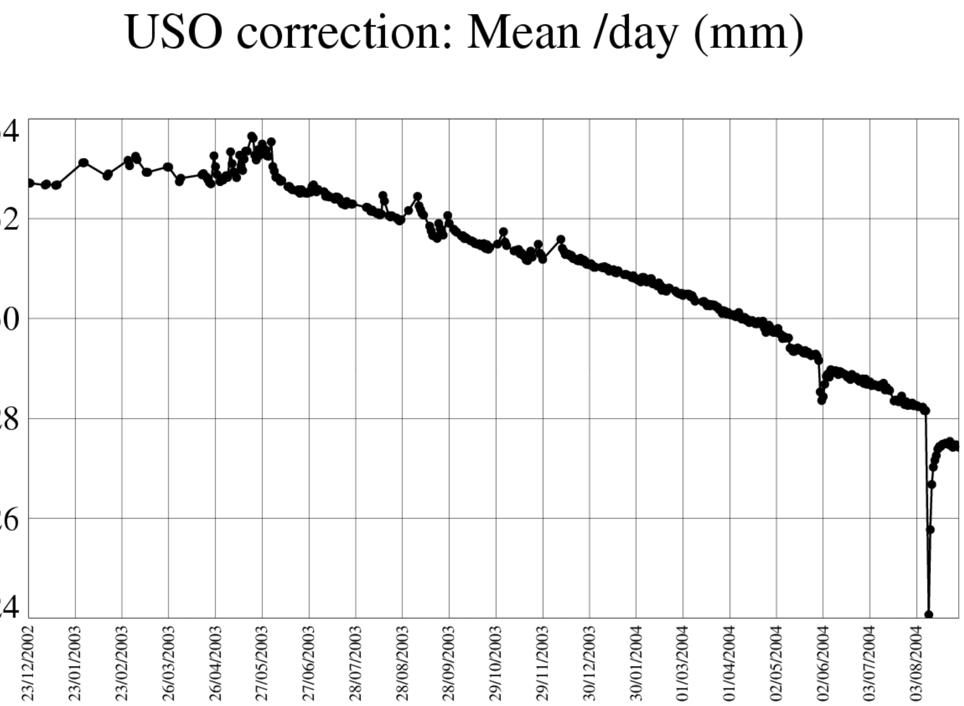

Figure 30 Mean of range error estimations (mm)

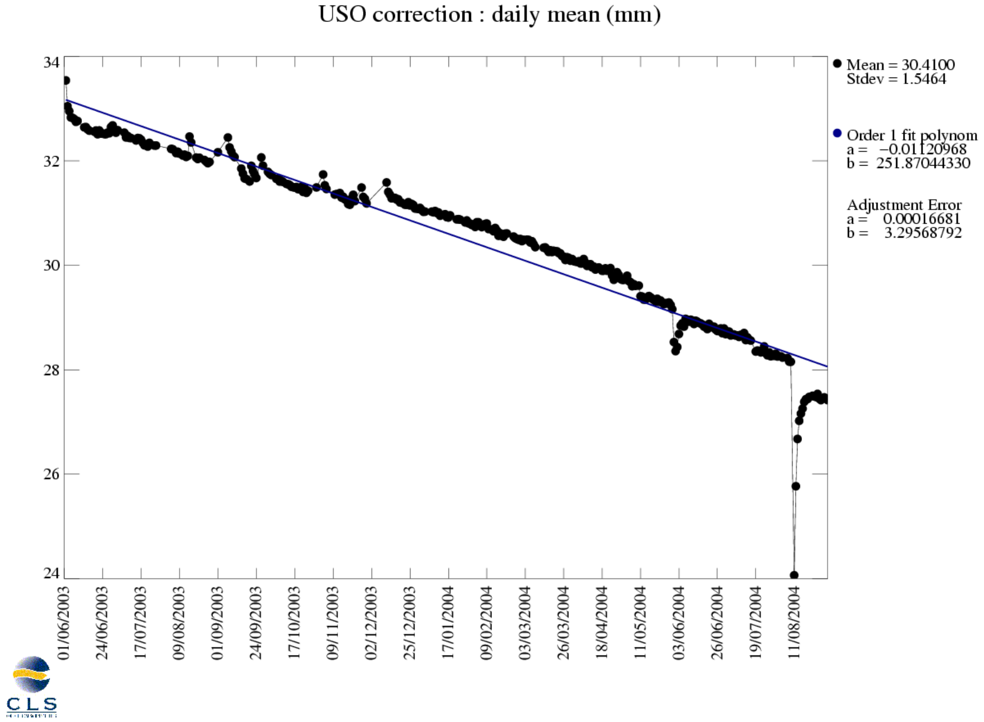

Figure 31 Mean of range error estimations since 01/06/2004 (mm)

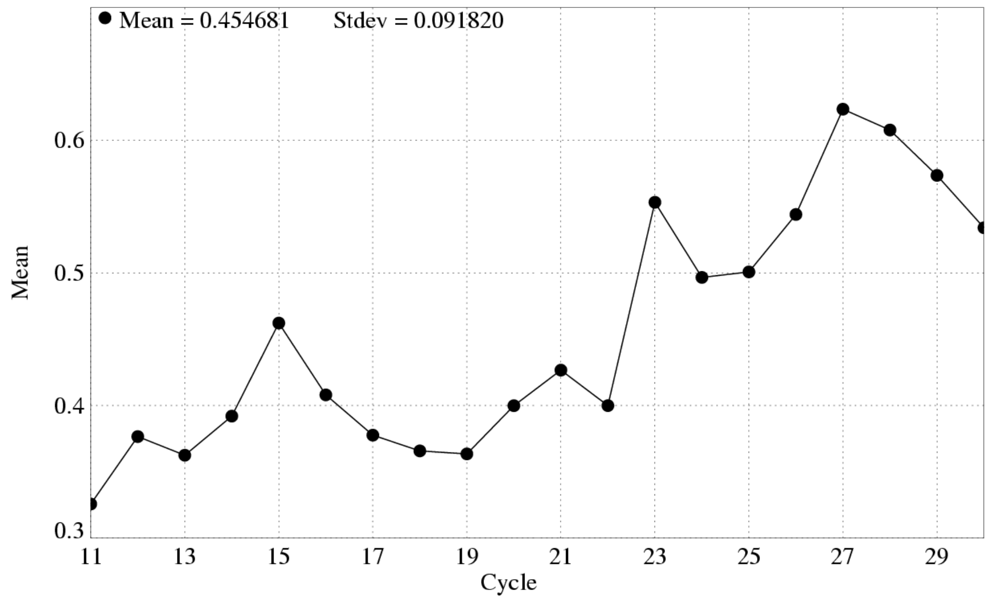

Figure 32 Mean of MWR-ECMWF model differences (cm)

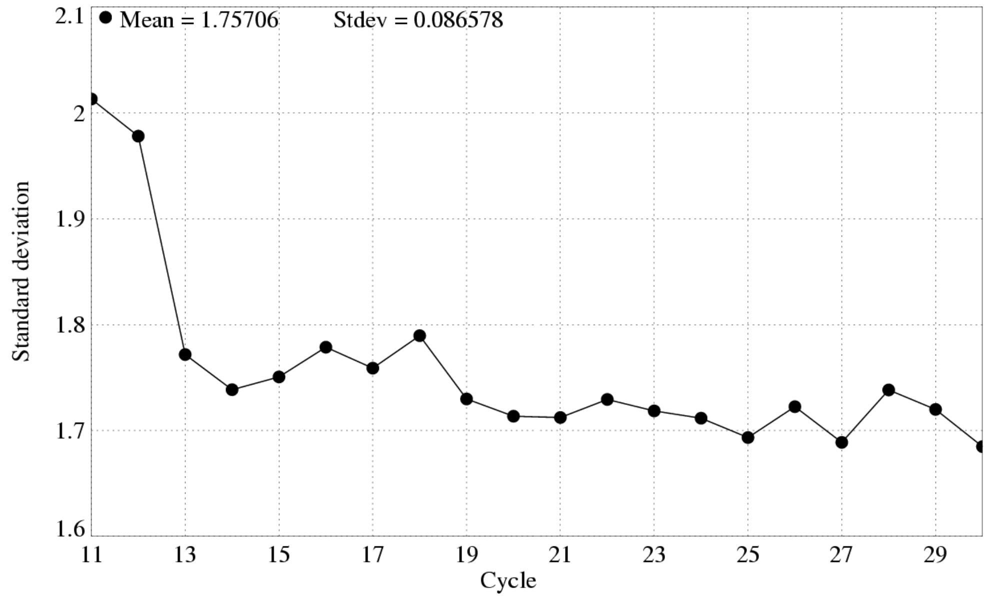

Figure 33 : Standard deviation of MWR-ECMWF model differences (cm)

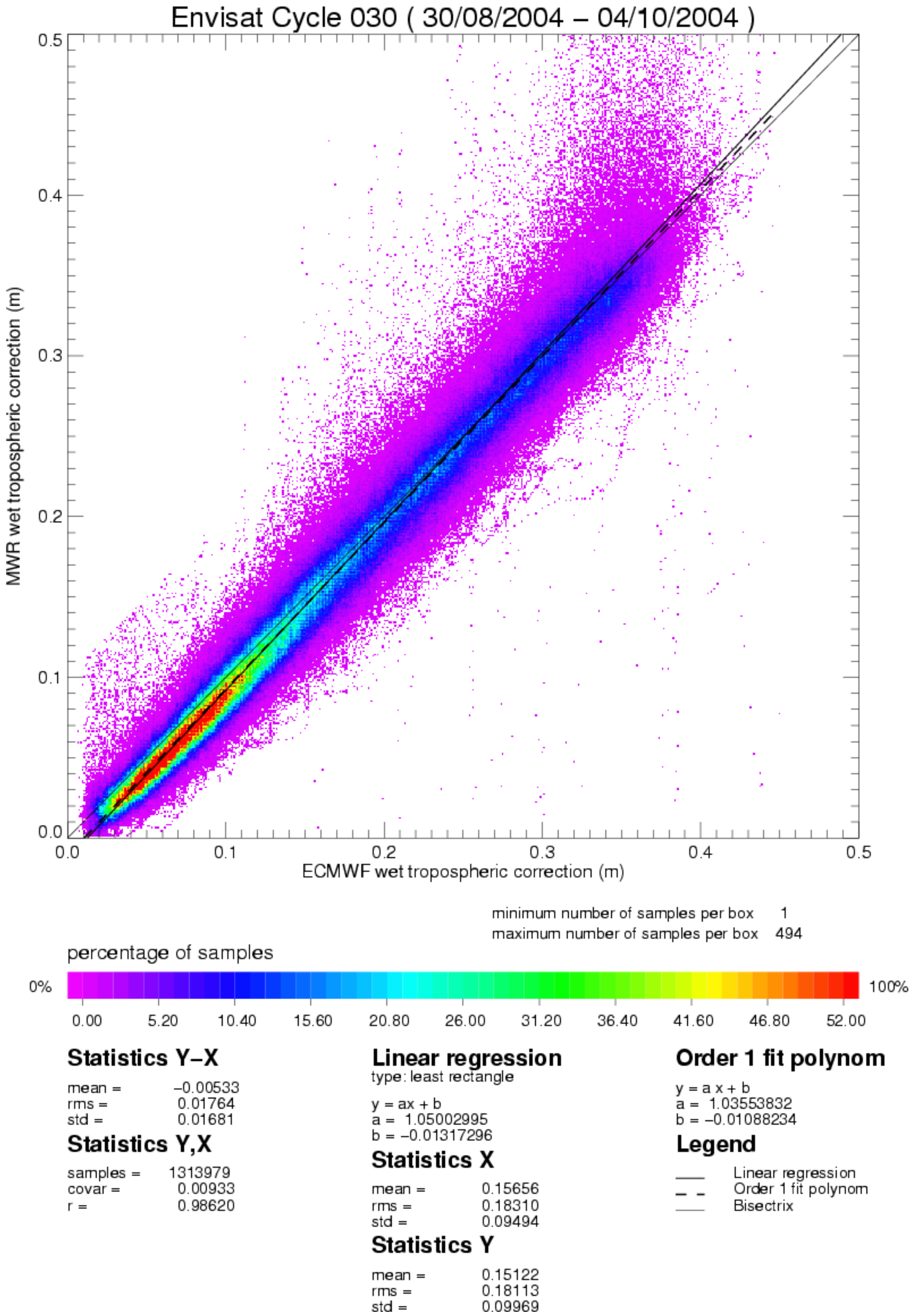

Figure 34 : Scatter plot of MWR correction according to ECMWF model (m)

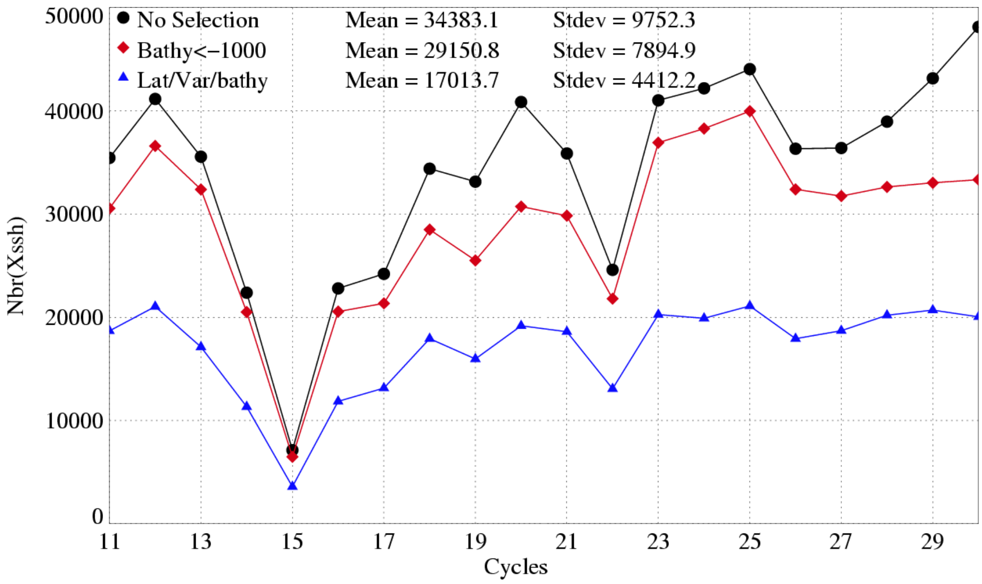

Figure 35 : Cycle by cycle number of crossovers, impact of selection

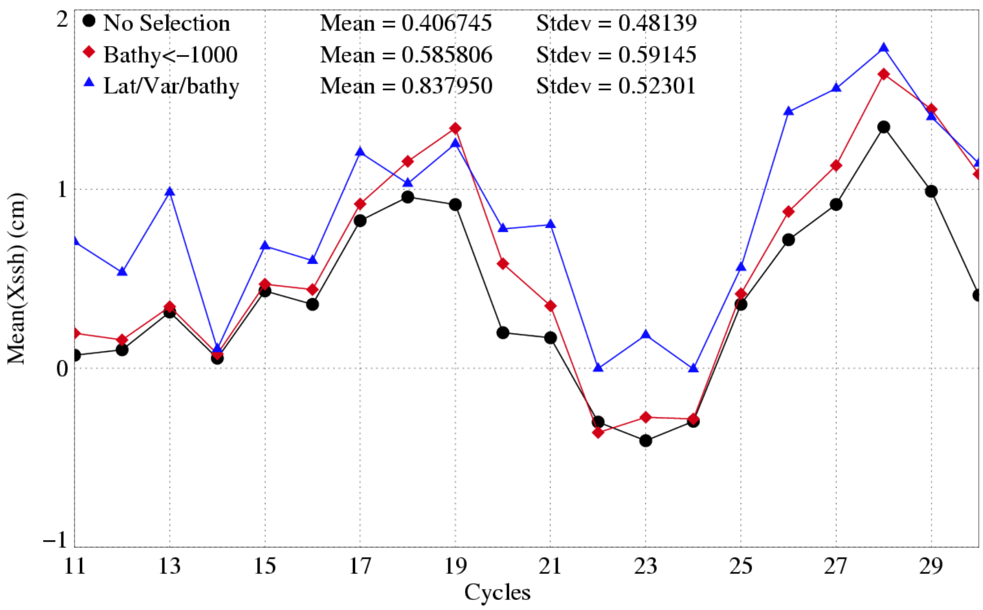

Figure 36 : Cycle by cycle mean at crossovers, impact of selection

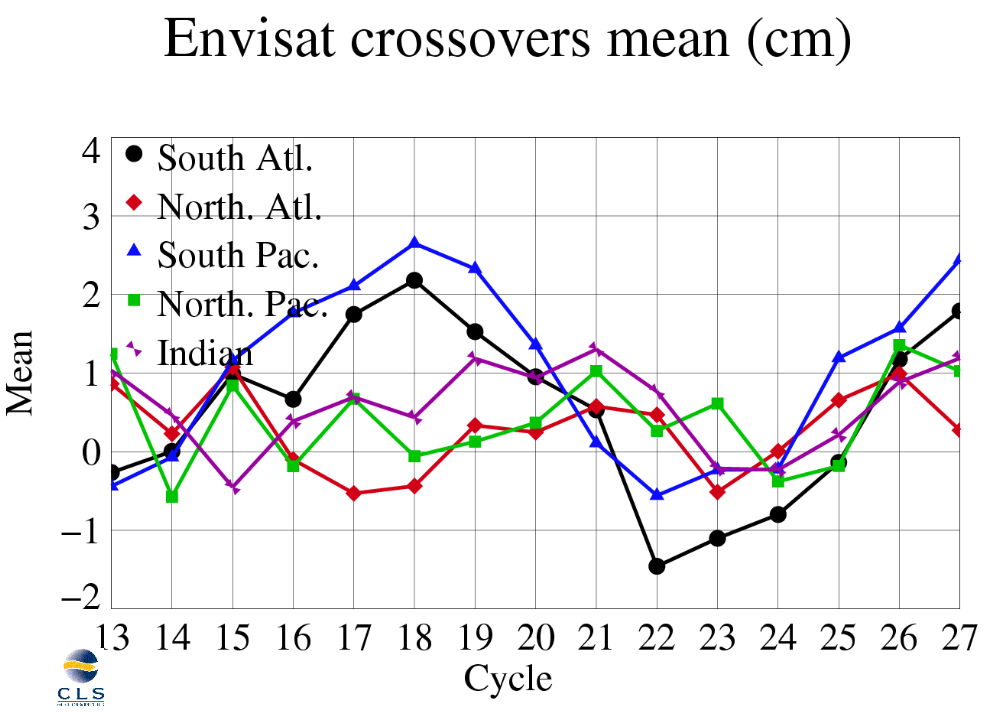

Figure 37 Cycle by cycle mean at crossovers in 5 areas

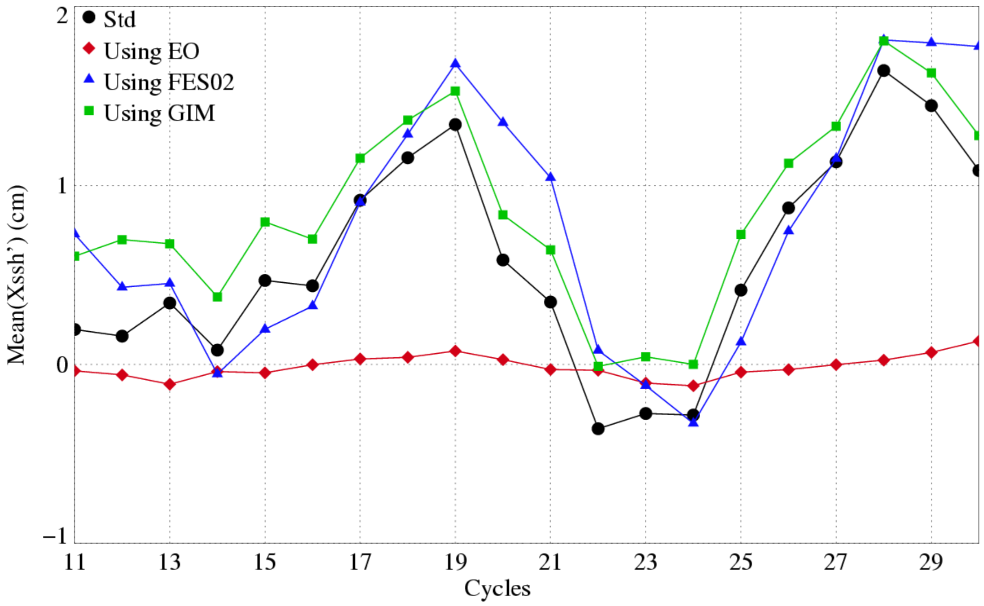

Figure 38 : Cycle by cycle mean at crossovers, impact of correction, Bathy<-1000

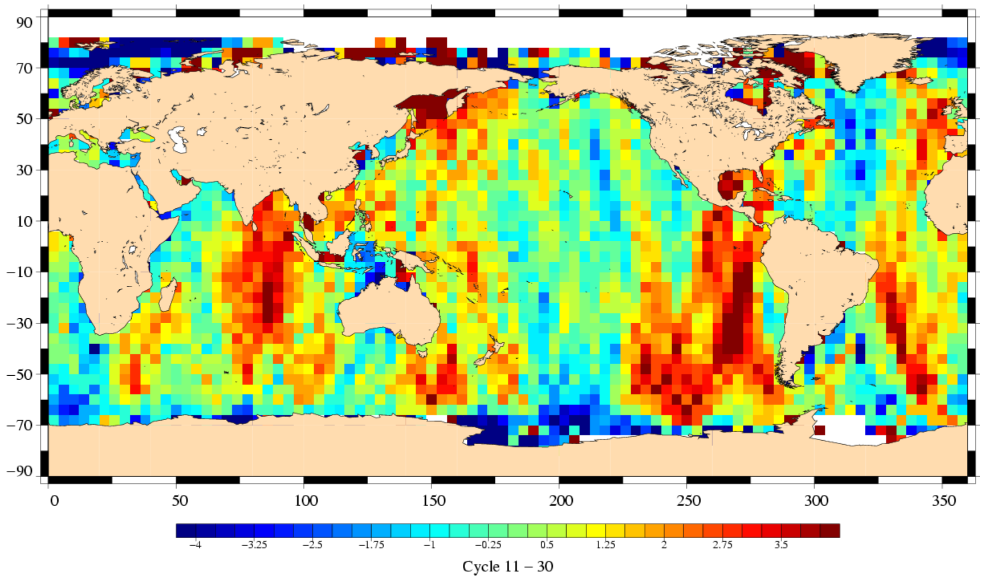

Figure 39 : Geographical pattern (4x4 degree bins) of crossover standard deviation (cm), from cycle 11 to cycle 30

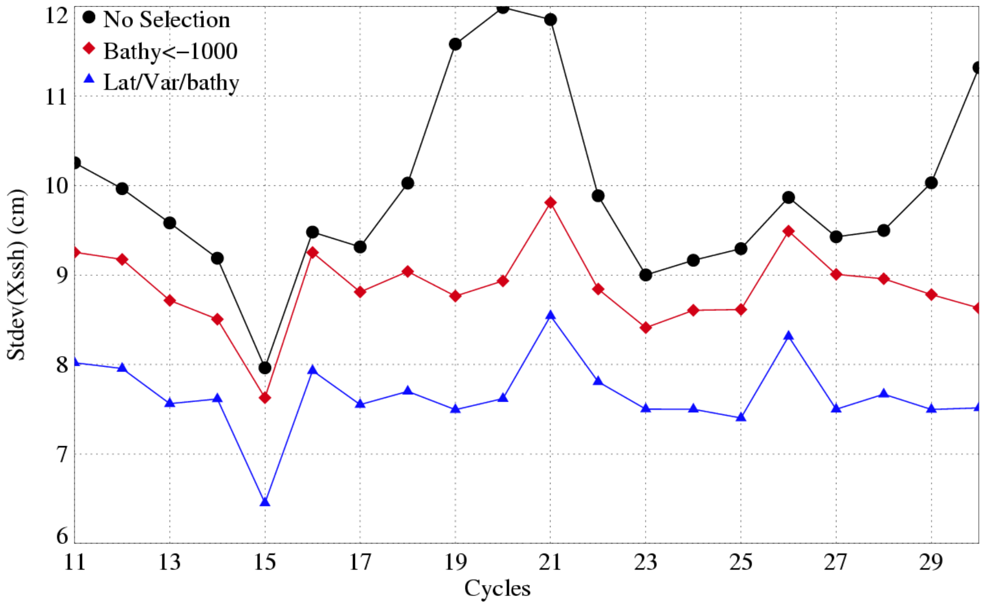

Figure 40 : Cycle by cycle standard deviation at crossovers, impact of selection

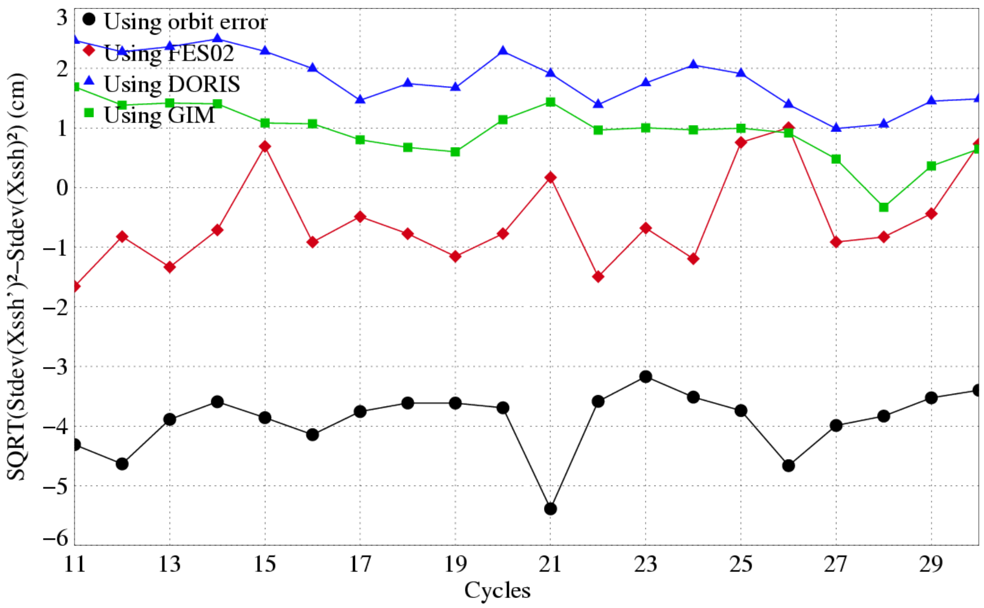

Figure 41 : Cycle by cycle gain at crossovers, impact of correction, Bathy<-1000

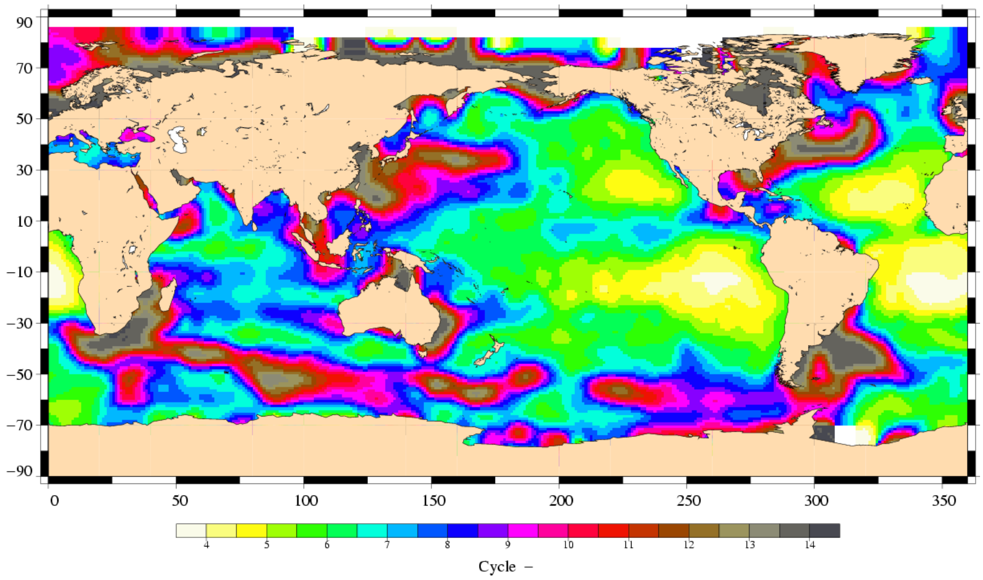

Figure 42 : Geographical pattern (4x4 degree bins) of the standard deviation of crossover differences, from cycle 11 to cycle30

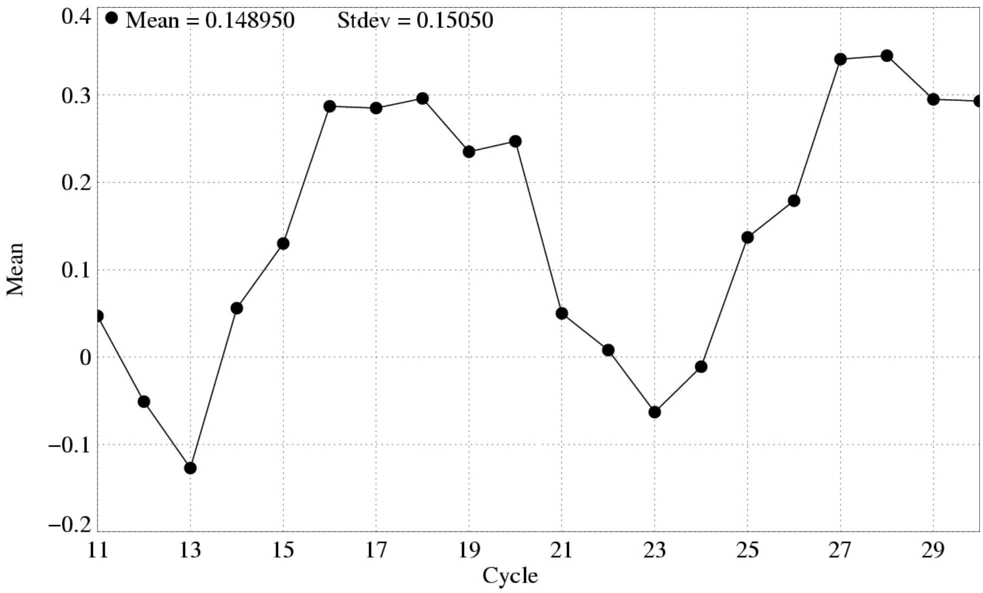

Figure 43 Mean of pseudo time tag bias (ms)

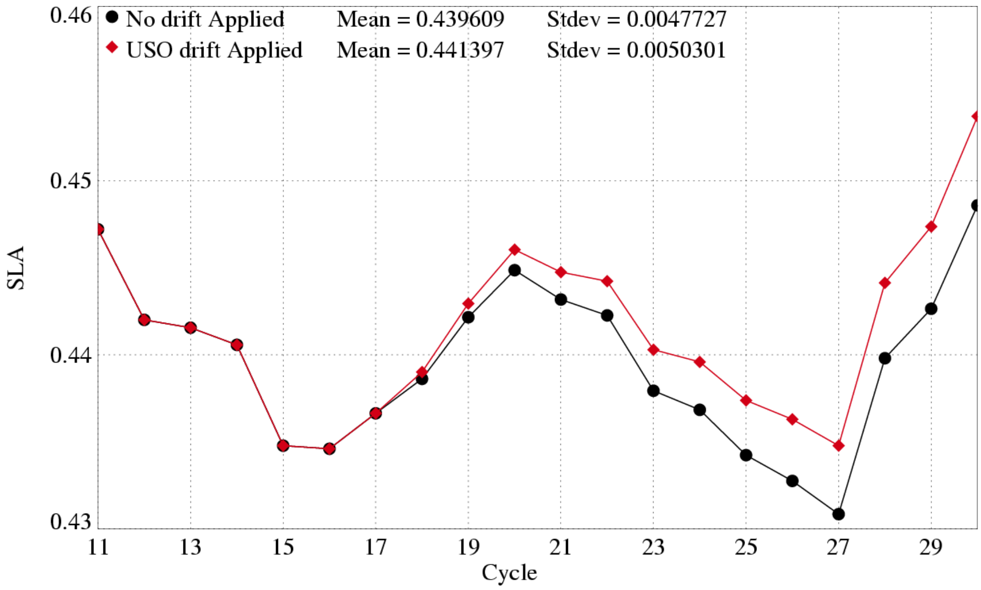

Figure 44 : Cycle by cycle mean of SSH-MSS (no selection)

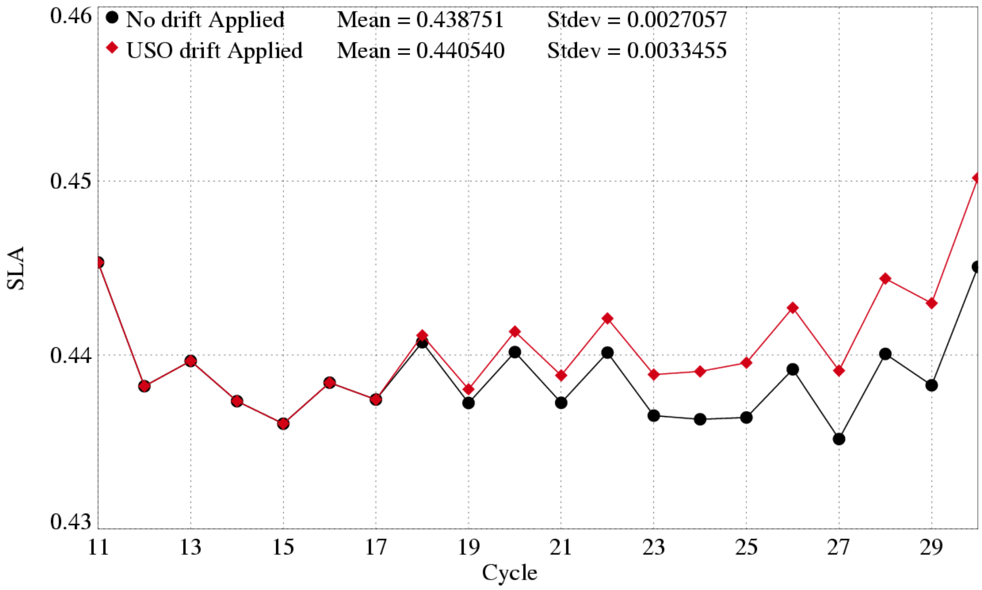

Figure 45 Cycle by cycle mean of SSH-MSS (lat/bathy/var)

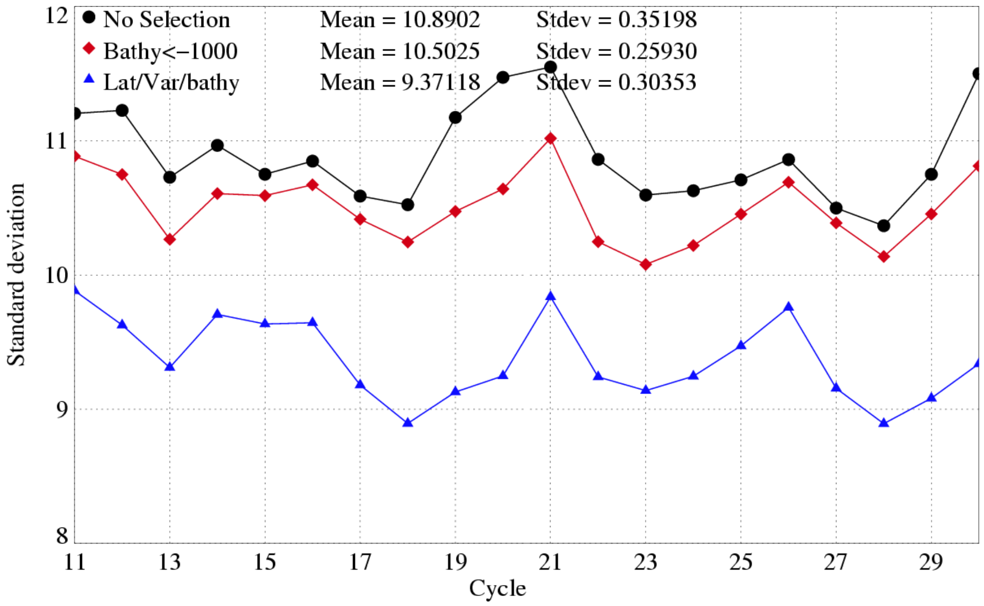

Figure 46 Cycle by cycle standard deviation of SSH-MSS

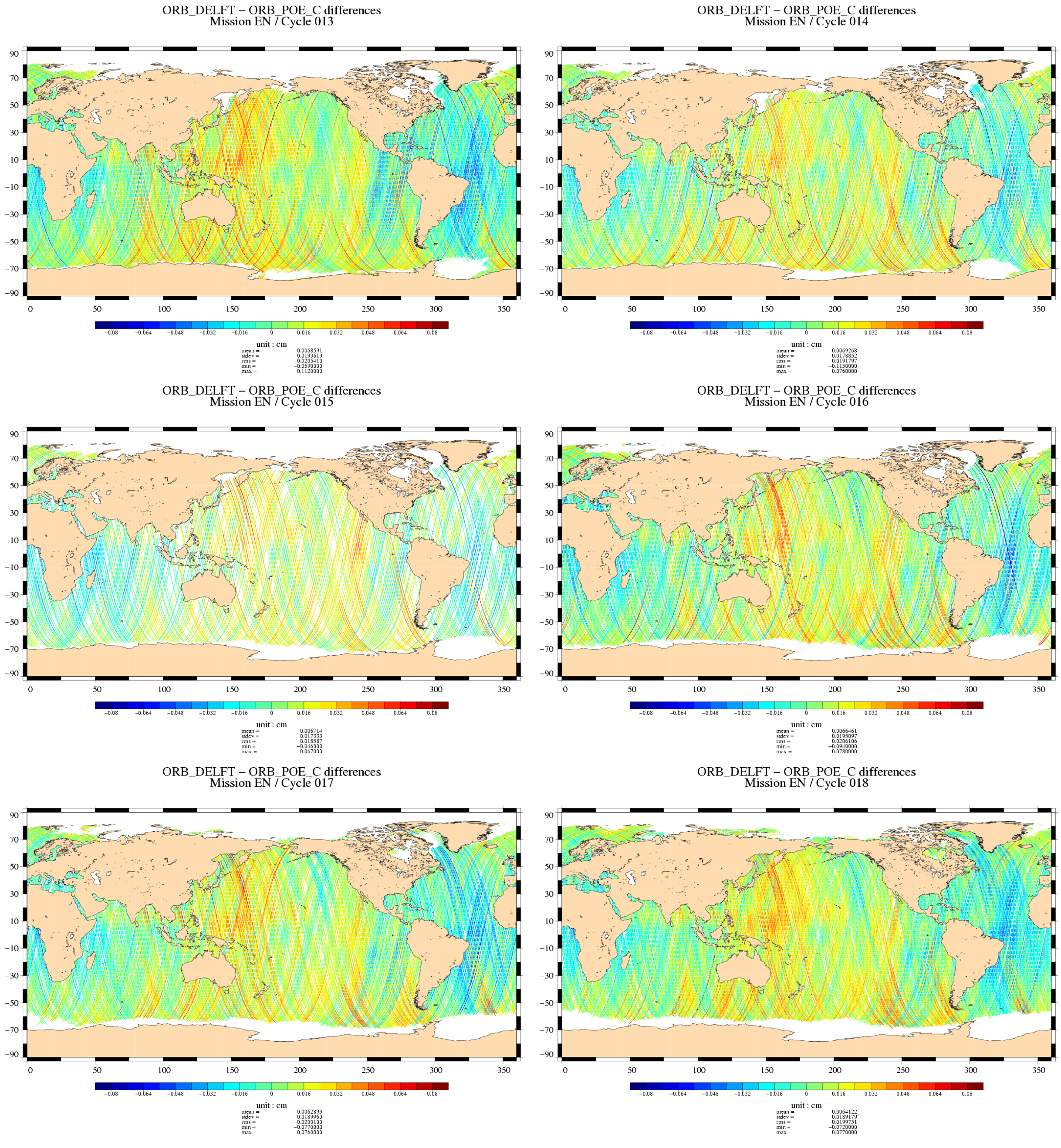

Figure 47 : Delft-GDR orbit, cycle 13, 14, 15, 16, 17, 18 scale [-8cm;8 cm]

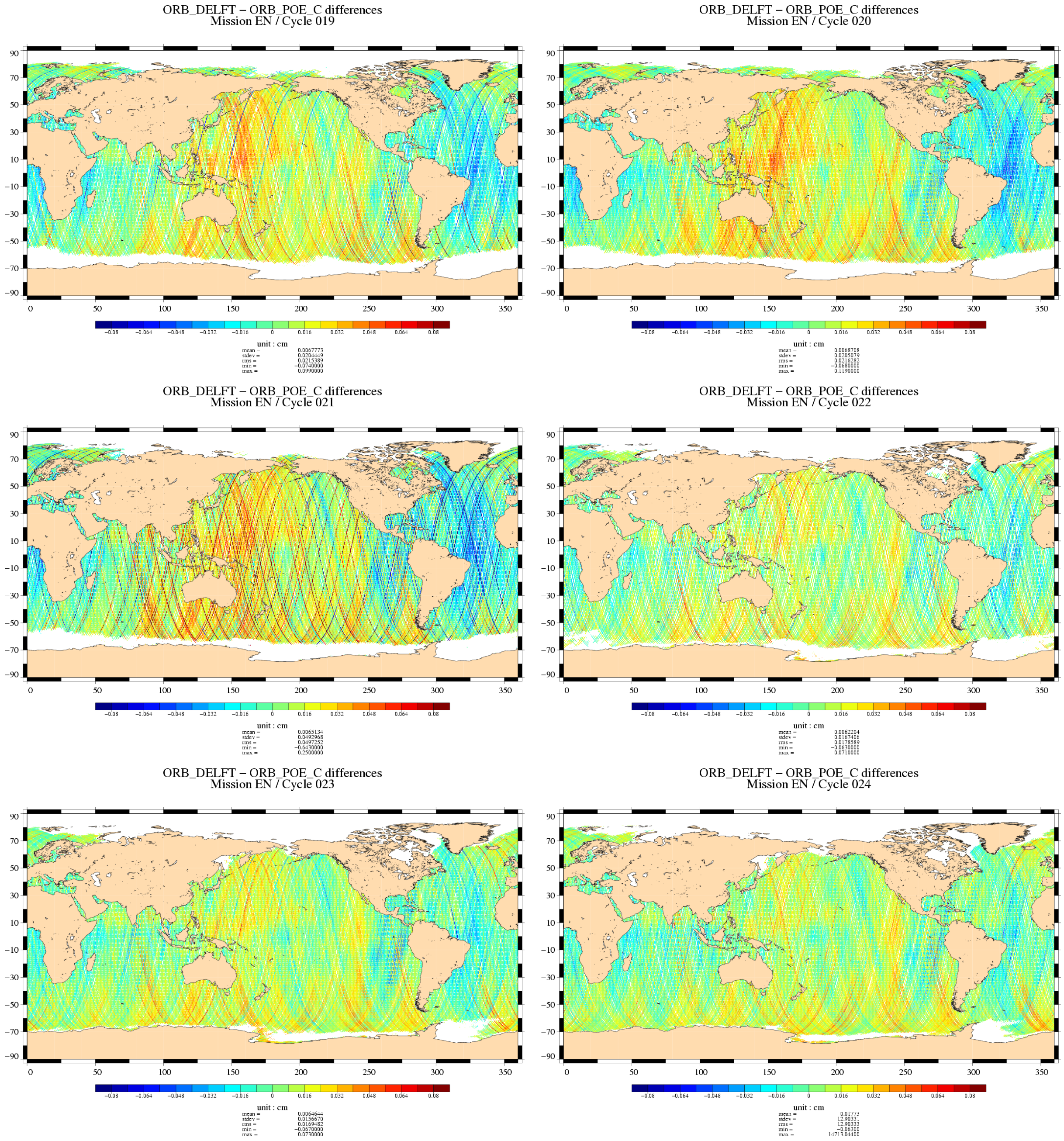

Figure 48 Delft-GDR orbit, cycle 19, 20, 21, 22, 23, 24 scale [-8 cm;8 cm]

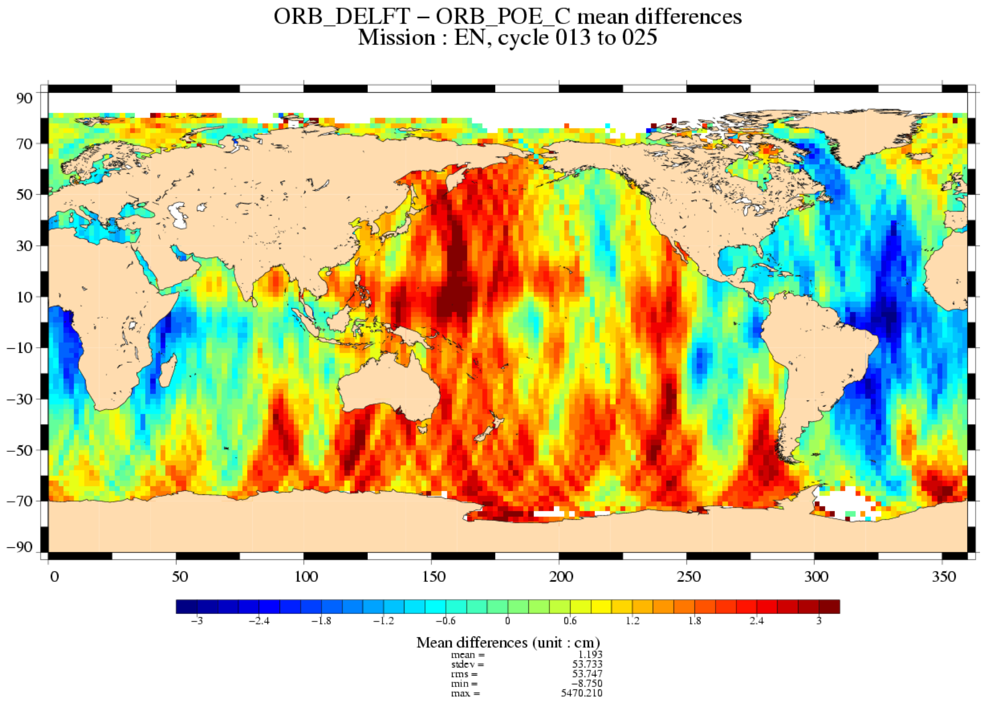

Figure 49 Delft-GDR orbit, mean over cycle 13-25

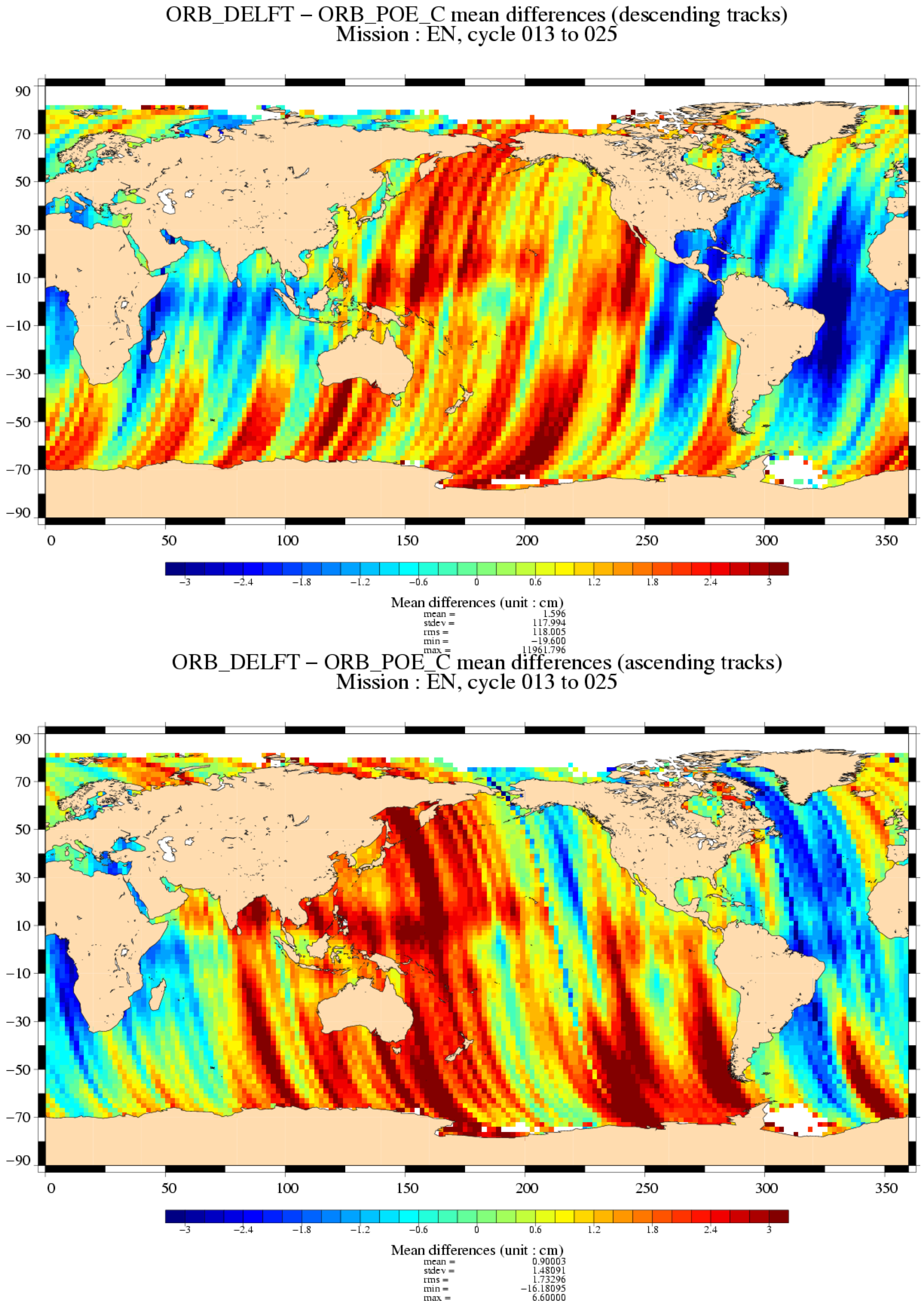

Figure 50 Delft-GDR orbit, mean over cycle 13-25, descending and ascending passes

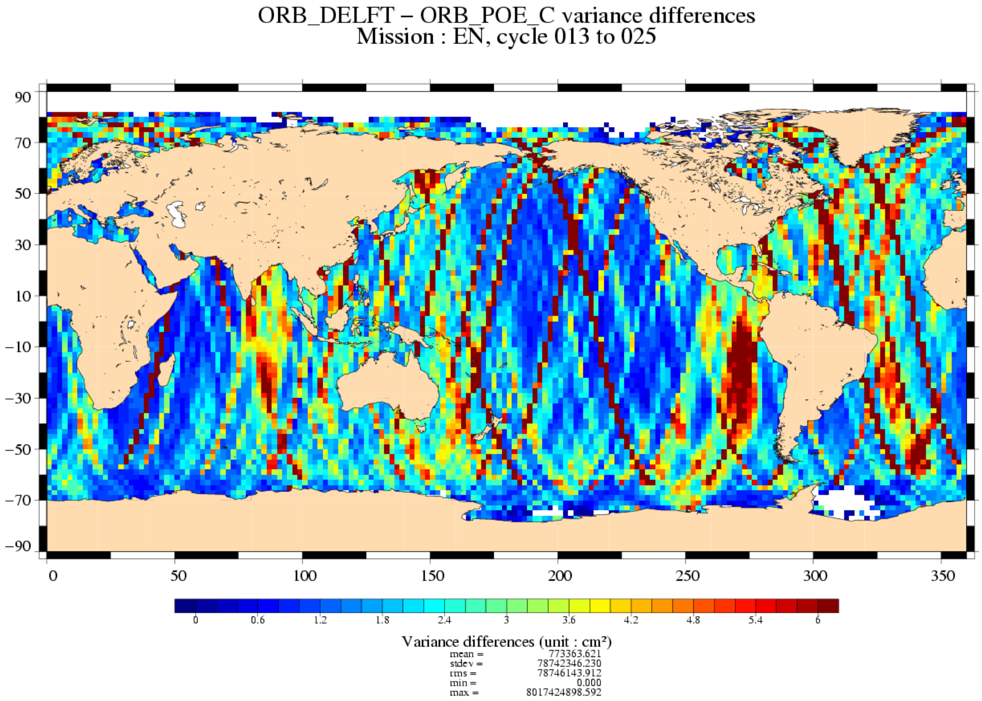

Figure 51 Delft-GDR orbit, standard deviation over cycle 13-25

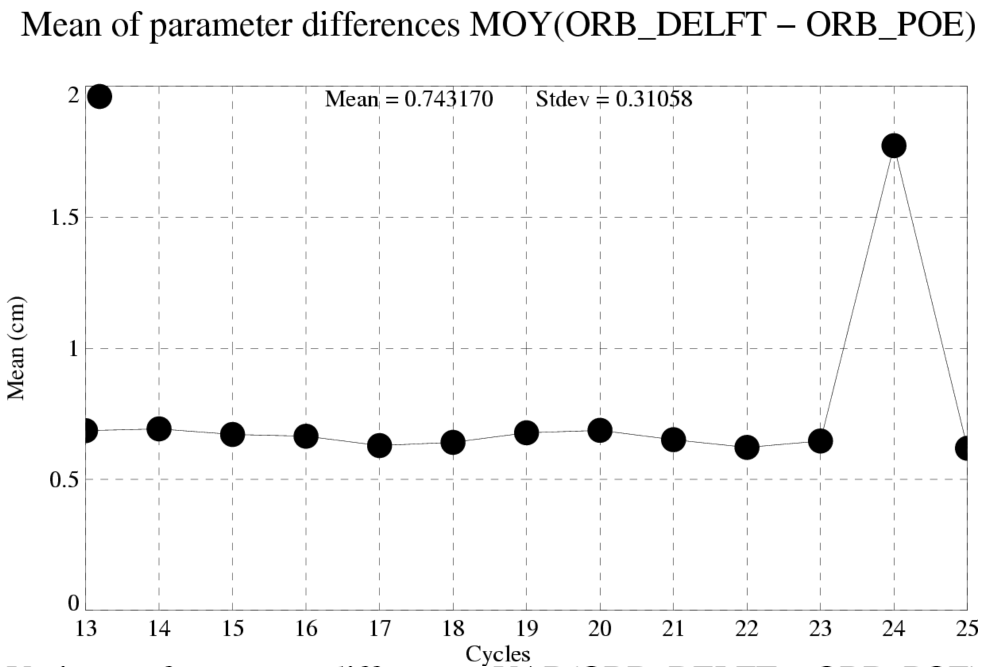

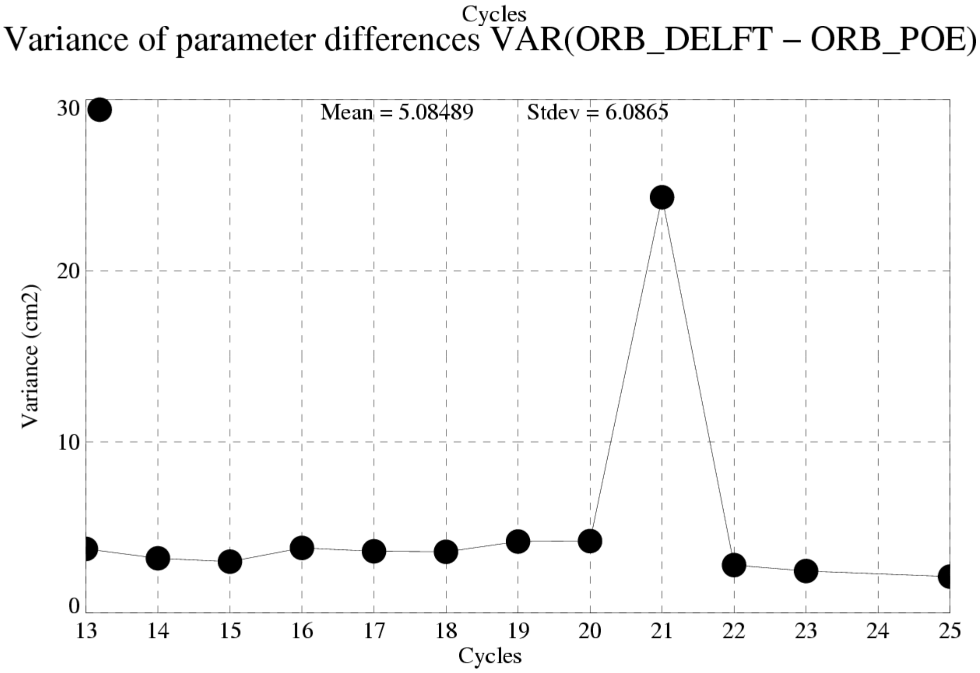

Figure 52 Delft-GDR orbit, cycle by cycle mean and variance

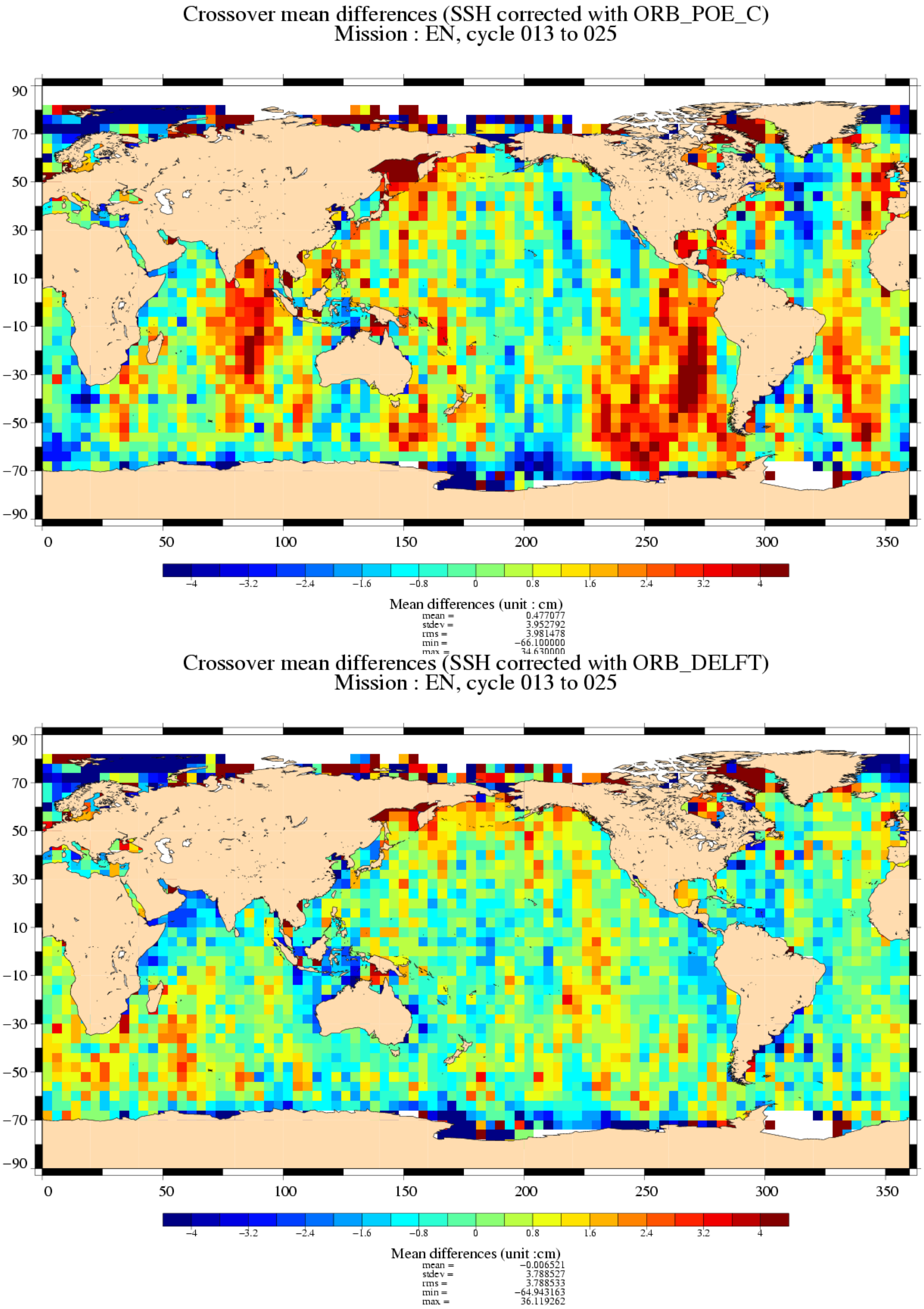

Figure 53 Mean SSH differences at crossovers with GDR and Delft orbit

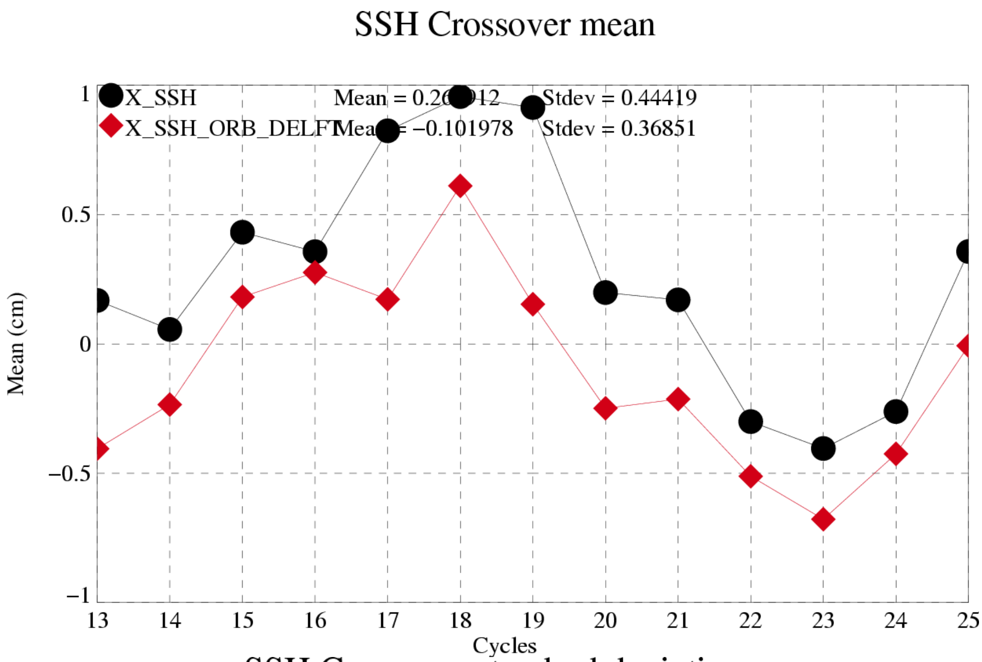

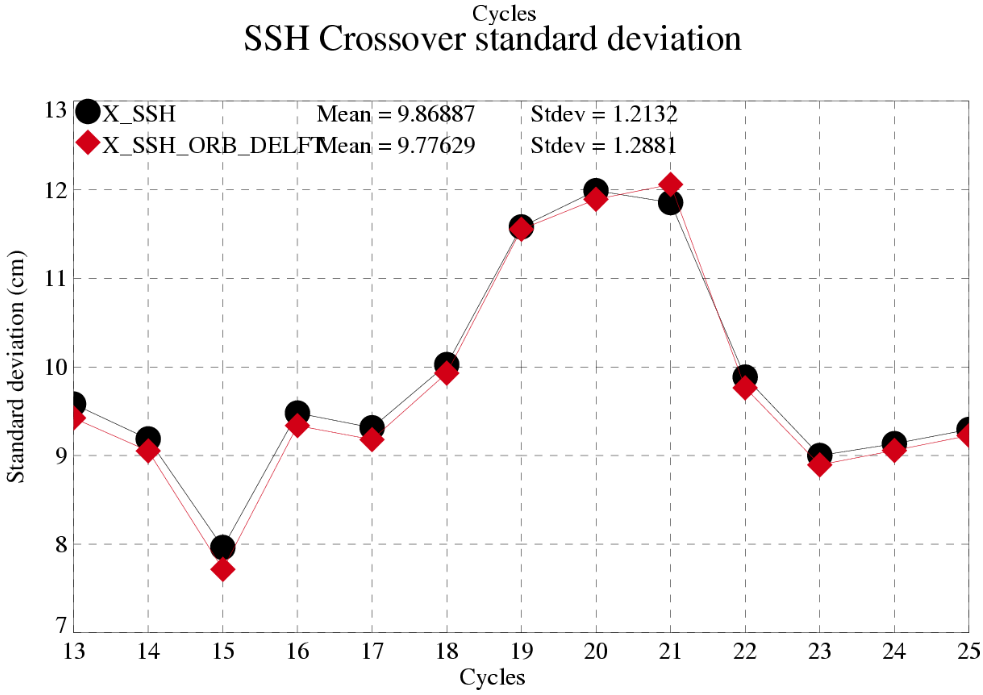

Figure 54 Cycle by cycle mean and standard deviation SSH differences at crossovers with GDR and Delft orbit

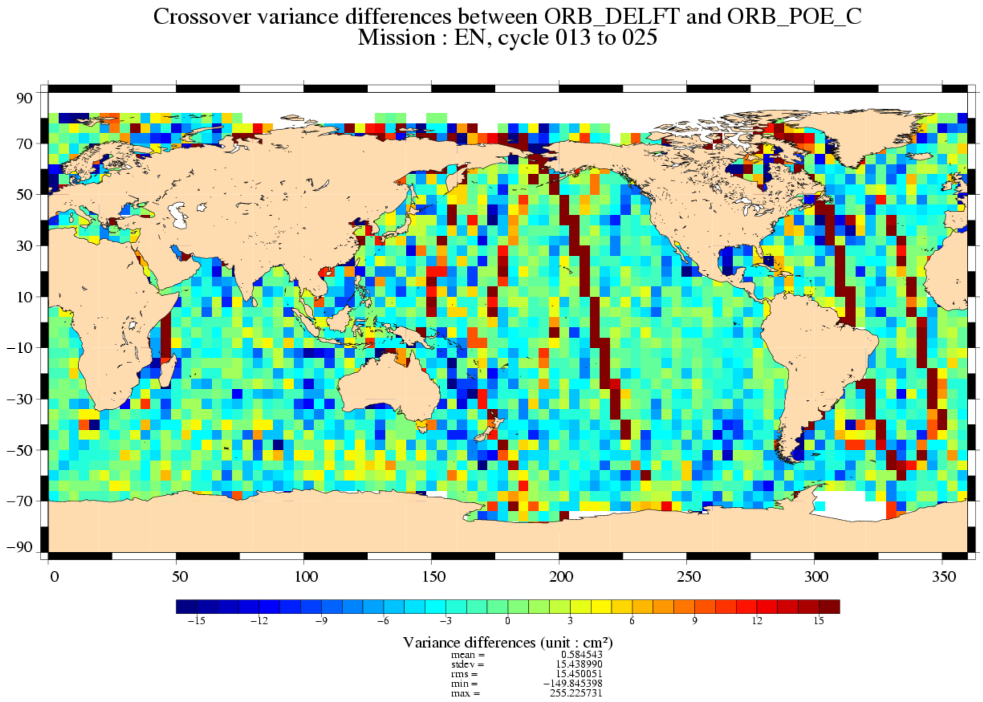

Figure 55 Variance[SSH_{Delft} differences at crossovers] - Variance[SSH_{GDR} differences at crossovers]

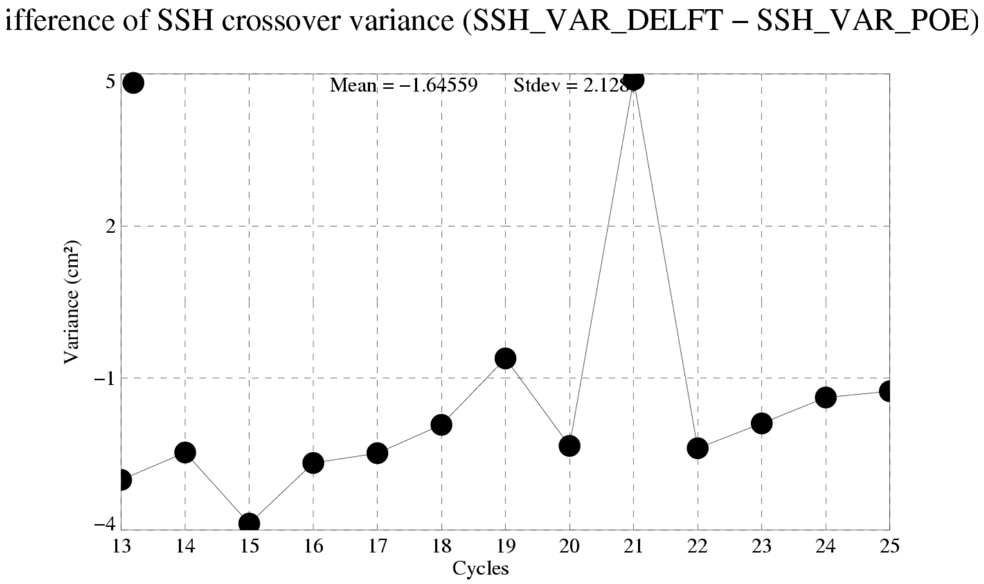

Figure 56 Cycle by cycle Variance[SSH_{Delft} differences at crossovers] - Variance[SSH_{GDR} differences at crossovers]

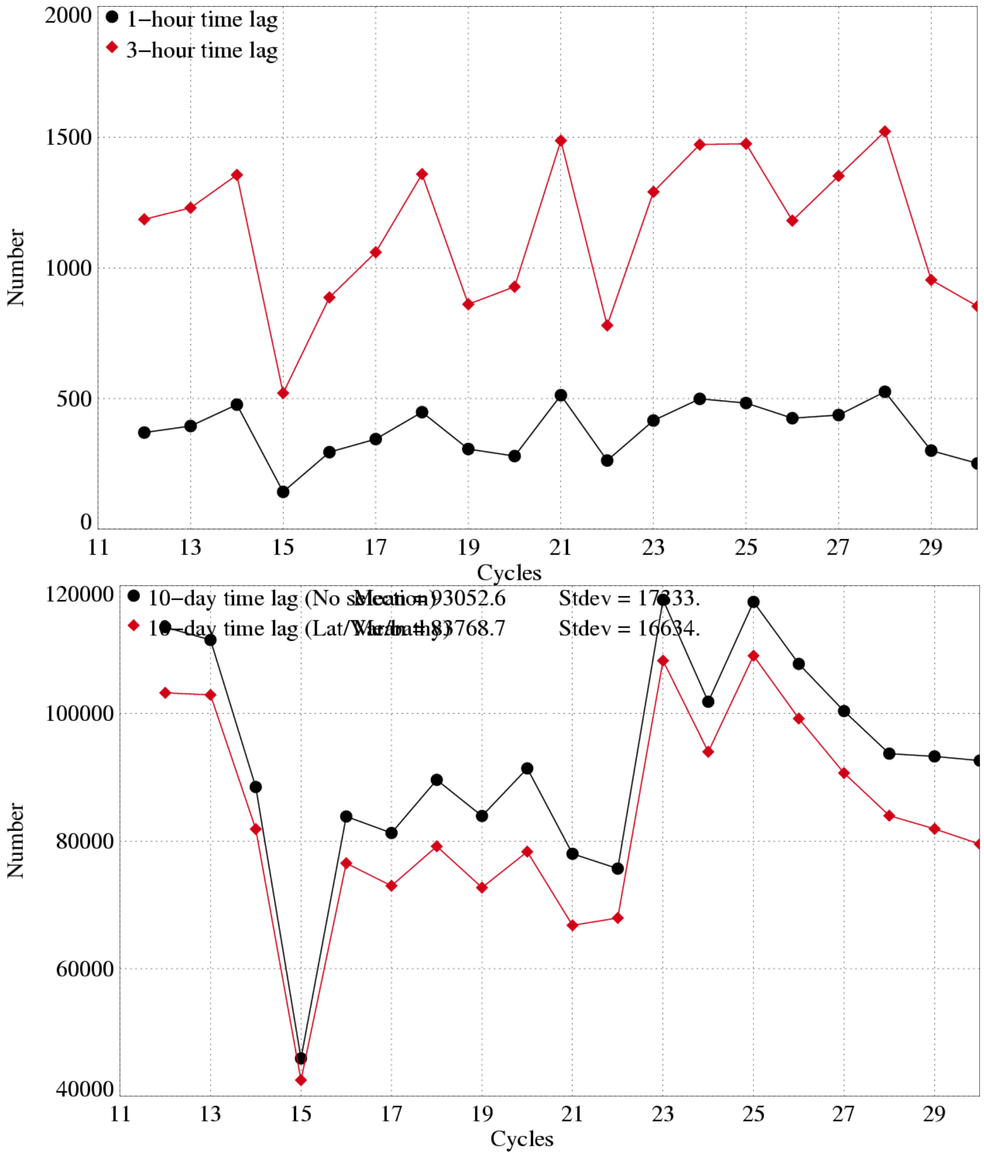

Figure 57 : Number of Jason-1/Envisat 1 hour, 3 hour and 10 days time lag dual crossover

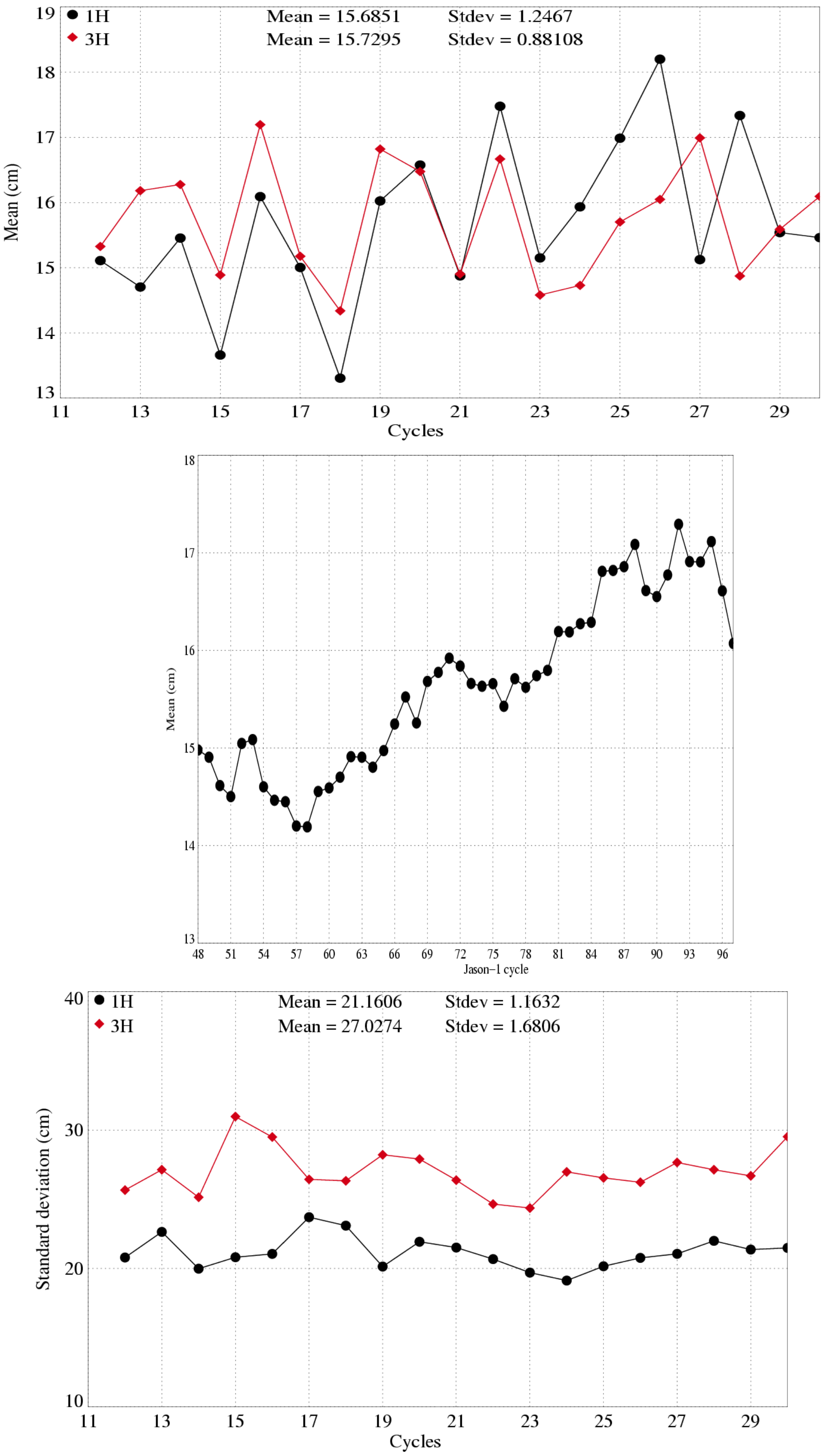

Figure 58 : Mean, running mean and standard deviation of [Envisat – Jason-1] Ku SWH differences at crossover (cm)

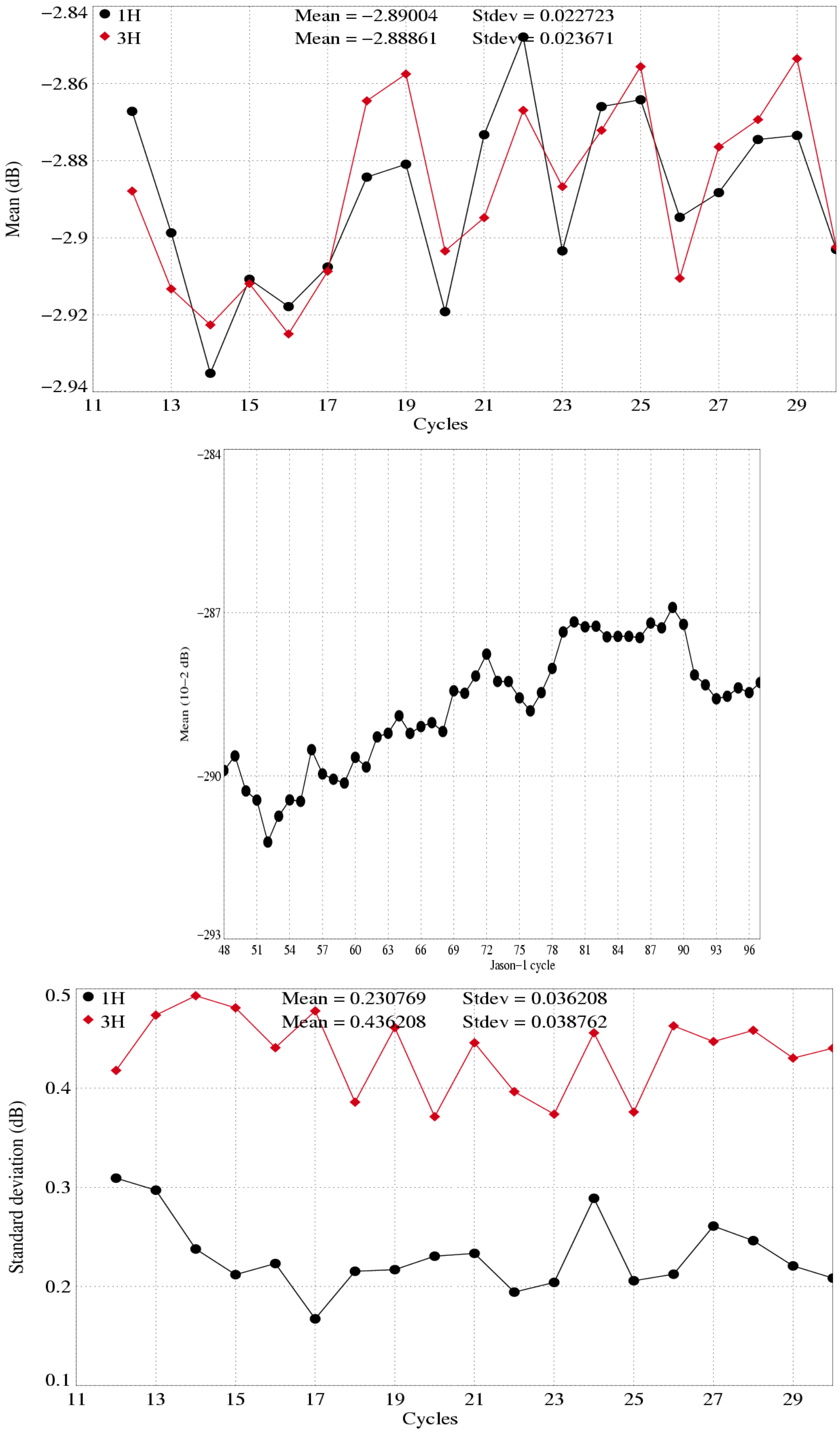

Figure 59 : Mean and standard deviation of [Envisat – Jason-1] Ku Sigma0 differences at crossover (dB)

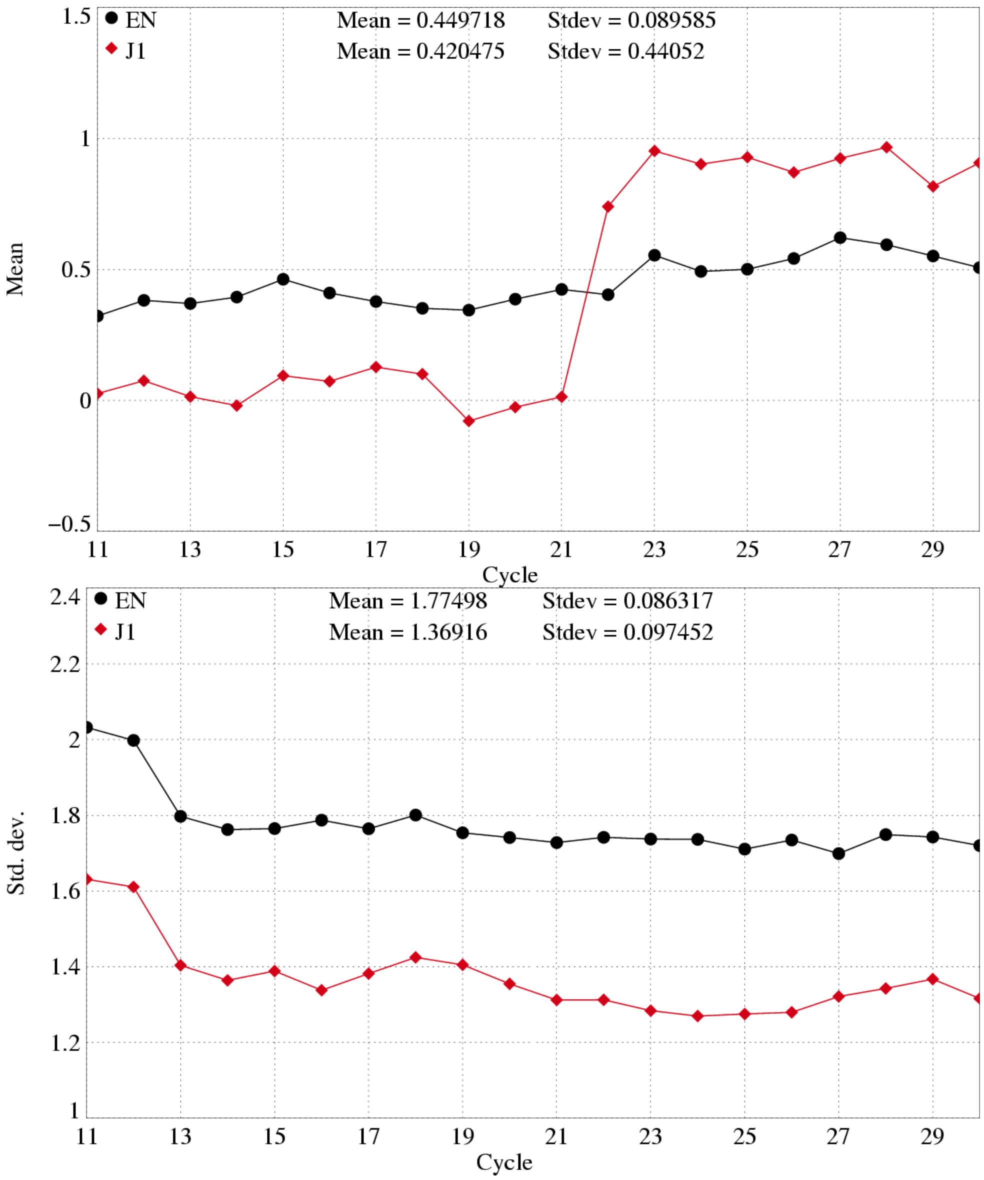

Figure 60 : Mean and standard deviation of [Envisat radiometer – ECMWF model] and [Jason radiometer – ECMWF model] differences at latitude<66 (cm)

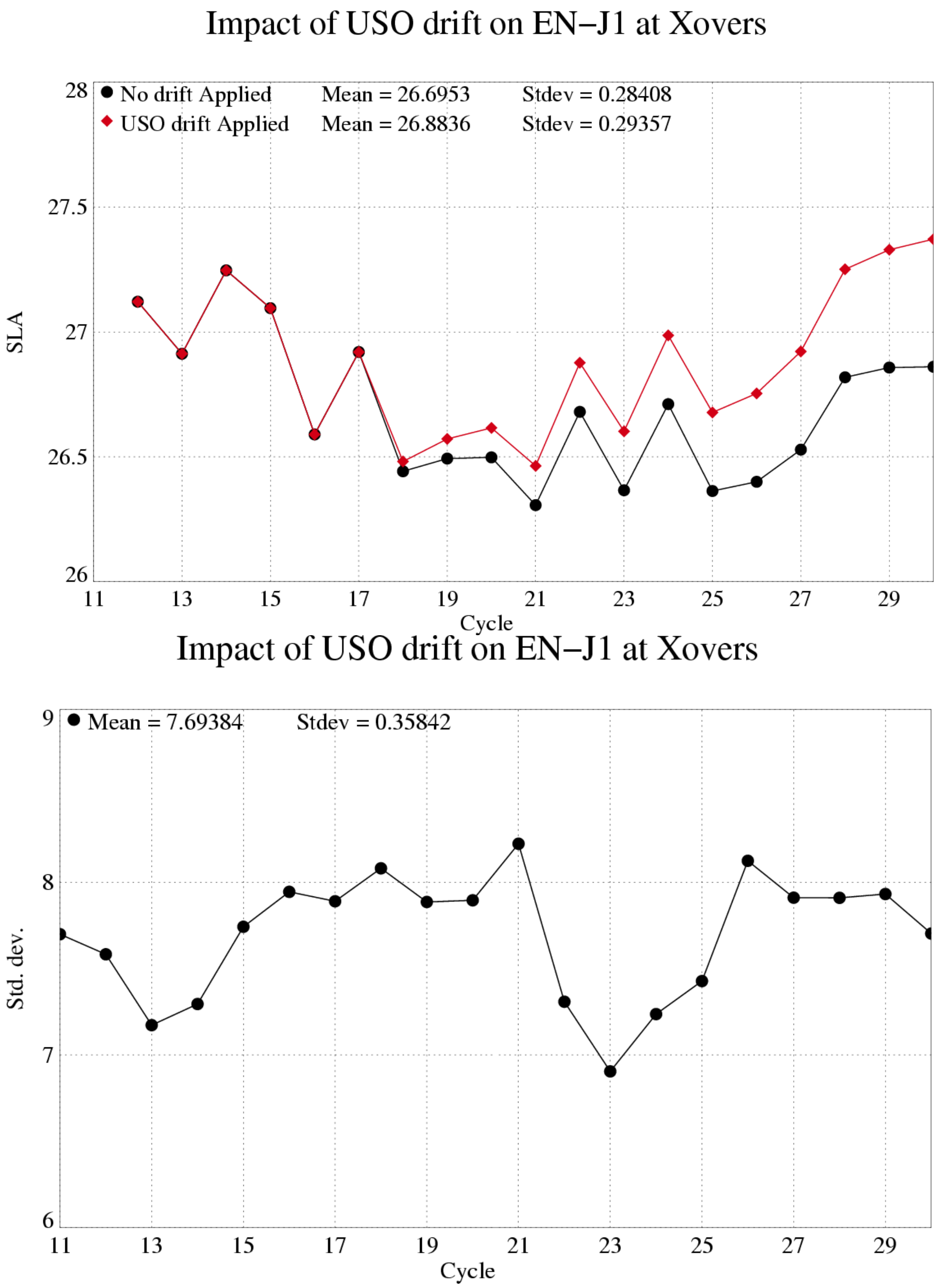

Figure 61 : Mean and standard deviation of [Envisat – Jason-1] SSH differences at crossover (cm), Bathy<-1000m

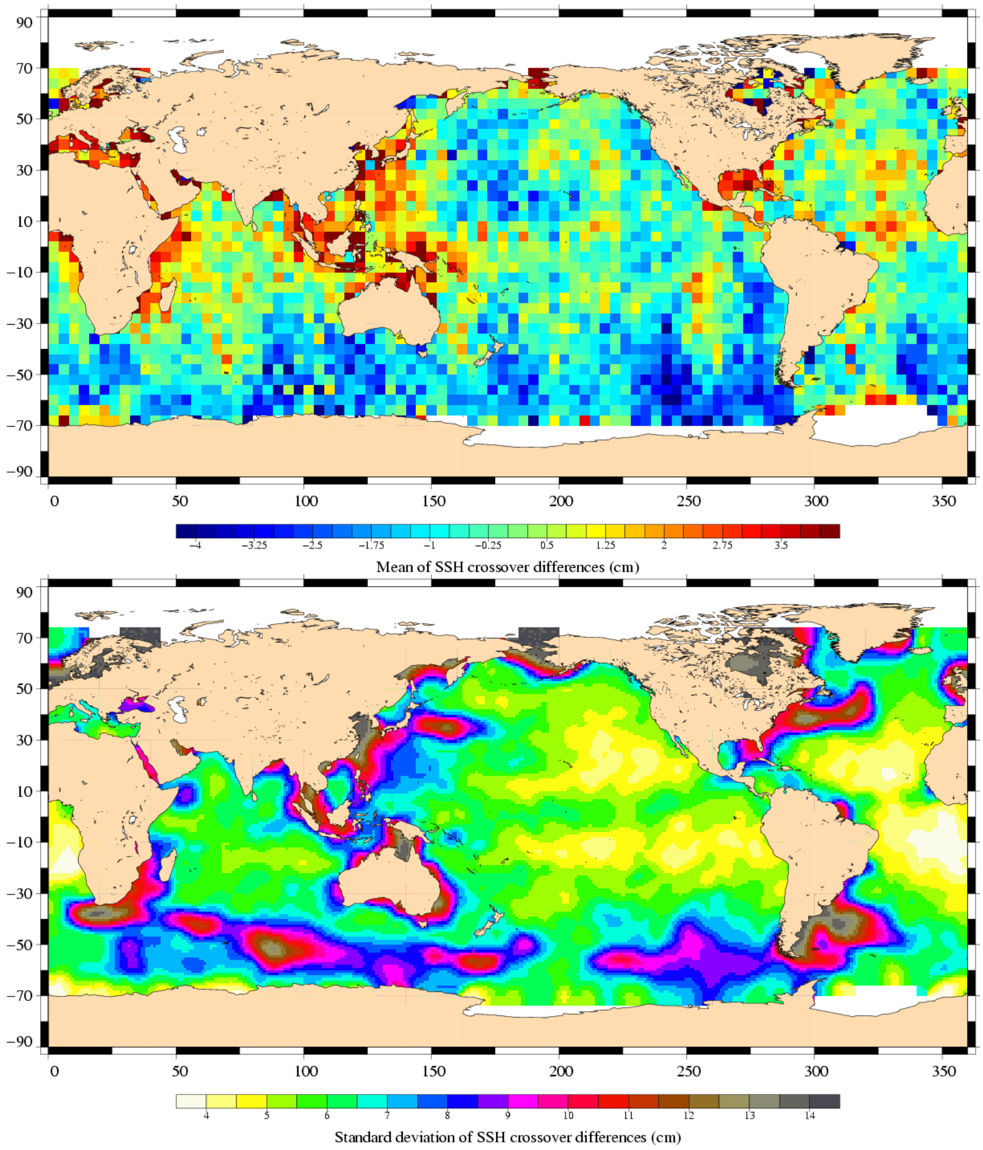

Figure 62 : Geographical pattern (4x4 degree bins) of crossover [Envisat – Jason-1] mean and standard deviation SSH differences (cm), from cycle 12 to cycle 30

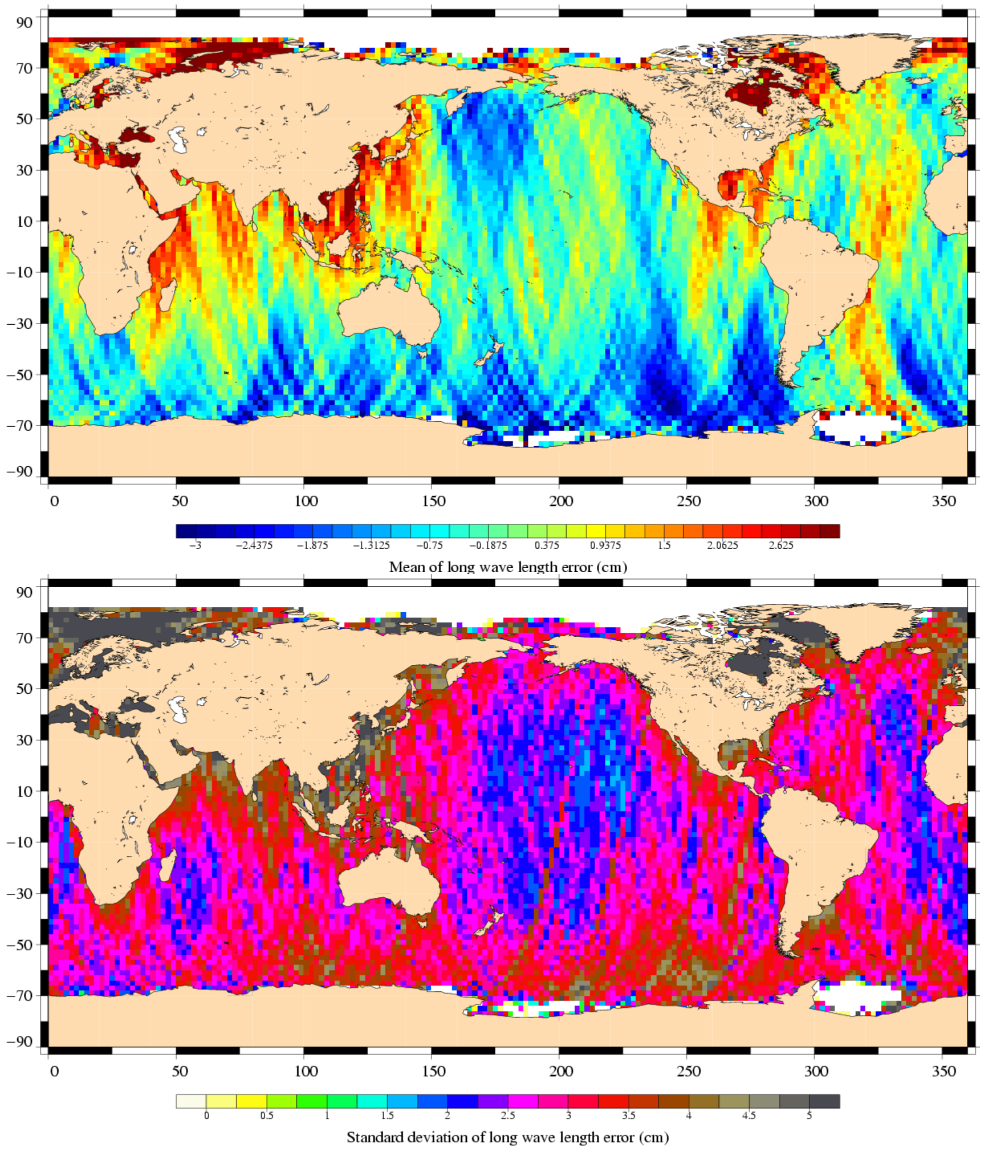

Figure 63 : Geographical pattern (2x2 degree bins) of mean (centred about the Global mean value) and standard deviation of the Envisat adjusted long wave length error (cm), from cycle 12 to cycle 30

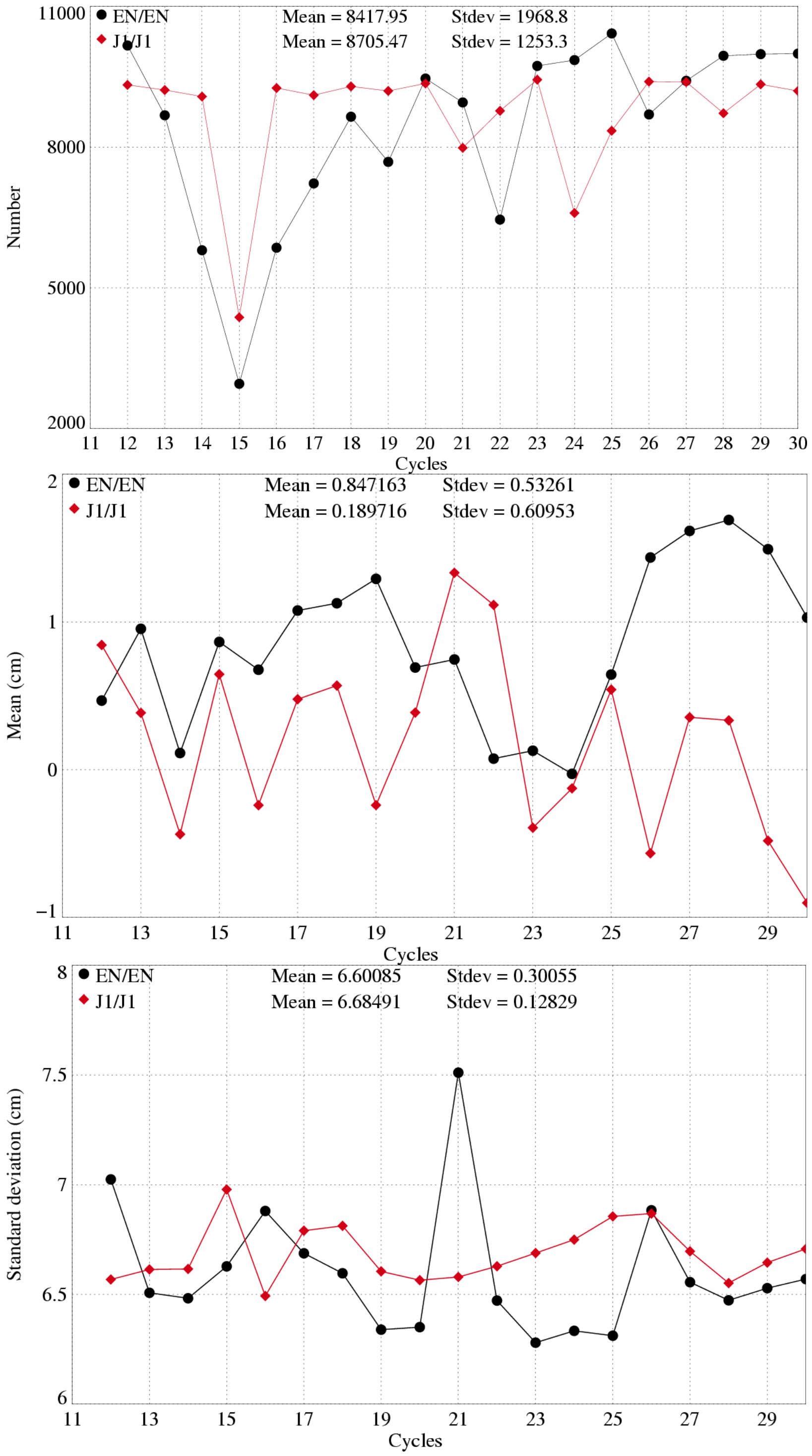

Figure 64 : Number, mean and standard deviation of SSH differences at crossover (cm), |latitude|<50°, Bathy<-1000m, Variability<20cm

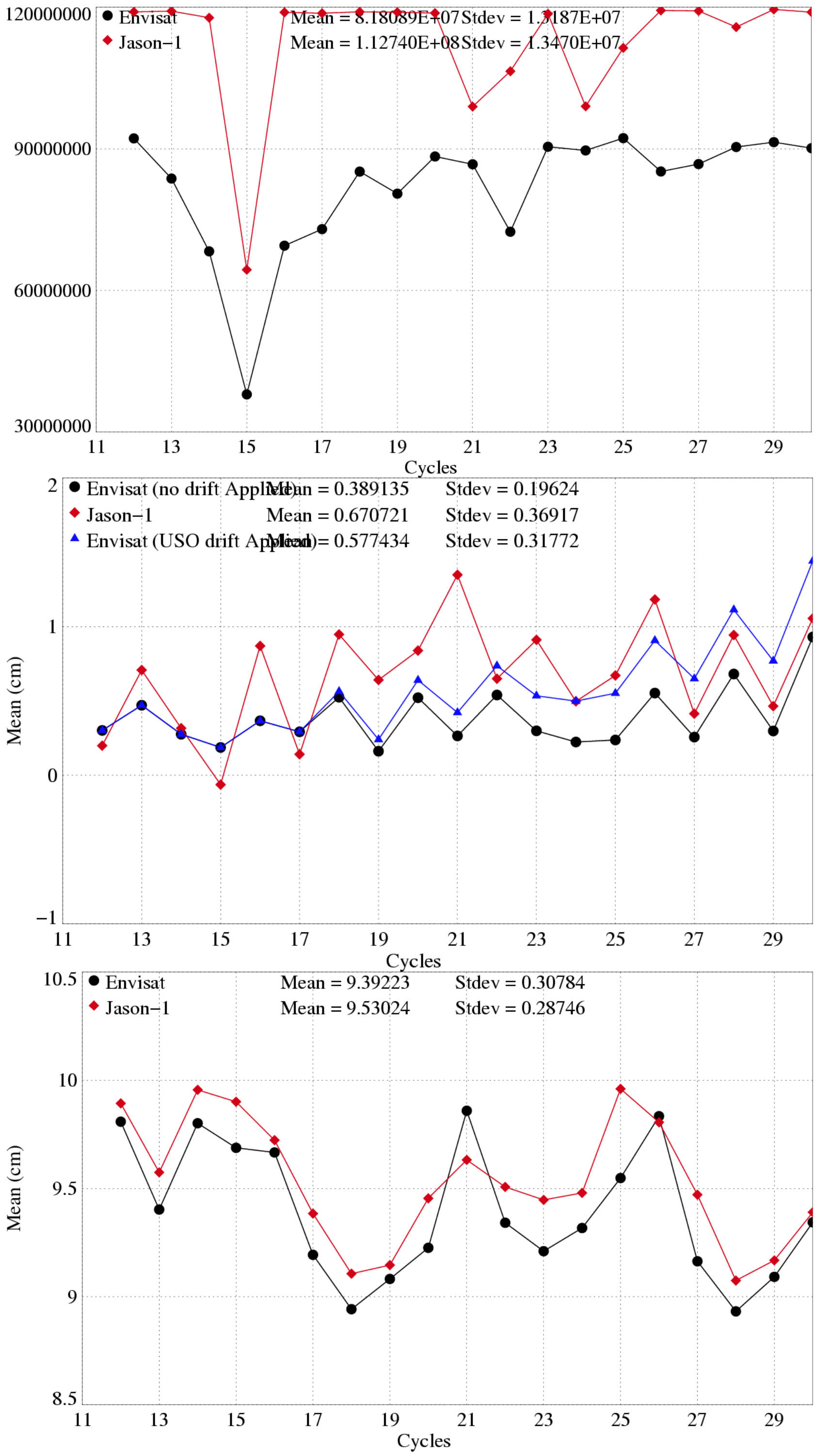

Figure 65 Number, mean and standard deviation of SSH-MSS differences (cm), |latitude|<50°, Bathy<-1000m, Variability<20cm

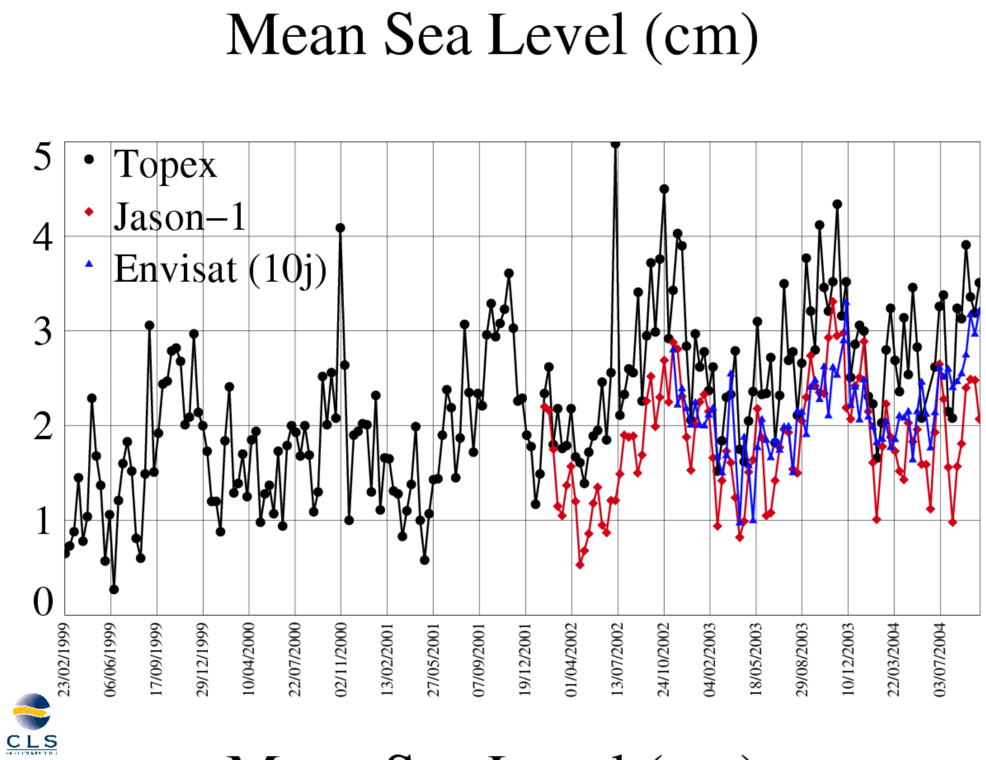

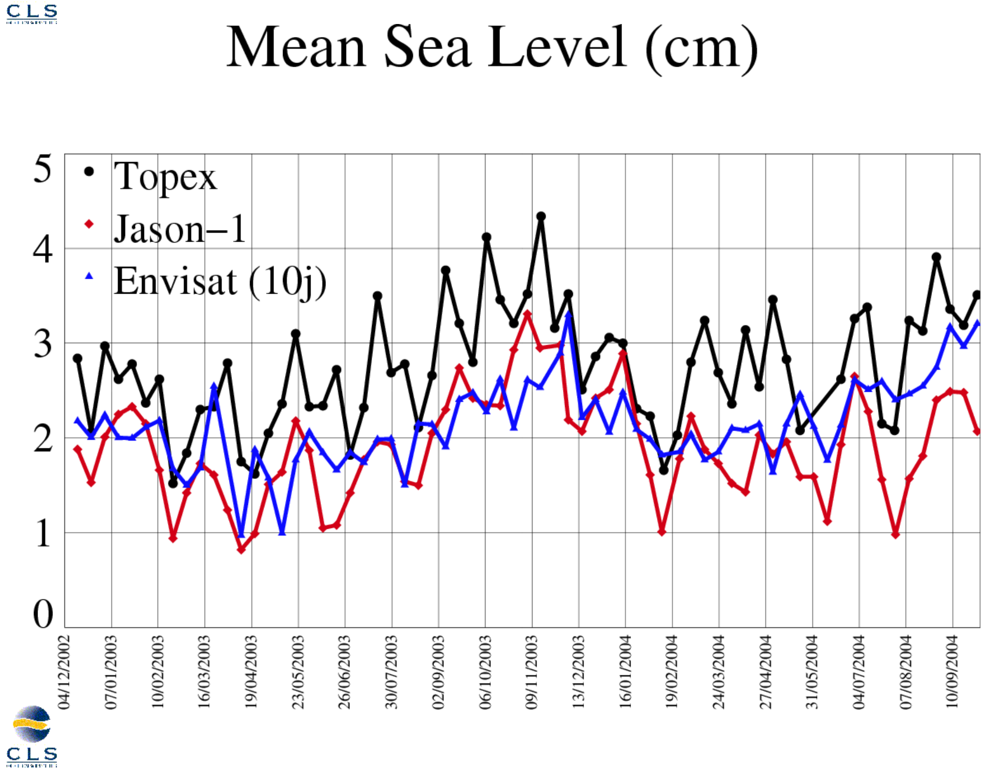

Figure 66 Mean Sea Level estimation of Topex, Jason and Envisat

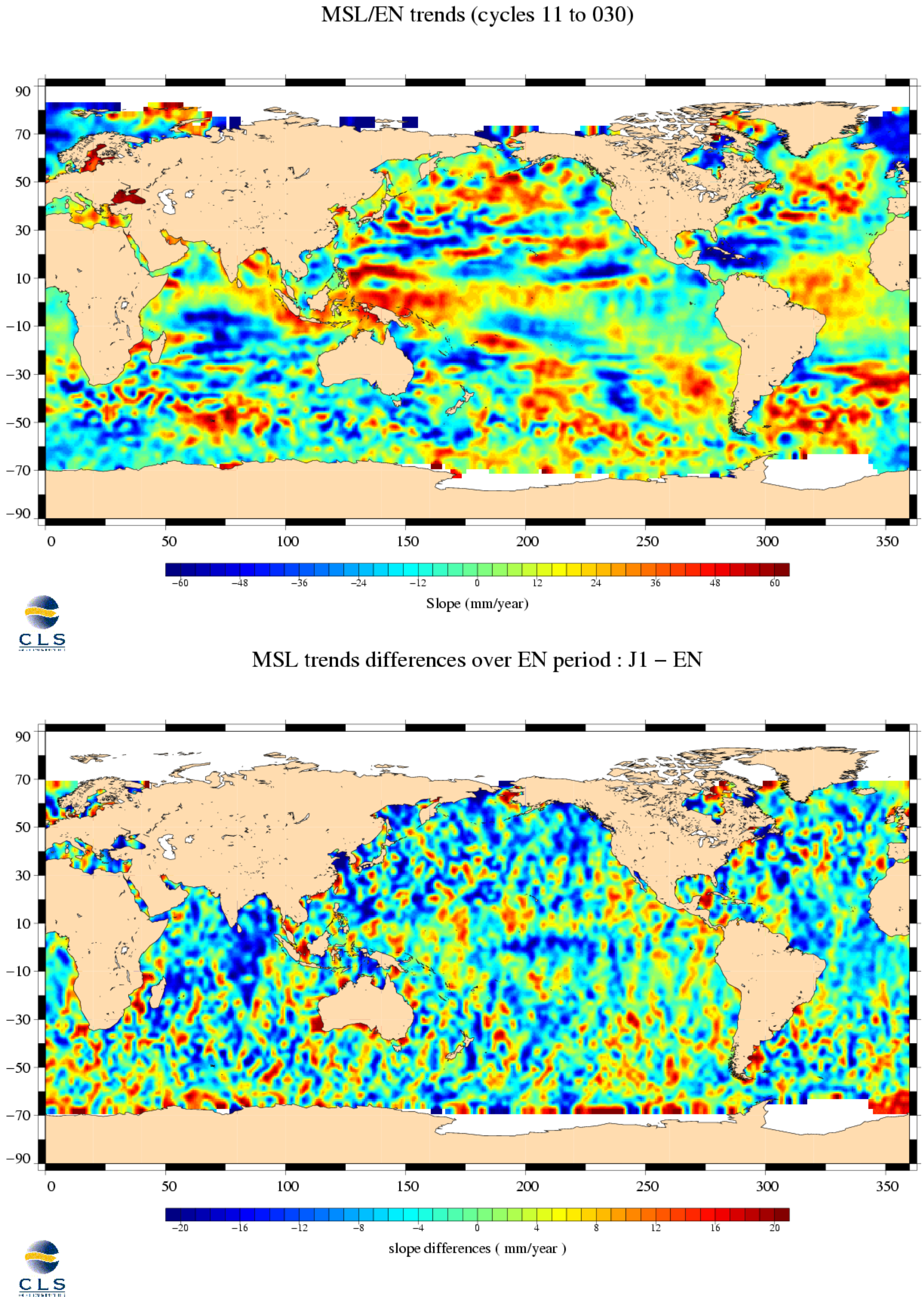

Figure 67 EN MSL trend (above) and [J1-EN] MSL trend (below)

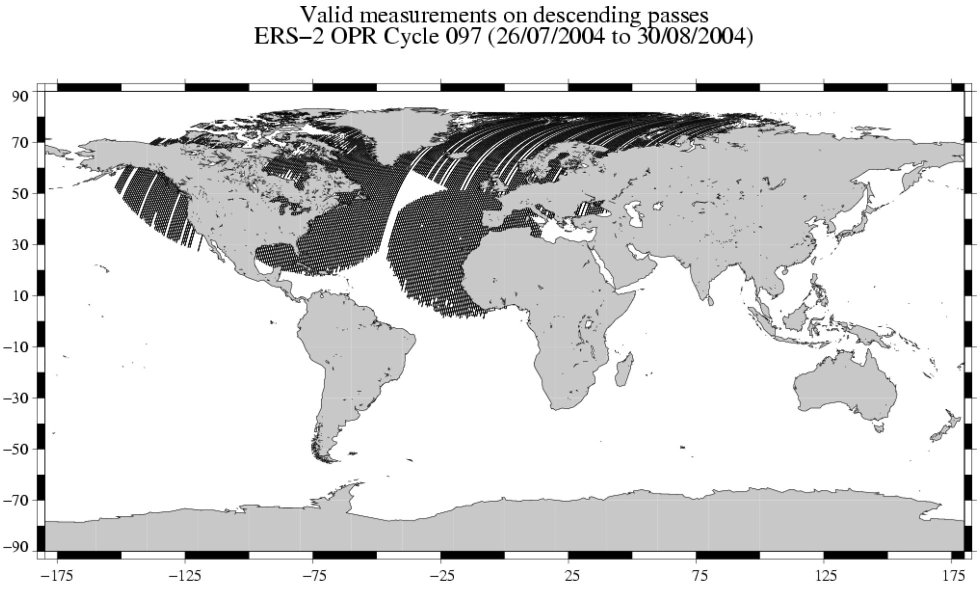

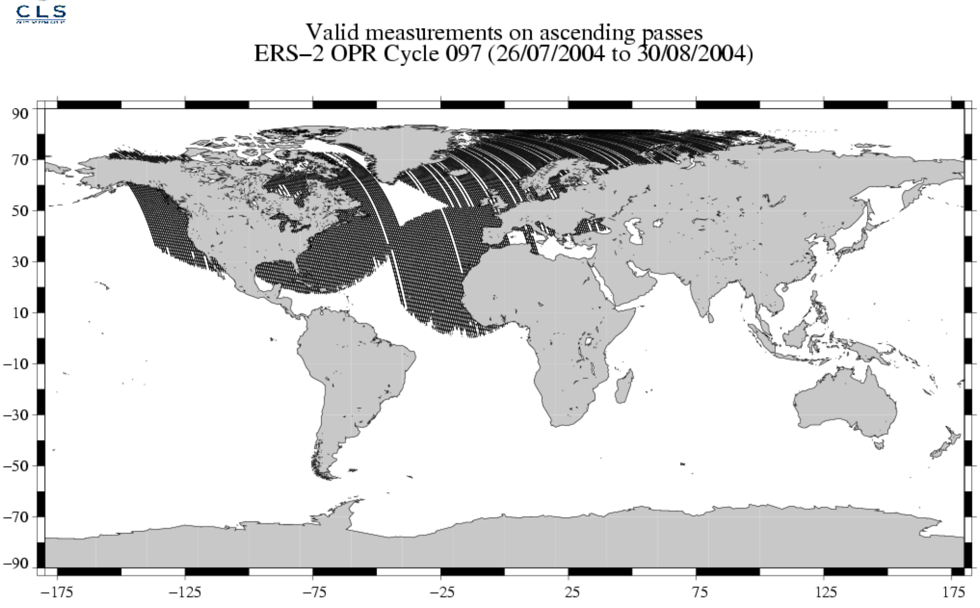

Figure 68 : Map of valid measurements of ERS-2 on cycle 97.

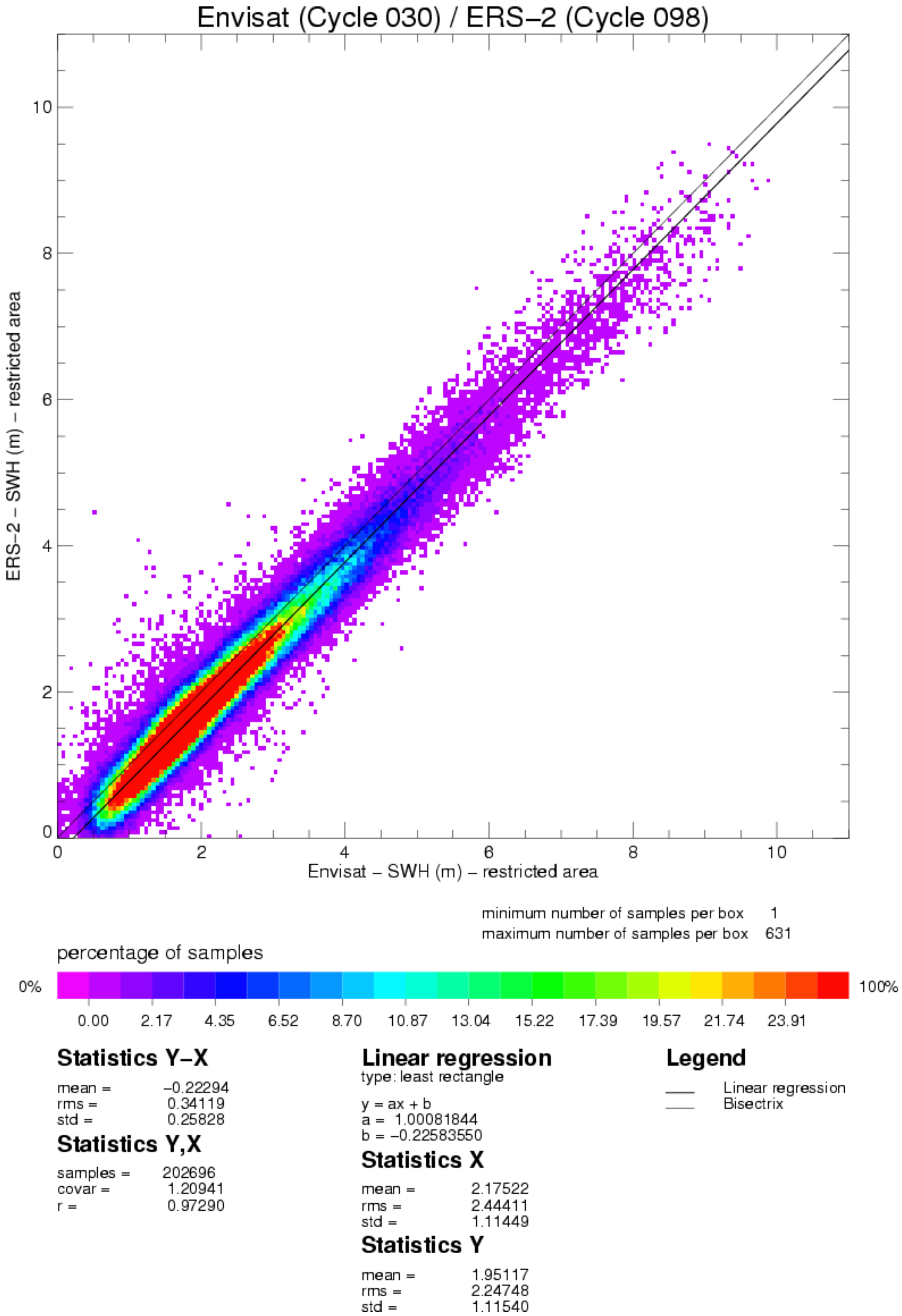

Figure 69 : Scatter plot of ERS-2 SWH versus ENVISAT SWH in meters.

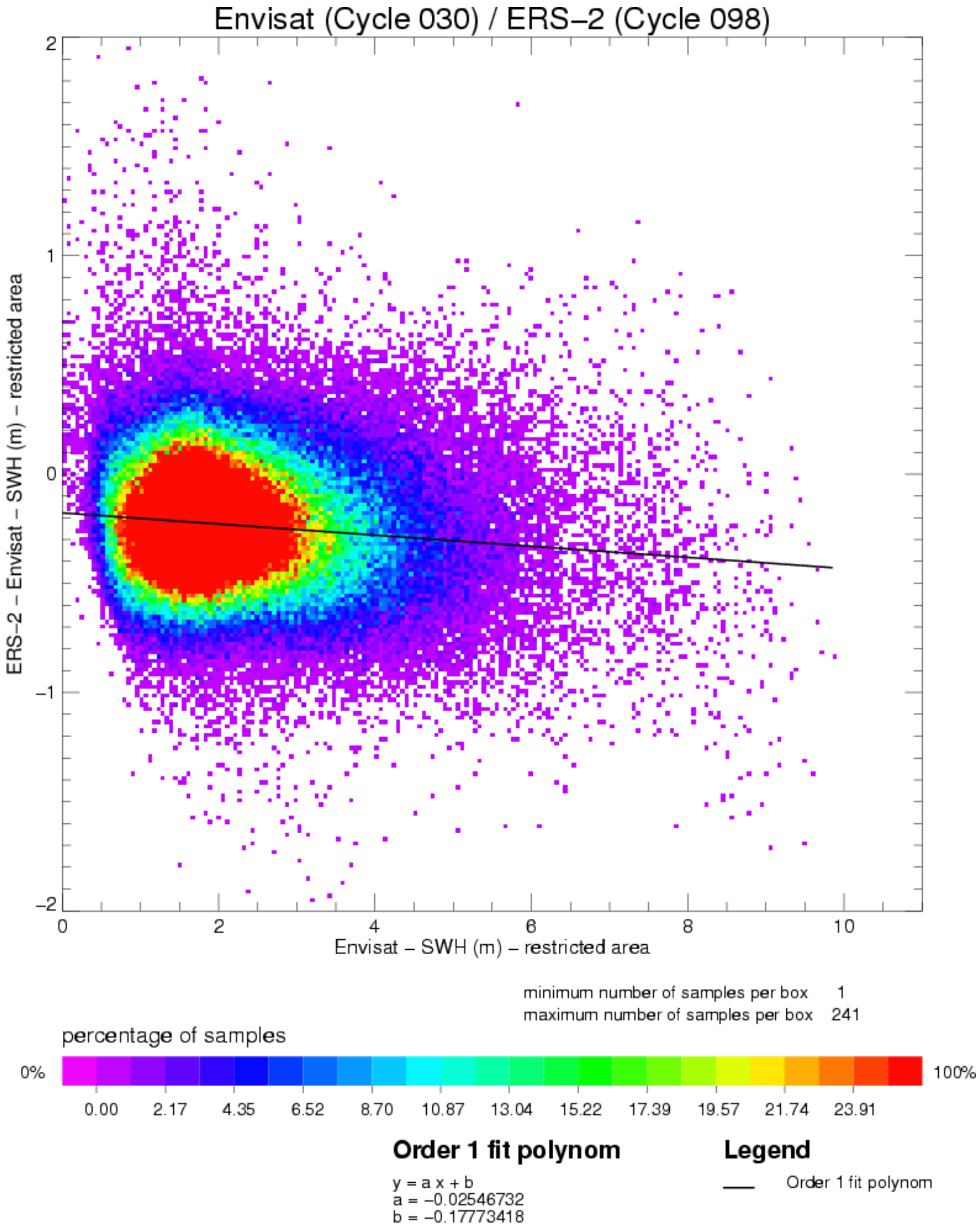

Figure 70 : Scatter plot of (ERS-2-ENVISAT) SWH differences (m) versus ENVISAT SWH.

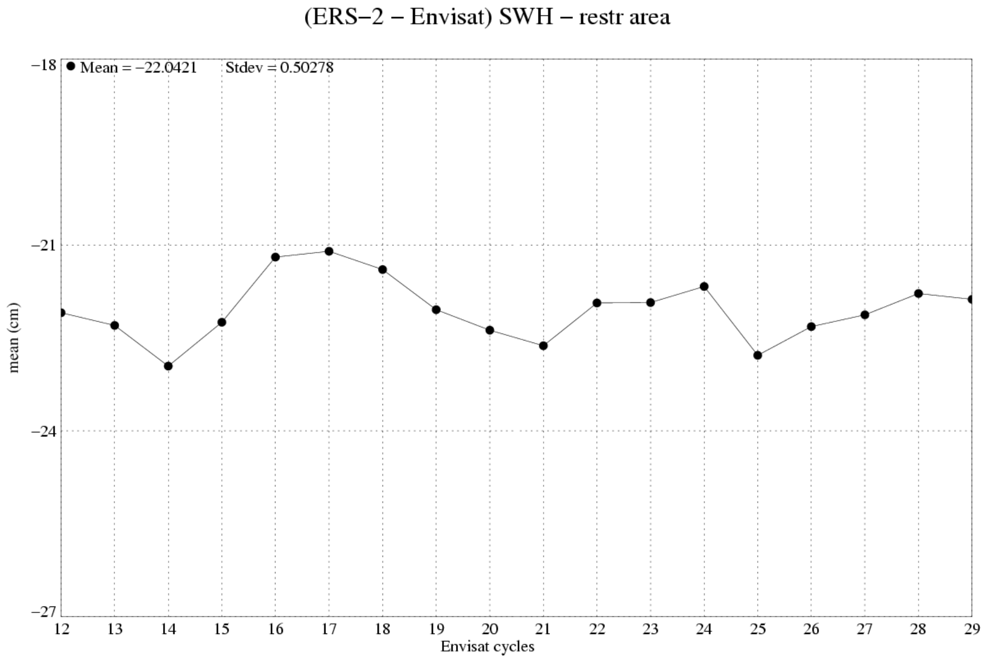

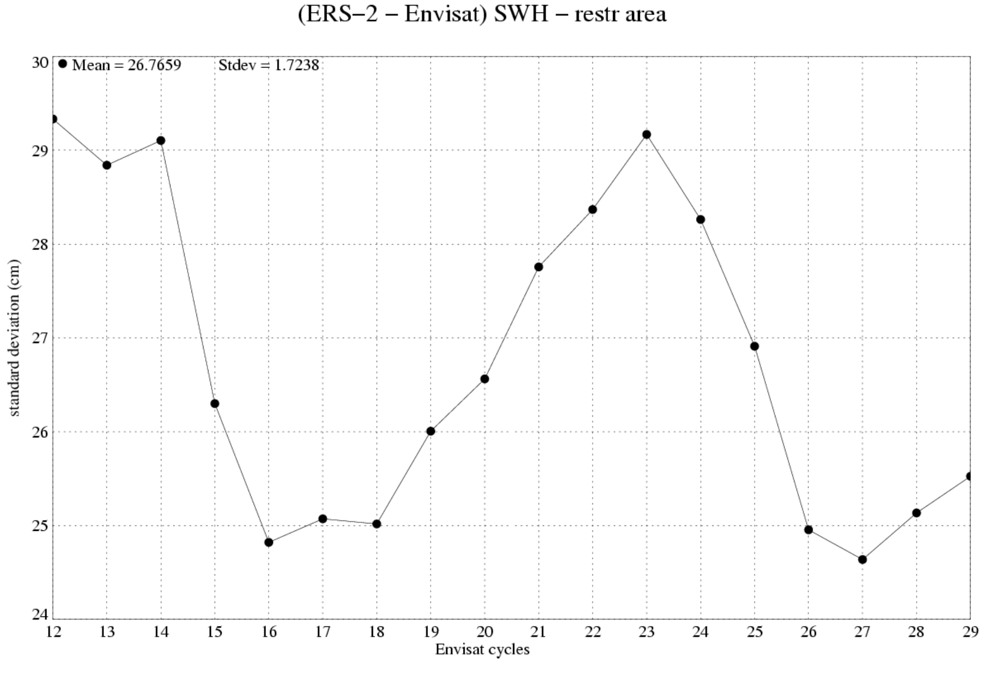

Figure 71 : Mean and standard deviation of (ERS-2 – Envisat) SWH along track residuals for each cycle over the restricted area.

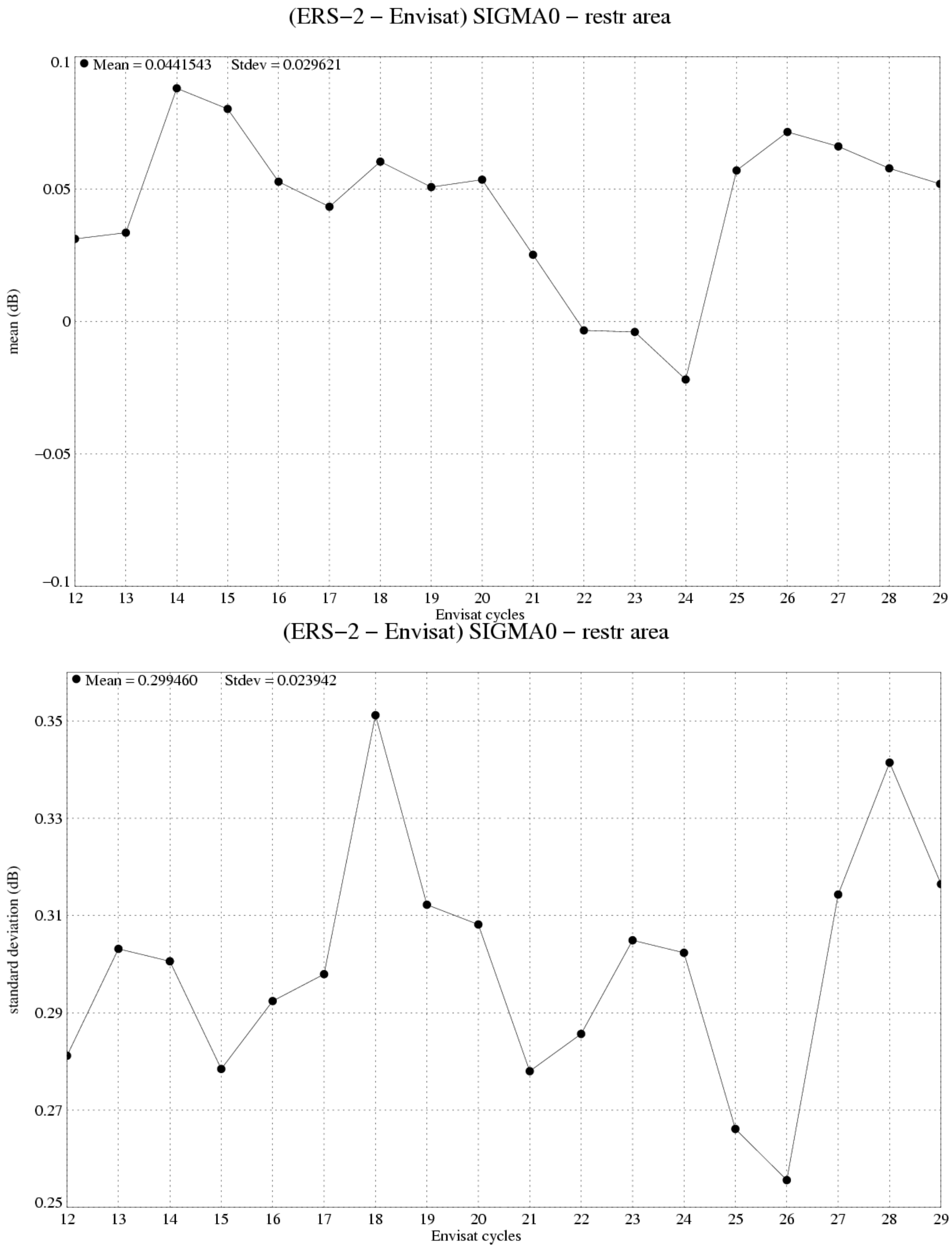

Figure 72 : Mean and standard deviation of (ERS-2 – Envisat) SIGMA-0 along track residuals for each cycle over the restricted area.

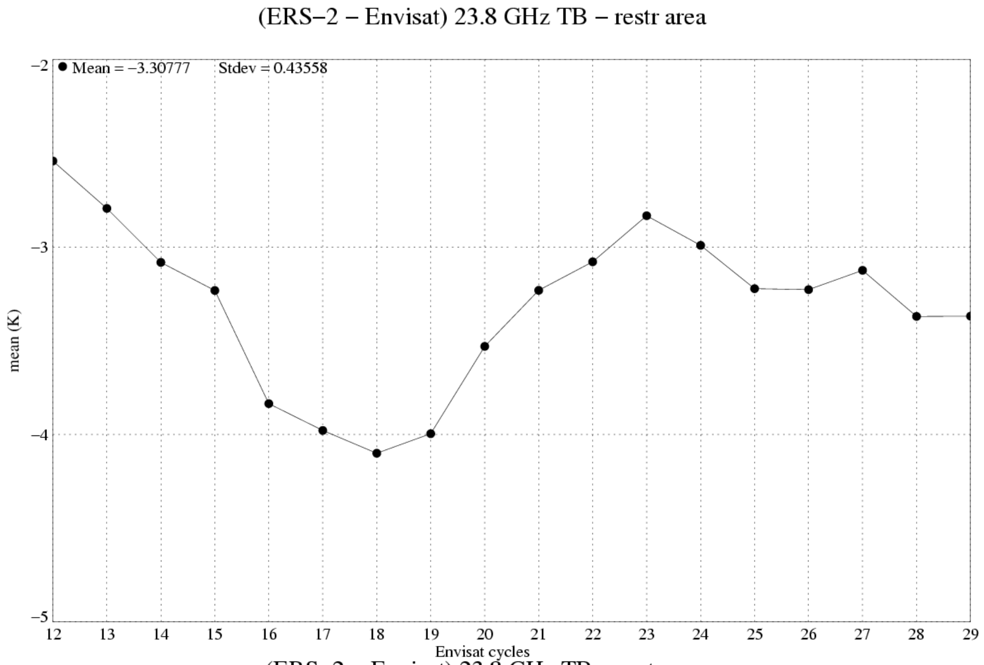

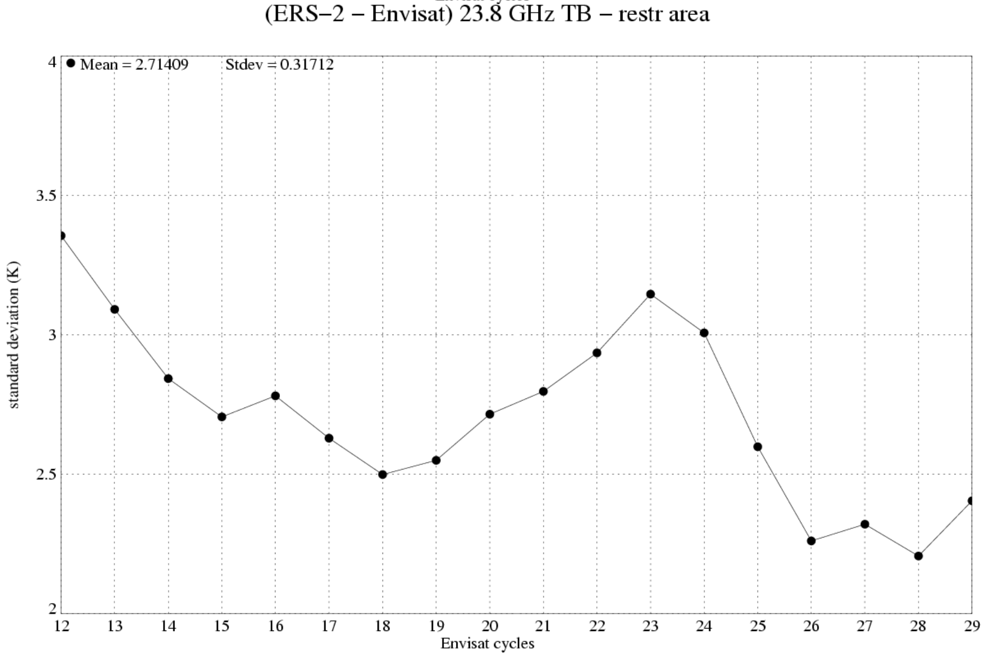

Figure 73 : Mean and standard deviation of (ERS-2 – Envisat) TB 23 GHz along track residuals for each cycle over the restricted area.

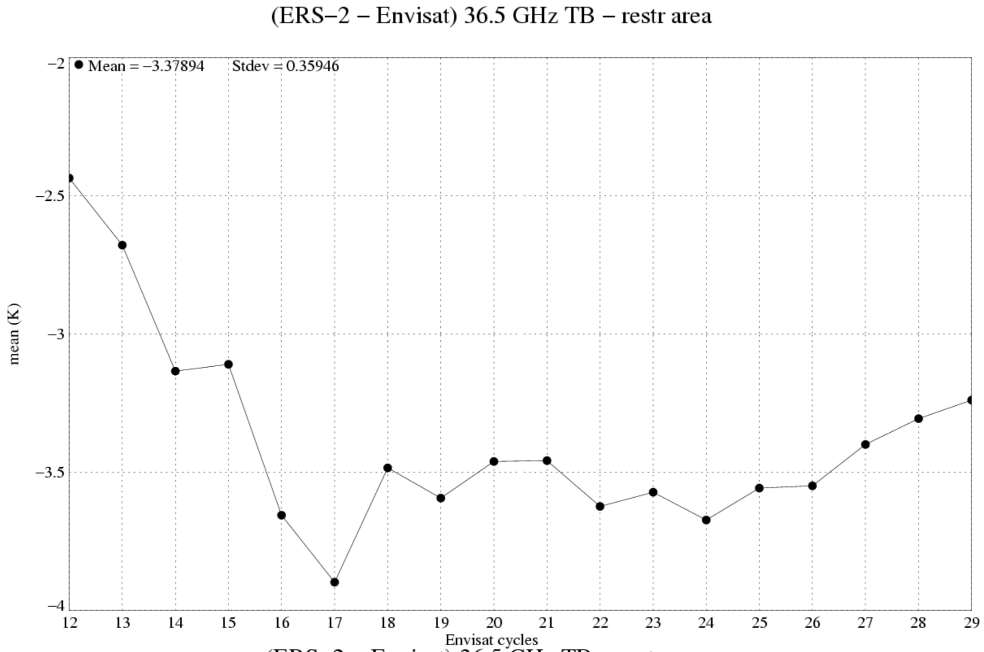

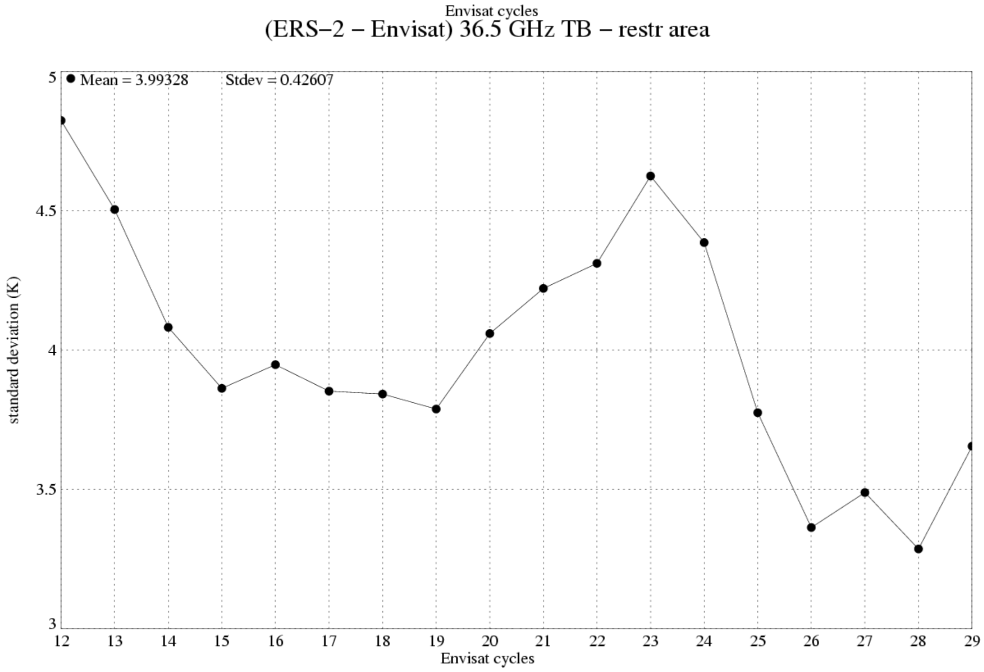

Figure 74 : Mean and standard deviation of (ERS-2 – Envisat) TB 36 GHz along track residuals for each cycle over the restricted area.

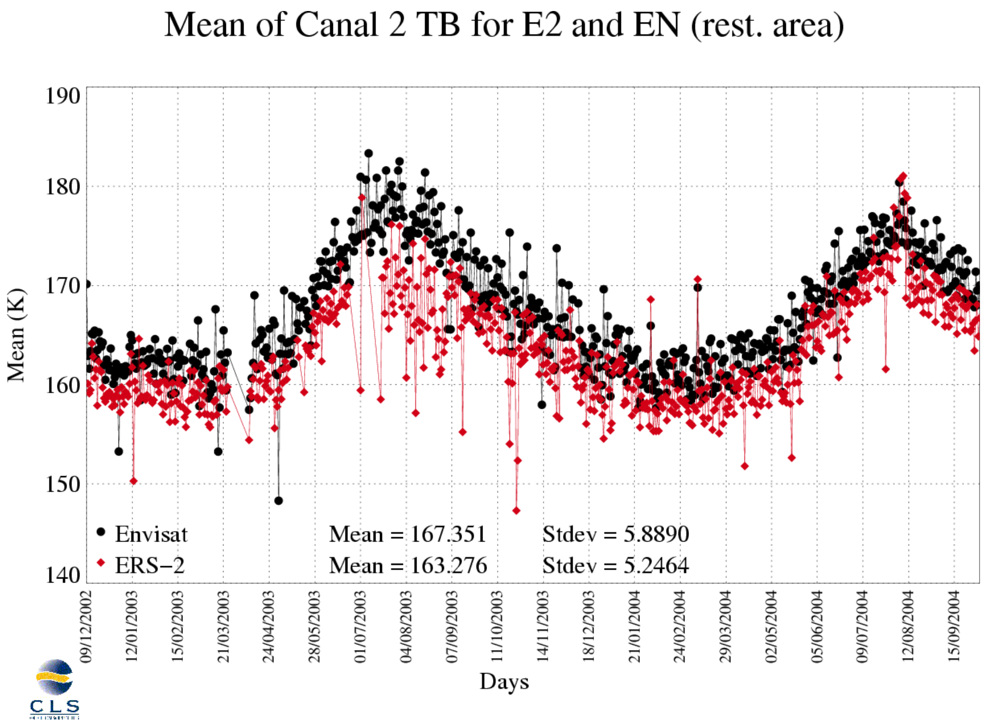

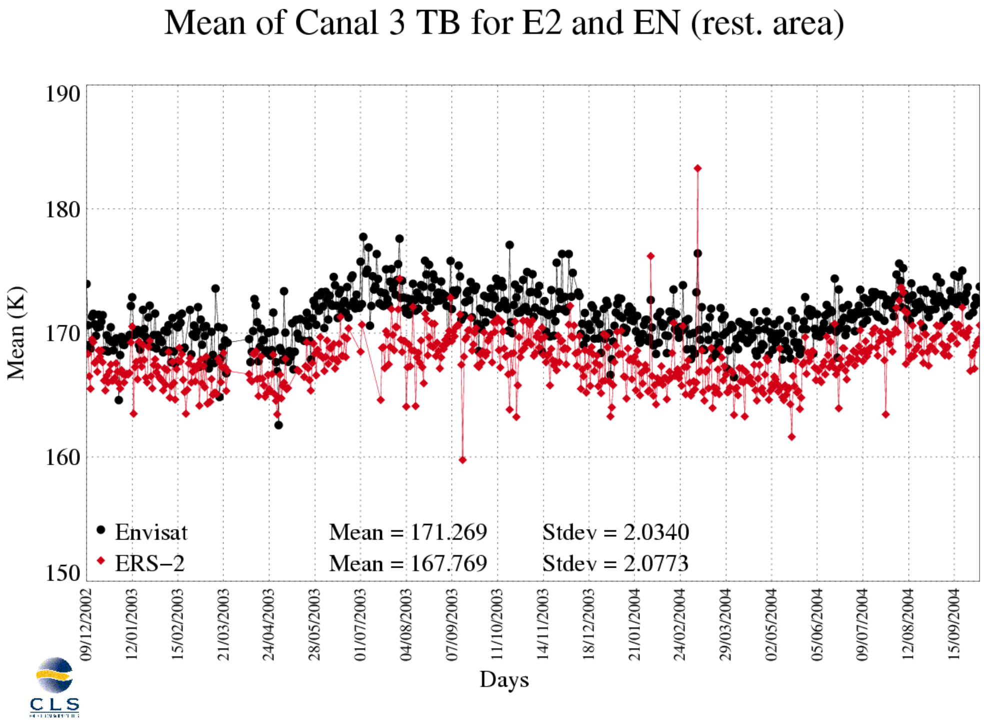

Figure 75 : **Mean of (ERS-2 – Envisat) TB 23.8 and 36.5 GHz along track residuals for each day over the restricted area.**

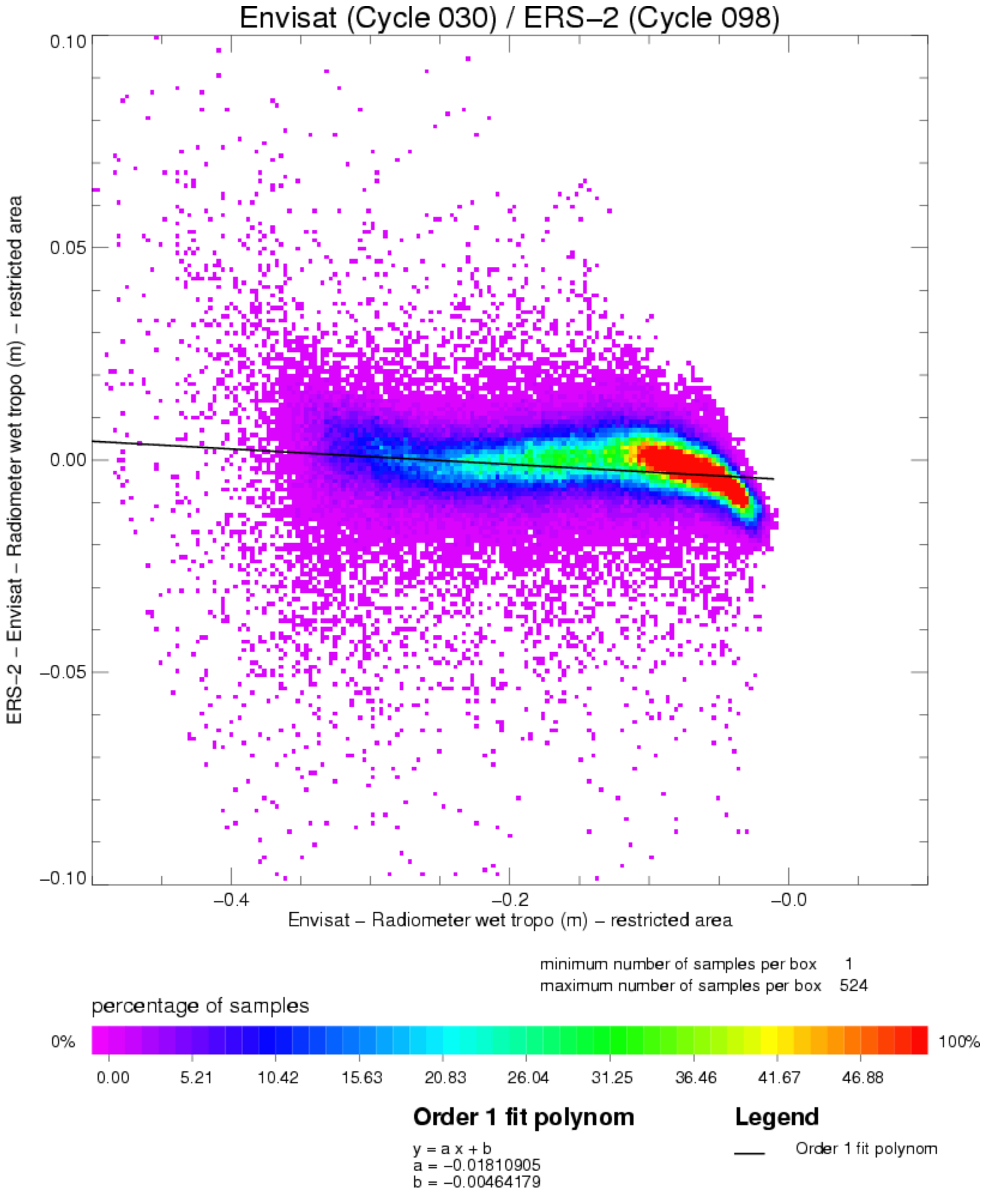

Figure 76 : Scatter plot of (ERS-2-ENVISAT) radiometer wet tropo differences (m) versus ENVISAT radiometer wet tropo.

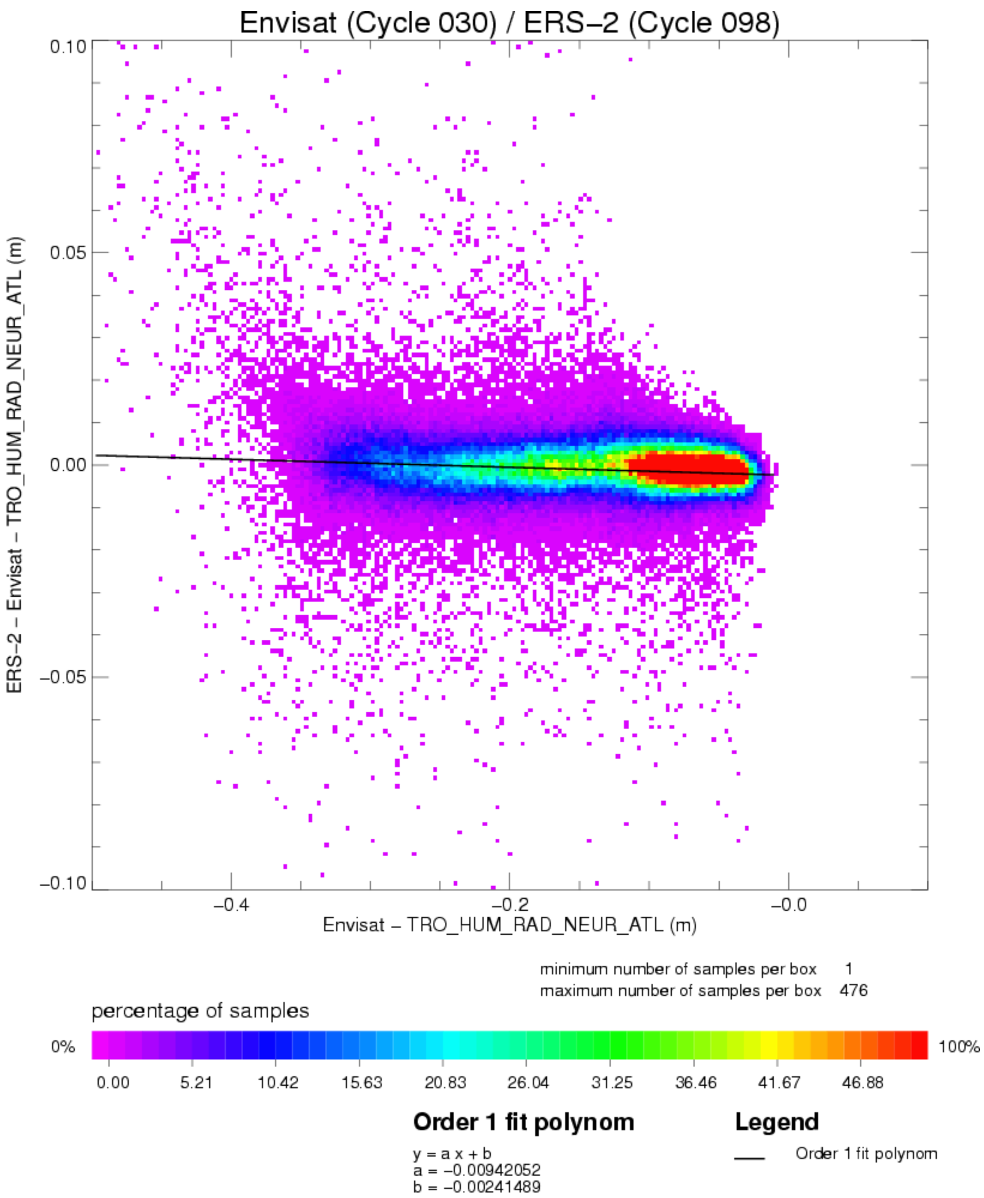

Figure 77 : Same as Figure 76 but with neural algorithm.

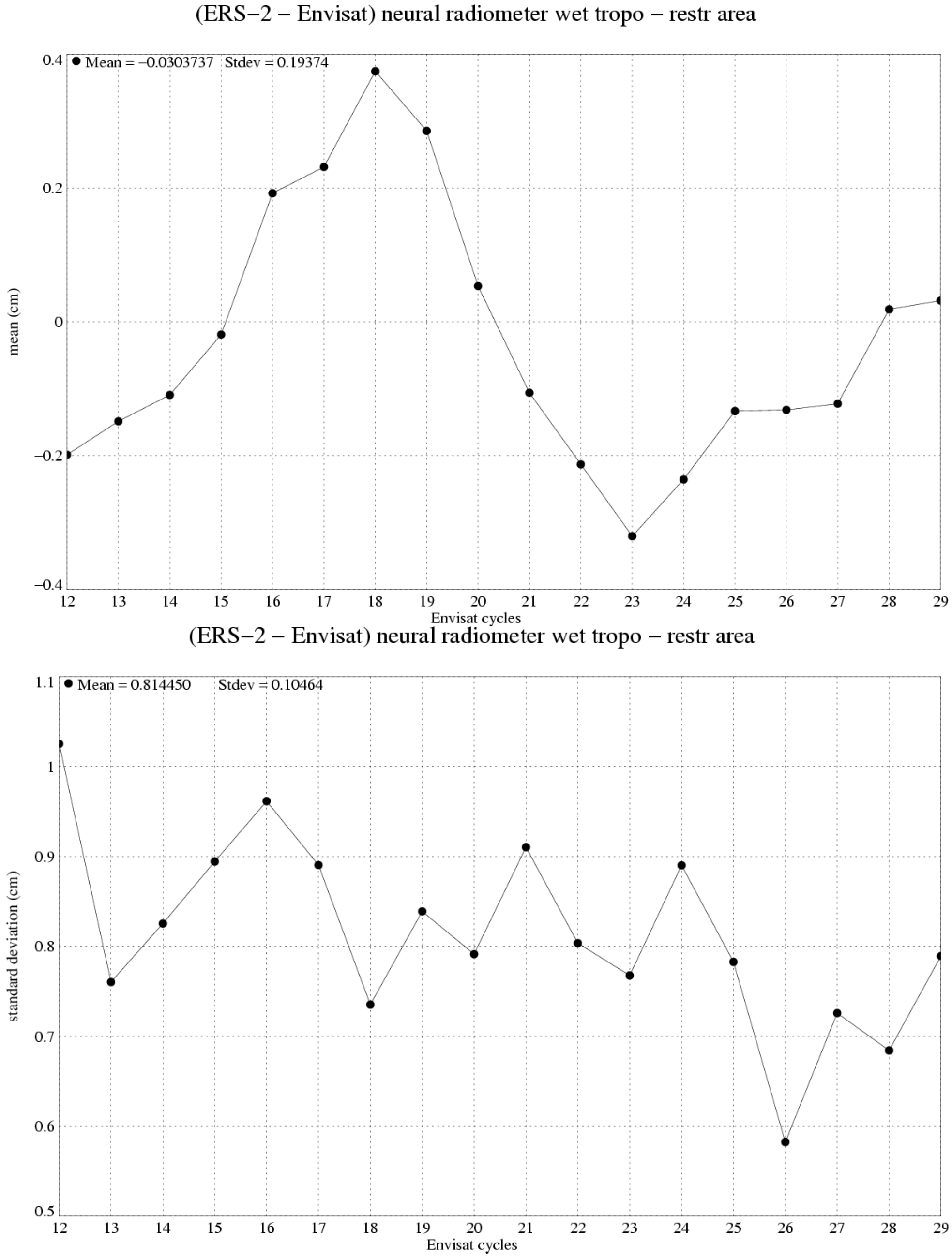

Figure 78 : Mean and standard deviation of (ERS-2 – Envisat) Radiometer wet troposphere correction along track residuals for each cycle over the restricted area.

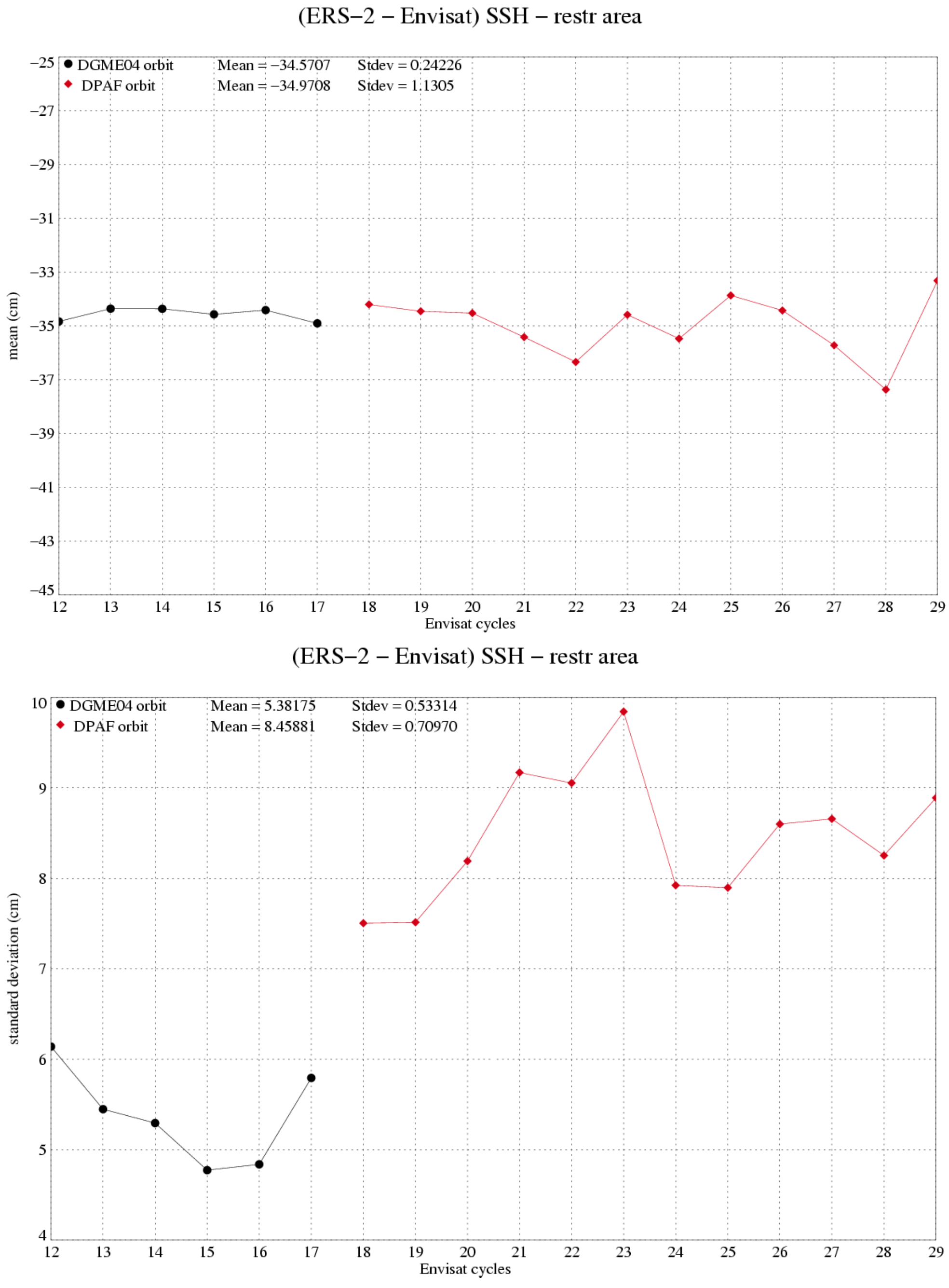

Figure 79 : Mean and standard deviation of (ERS-2 – Envisat) SSH along track residuals for each cycle computed with DGME04 orbit (black) and DPAF orbit (red).

11. APPENDIX A: MEAN SEA LEVEL AND SEA SURFACE TEMPERATURE COMPARISONS

This study has been carried out in order to monitor the MSL seen by all the operational altimeter missions. Long-term MSL change is a variable of considerable interest in the studies of global climate change. Then the objective here is on the one hand to survey the mean sea level trends and on the other hand to assess the consistency between all the MSL. Besides, the Reynolds SST is used to compare the MSL with an external data source. The mean SST is calculated as the same way as the MSL.
The following missions have been used : TOPEX/Poseïdon (T/P), Jason-1 (J1), Geosat Follow-On (GFO) and Envisat. The MSL and SST time series have been plotted over global ocean and over main oceanic areas. This allows us to correlate the MSL trends seen by each mission and to compare them with the SST.
In addition to this analysis, the maps of regional MSL change and SST change have been plotted for each mission over the Jason-1 period and the Envisat period. The differences of these maps has been performed; this is a way to display eventual local drifts.
This study is still on going and the analysis of the plots presented here is very preliminary. Basically, it allows us to give an overview of results which can be achieved.

1.1 SSH definition for each mission

The main SSH calculation are defined for all the satelites as defined below as of the GDR products (Jason-1, Envisat) or MGDRs products (T/P) :

$$SSH = Orbit - Altimeter\ Range - \sum_{i=1}^{n} Correction_i$$

with :

$$\begin{aligned}
\sum_{i=1}^{n} Correction_i &= Dry\ troposhere\ correction \\
&+ Inverse\ barometer\ correction \\
&+ RadiometerWet\ troposhere\ correction \\
&+ AltimeterIonospheric\ correction \\
&+ Sea\ state\ bias\ correction \\
&+ Ocean\ tide\ correction \\
&+ Earth\ tide\ correction \\
&+ Polar\ tide\ correction
\end{aligned}$$

But some exceptions or additionnal corrections have been applied :

- For Jason-1 and Envisat the wet troposhere correction has been changed by the ECMWF model in order to remove the effects of abnormal changes or trends observed on the radiometer wet troposhere correction.
- For Envisat, the USO drift has been applied.
- For T/P, the radiometer wet troposhere correction has been corrected from Ruf correction (Ruf, 2002b [?])
- For T/P, the relative bias between TOPEX and Poseidon and between TOPEX A and TOPEX B has been taken into account
- For T/P, the drift between the TOPEX and DORIS ionosphere corrections has been corrected for on Poseidon cycles.
- For Geosat Follow-On, the GIM model has been used for the ionospheric correction.

1.2 MSL and SST time series over main oceanic areas

1.2.1 Methodology

The MSL and the Reynolds SST have been computed cycle per cycle according to the main oceanic areas for each altimeter mission. For each plot, the MSL scale is described on the left and the SST scale on the right. The MSL and the SST don't have the same unit ("cm" and "degree"), thus to compare the 2 quantities, the SST scale is adjusted on the MSL scale so that the SST trend and the MSL trend are visually the same. Thus the SST and the MSL dynamics can be compared.
For each area, 2 charts have been plotted: olny the MSL have been plotted on the right whereas the SST has been plotted on the left in addition. For each plot, the 60-day signal has been smoothed. Notice that an articial MSL bias has been applied in order to not superimpose each curve.

1.2.2 Global ocean

MSL and SST have been monitored over global ocean in figure 1 over T/P period and in figure 2 over Jason-1 period.

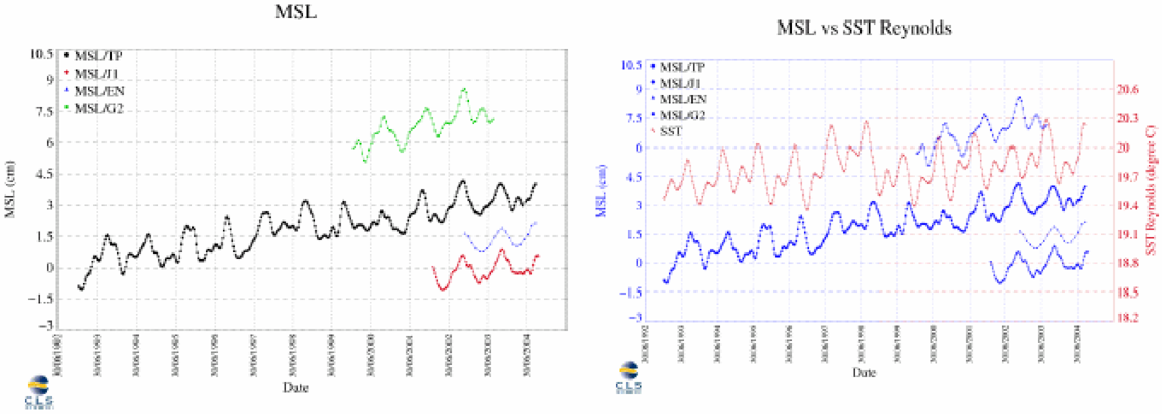

Figure 1: *MSL and SST over global ocean and over the T/P period*

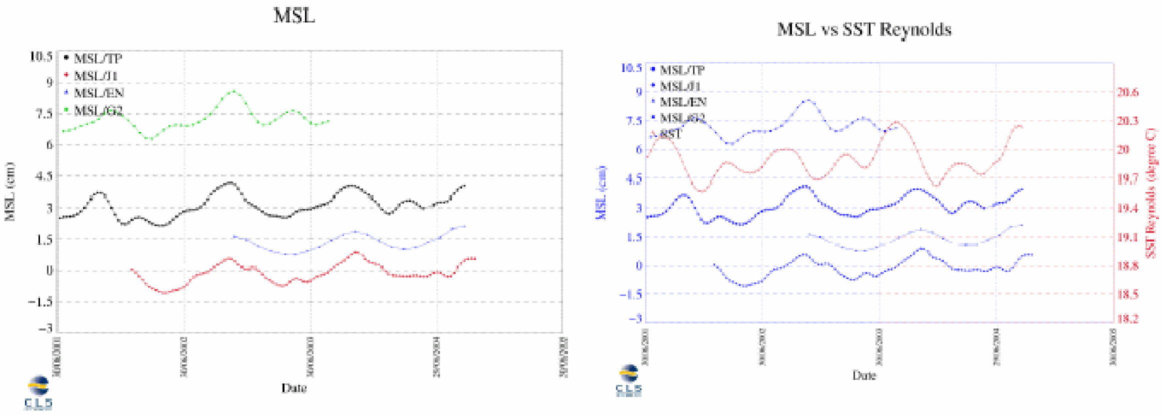

Figure 2: *MSL and SST over global ocean and over the Jason-1 period*

1.2.3 Monitoring over the Indian Ocean

Figure 3 and figure 4 are the same as in section 1.2.2 over the Indian Ocean.

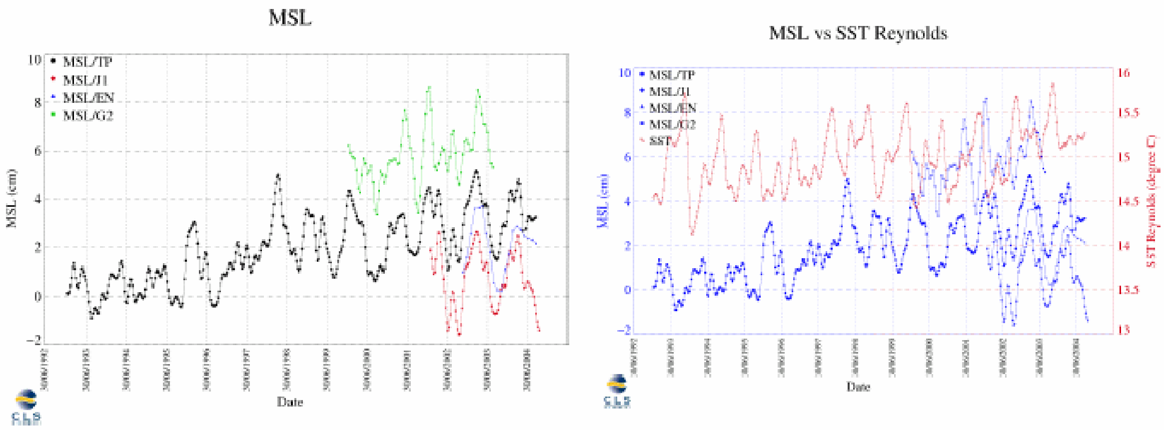

Figure 3: *MSL and SST over the Indian Ocean and over the T/P period*

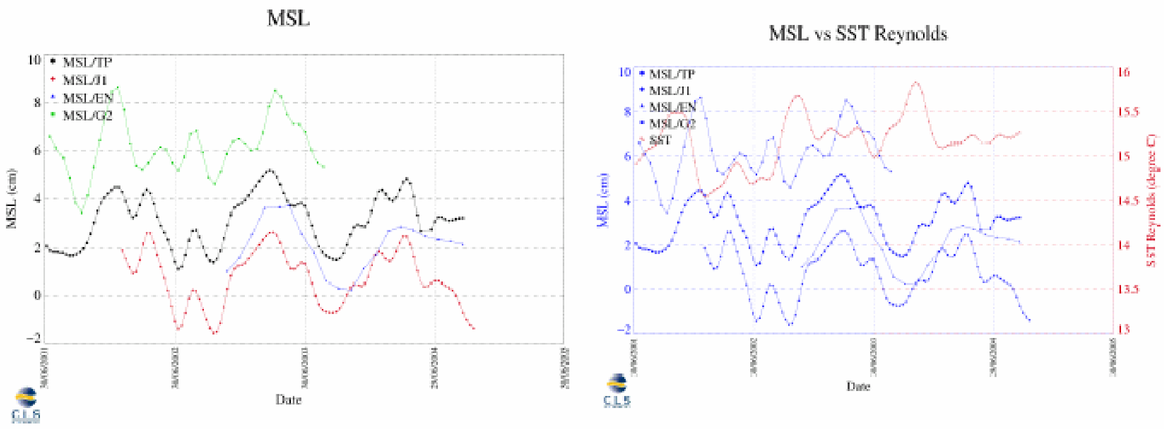

Figure 4: *MSL and SST over the Indian Ocean and over the Jason-1 period*

1.2.4 Monitoring on the Northern hemisphere

Figure 5 and figure 6 are the same as in section 1.2.2 on the Northern hemisphere.

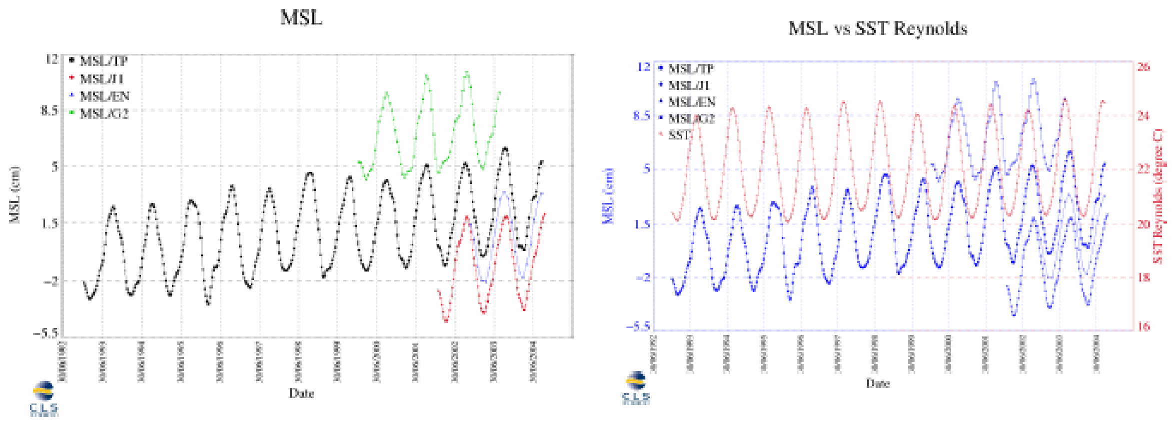

Figure 5: *MSL and SST on the Northern hemisphere and over the T/P period*

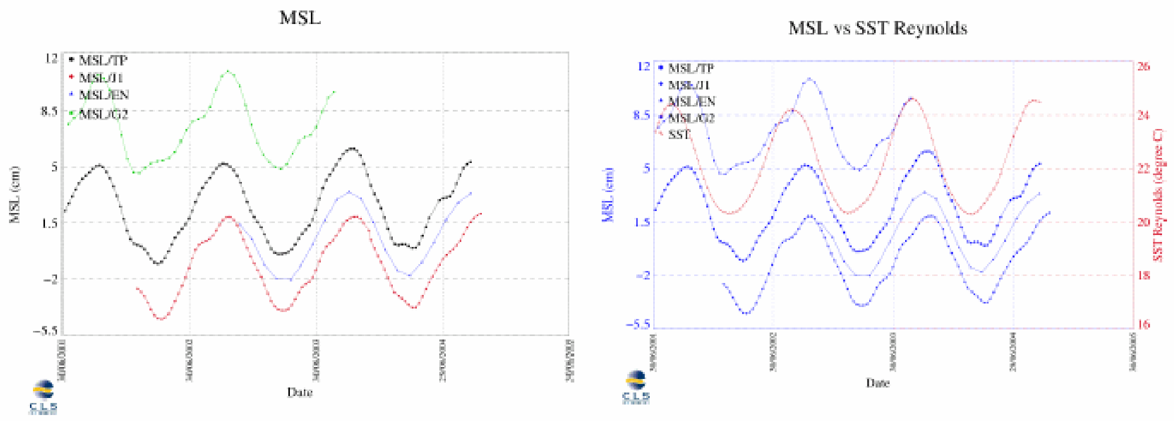

Figure 6: *MSL and SST on the Northern hemisphere and over the Jason-1 period*

1.2.5 Monitoring on Southern hemisphere

Figure 7 and figure 8 are the same as in section 1.2.2 on the Southern hemisphere.

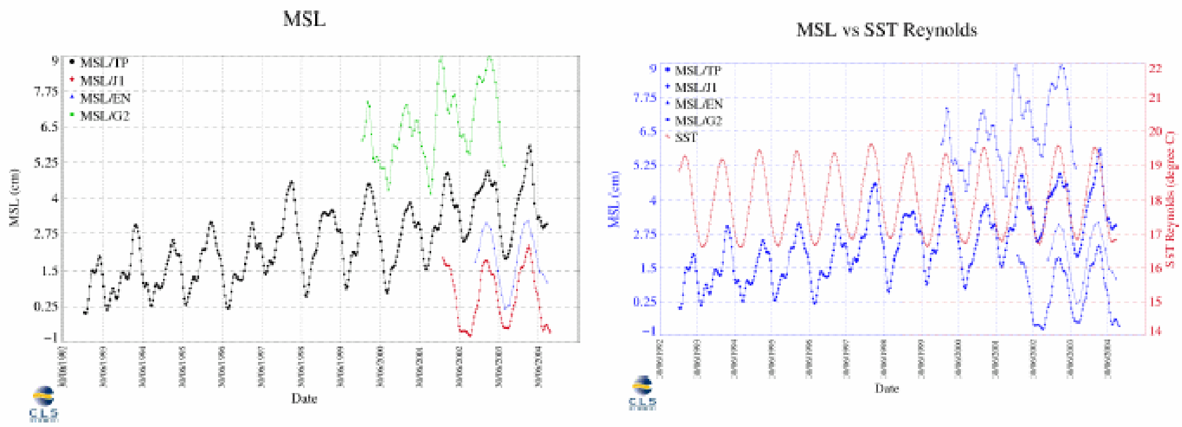

Figure 7: *MSL and SST on the Southern hemisphere and over the T/P period*

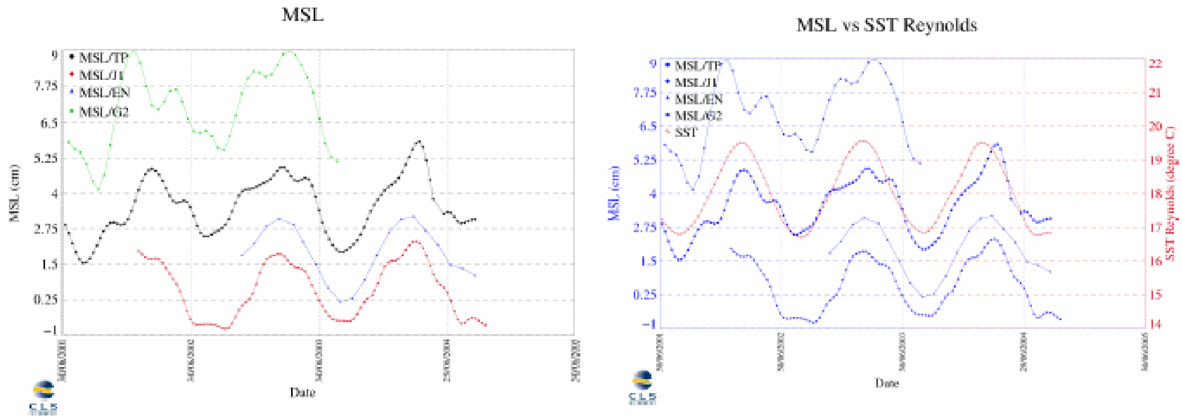

Figure 8: *MSL and SST on the Southern hemisphere and over the Jason-1 period*

1.2.6 Monitoring over the North Atlantic Ocean

Figure 9 and figure 10 are the same as in section 1.2.2 over the North Atlantic Ocean.

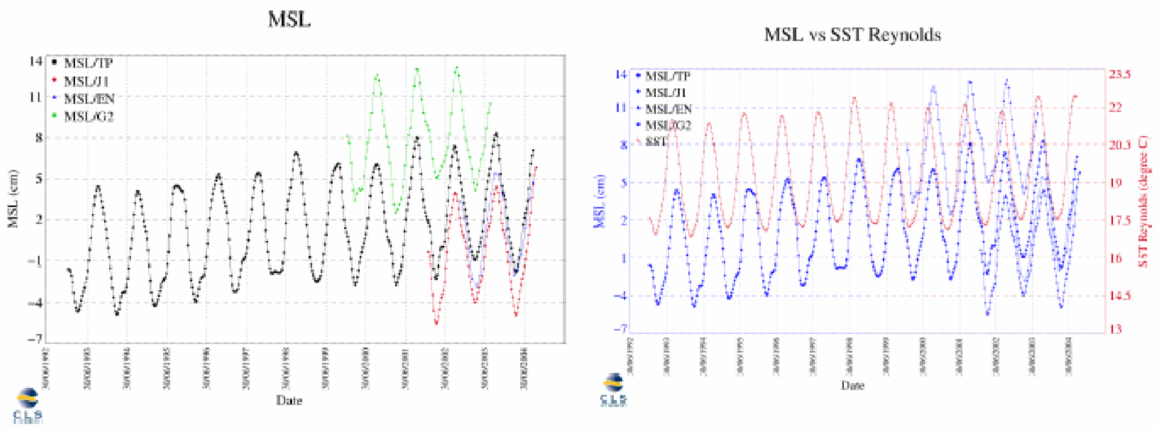

Figure 9: *MSL and SST over the North Atlantic Ocean and over the T/P period*

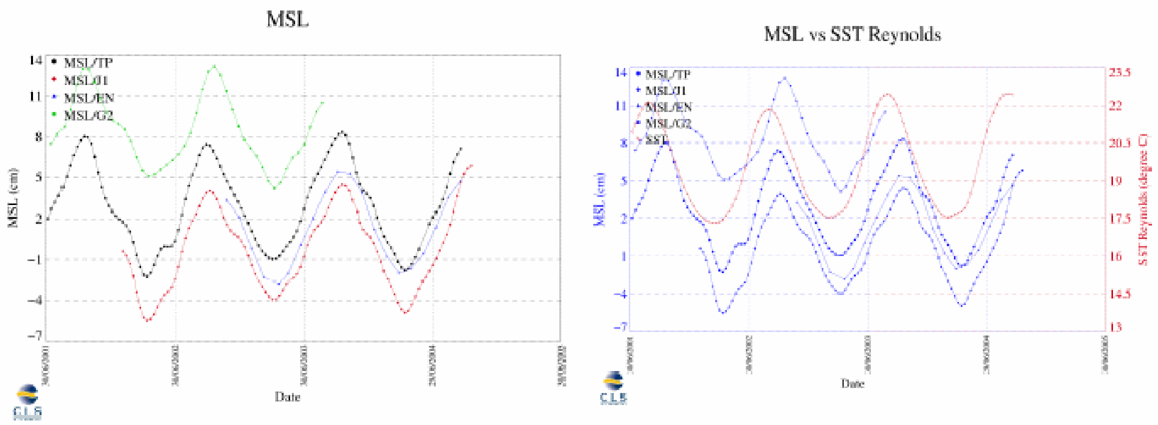

Figure 10: *MSL and SST over the North Atlantic Ocean and over the Jason-1 period*

1.2.7 Monitoring over the South Atlantic Ocean

Figure 11 and figure 12 are the same as in section 1.2.2 over the South Atlantic Ocean.

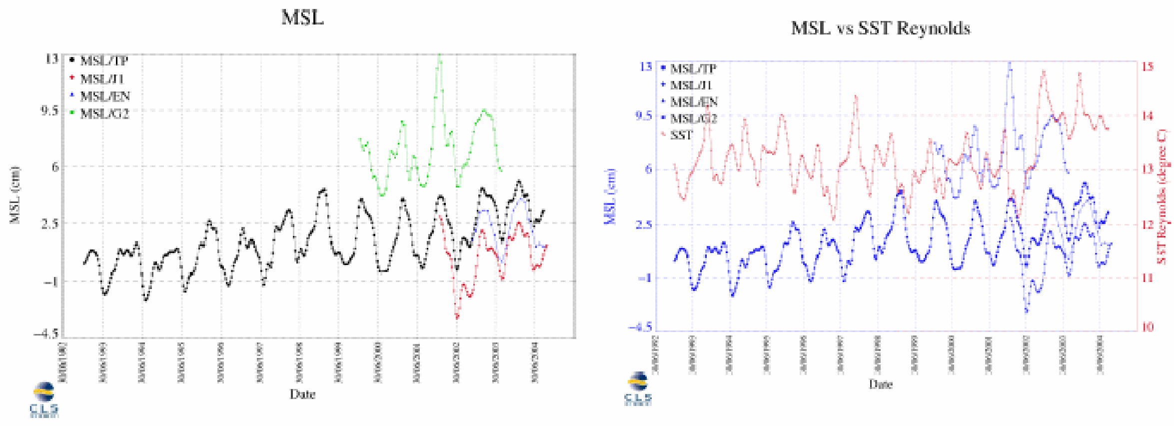

Figure 11: *MSL and SST over the South Atlantic Ocean and over the T/P period*

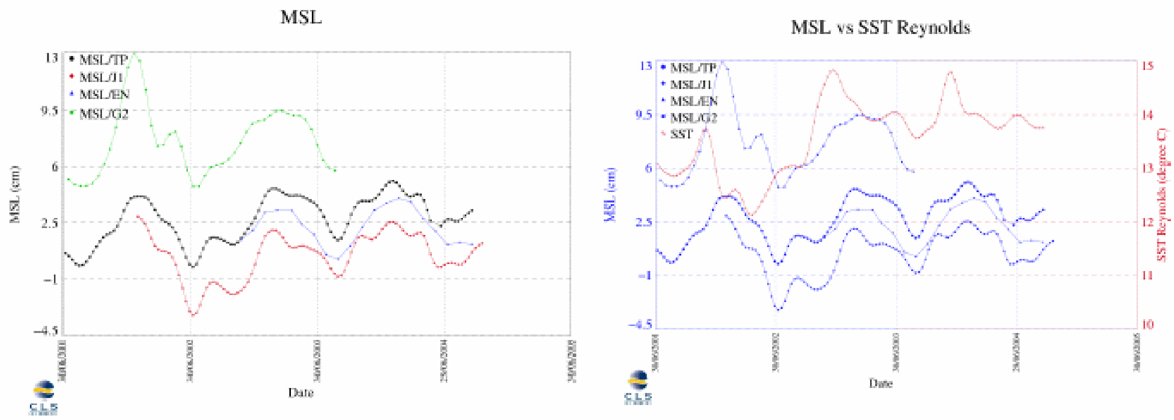

Figure 12: *MSL and SST over the South Atlantic Ocean and over the Jason-1 period*

1.2.8 Monitoring over the North Pacific Ocean

Figure 13 and figure 14 are the same as in section 1.2.2 over the North Pacific Ocean.

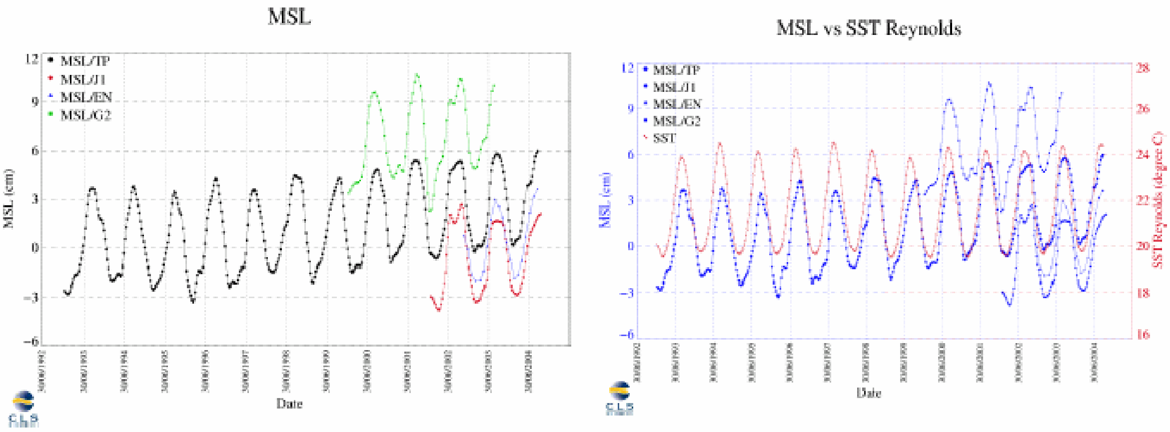

Figure 13: *MSL and SST over the North Pacific Ocean and over the T/P period*

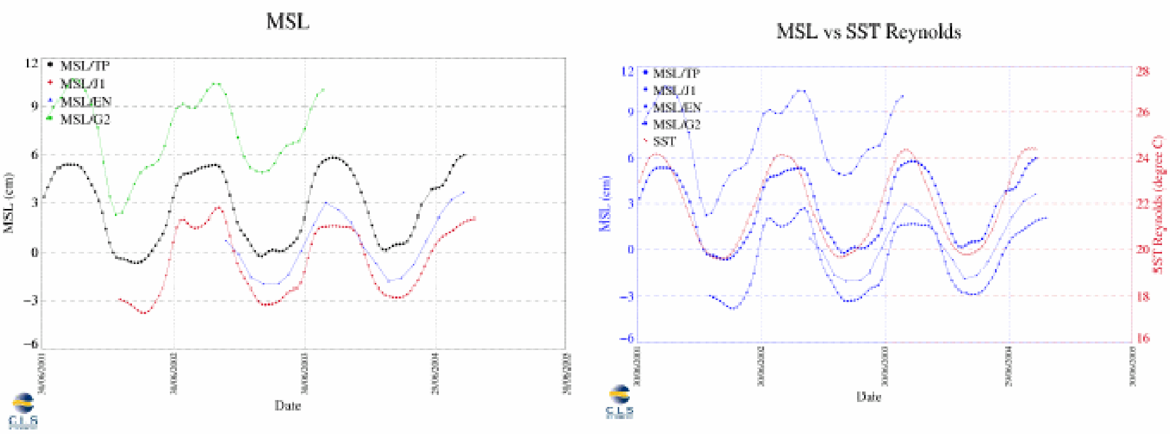

Figure 14: *MSL and SST over the North Pacific Ocean and over the Jason-1 period*

1.2.9 Monitoring over the South Pacific Ocean

Figure 15 and figure 16 are the same as in section 1.2.2 over the South Pacific Ocean.

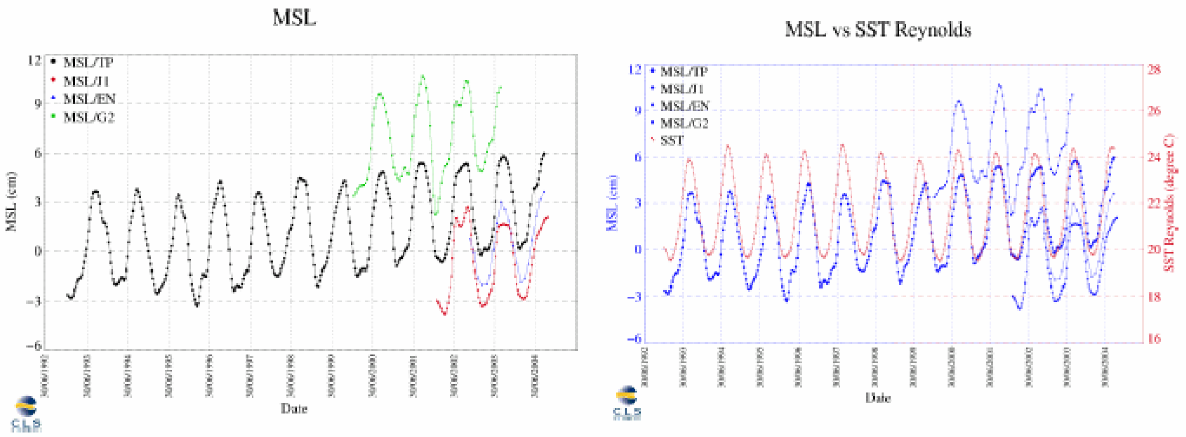

Figure 15: *MSL and SST over the South Pacific Ocean and over the T/P period*

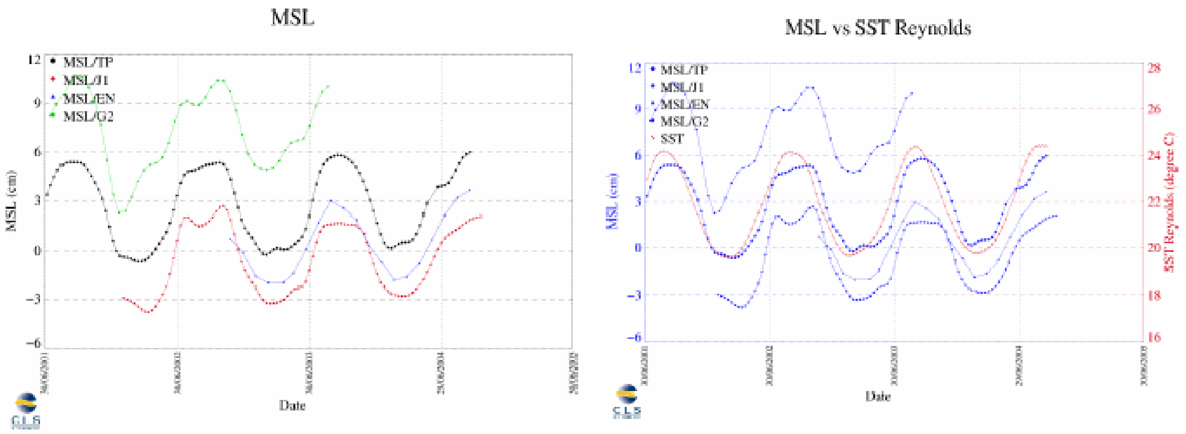

Figure 16: *MSL and SST over the South Pacific Ocean and over the Jason-1 period*

1.2.10 Monitoring over the Mediterranean Sea

Figure 17 and figure 18 are the same as in section 1.2.2 over the Mediterranean Sea.

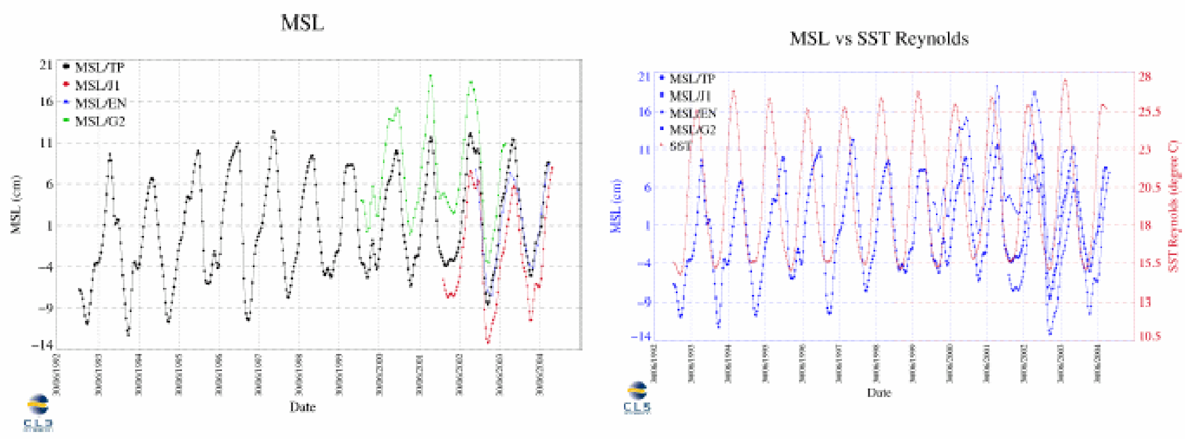

Figure 17: *MSL and SST over the Mediterranean Sea and over the T/P period*

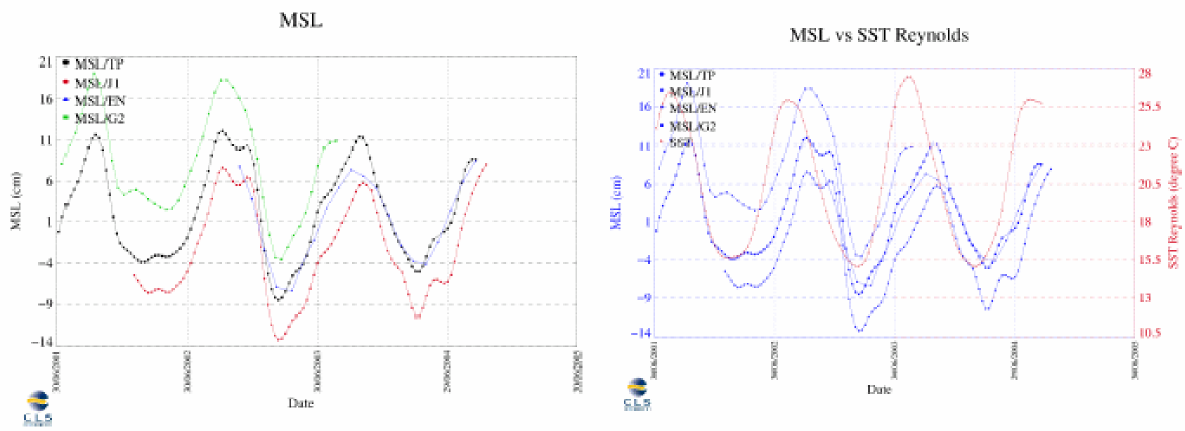

Figure 18: *MSL and SST over the Mediterranean Sea and over the Jason-1 period*

1.2.11 Monitoring over the Black Sea

Figure 19 and figure 20 are the same as in section 1.2.2 over the Black Sea.

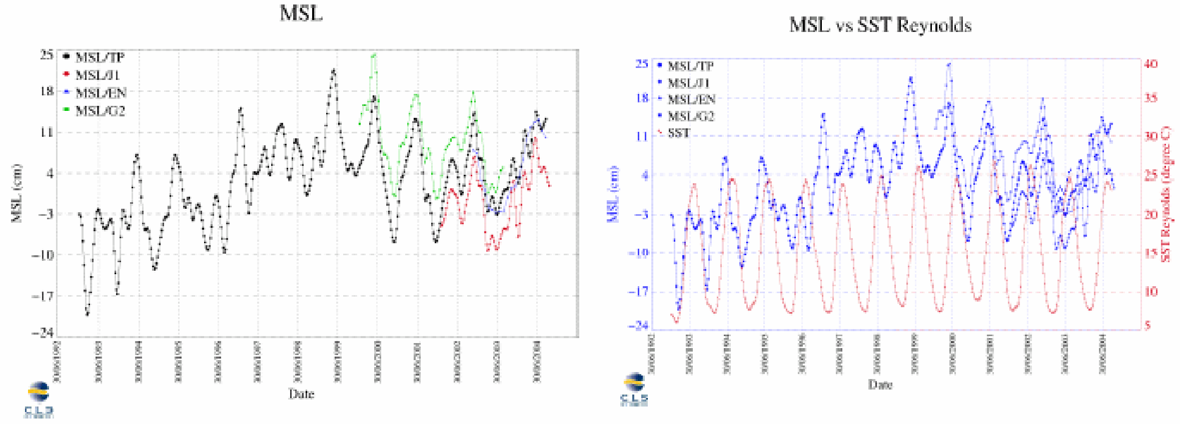

Figure 19: *MSL and SST over the Black Sea and over the T/P period*

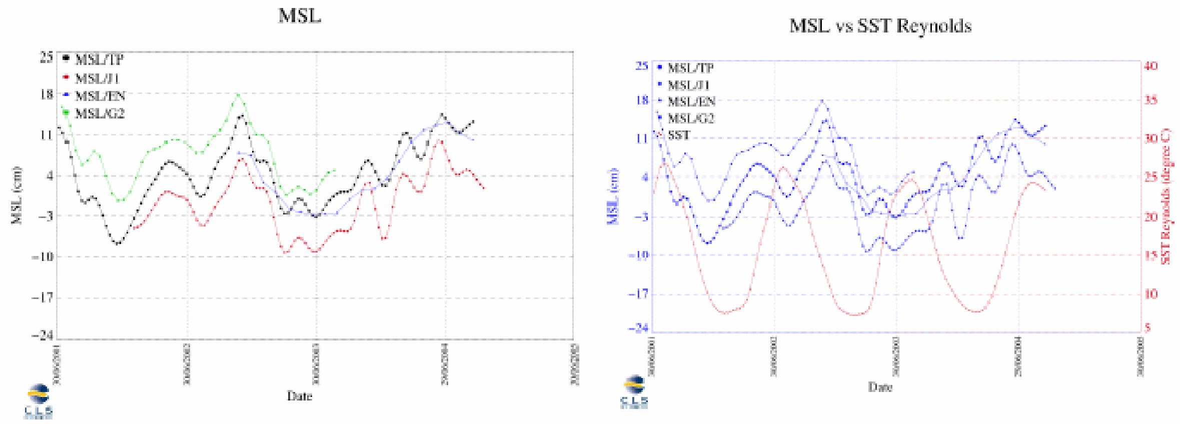

Figure 20: *MSL and SST over the Black Sea and over the Jason-1 period*

1.3 Spatial MSL and SST slopes

1.3.1 Methodology

In order to monitor the MSL, the spatial MSL slopes have been calculated. The SLA grids (2x2 degree bins) have been computed cycle per cycle, and the slope has been performed on each grid point. As for time analysis, 60 day, semi-annual and annual signals have been removed before estimating the slopes. Then, the MSL slopes have been mapped for each mission. These maps are used to compare the MSL slopes between each altimetrer mission. This allows us to detect potential local drifts.
Besides the SST slopes has been computed in a same way in order to correlate them with the MSL slopes.

1.3.2 Spatial MSL slopes over Jason-1 period

The MSL slopes has been plotted for Jason-1 (on the right) and T/P (on the left) over Jason-1 period in figure 21. The MSL trends seen by the two satellites seem very homogenous that is shown by the bottom map where the difference between the 2 previous maps have been plotted. However, differences can be observed in some areas: they are under investigation.

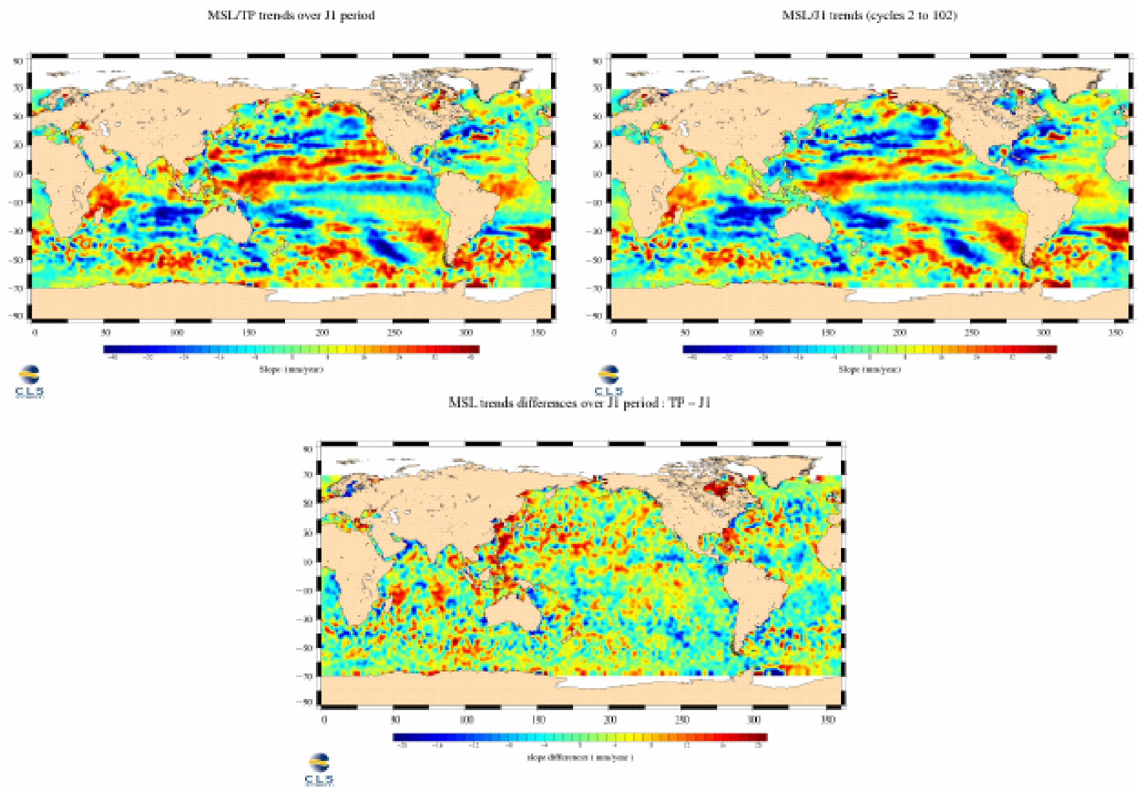

Figure 21: *MSL slopes over Jason-1 period for T/P (left) and Jason-1 (right), MSL slope differences between Jason-1 and T/P (bottom)*

1.3.3 Spatial MSL slopes over Envisat period

Same work has been performed over Envisat period using Envisat data in figure 22. The 3 maps seem very homogenous.
In figure 23, the slope differences between each mission have been plotted. They allow us to observe differences in equatorial area between T/P and Envisat, and between T/P and Jason-1. These differences are not visible between Envisat and Jason-1. Investigations are on-going to understand the reasons of this observation.

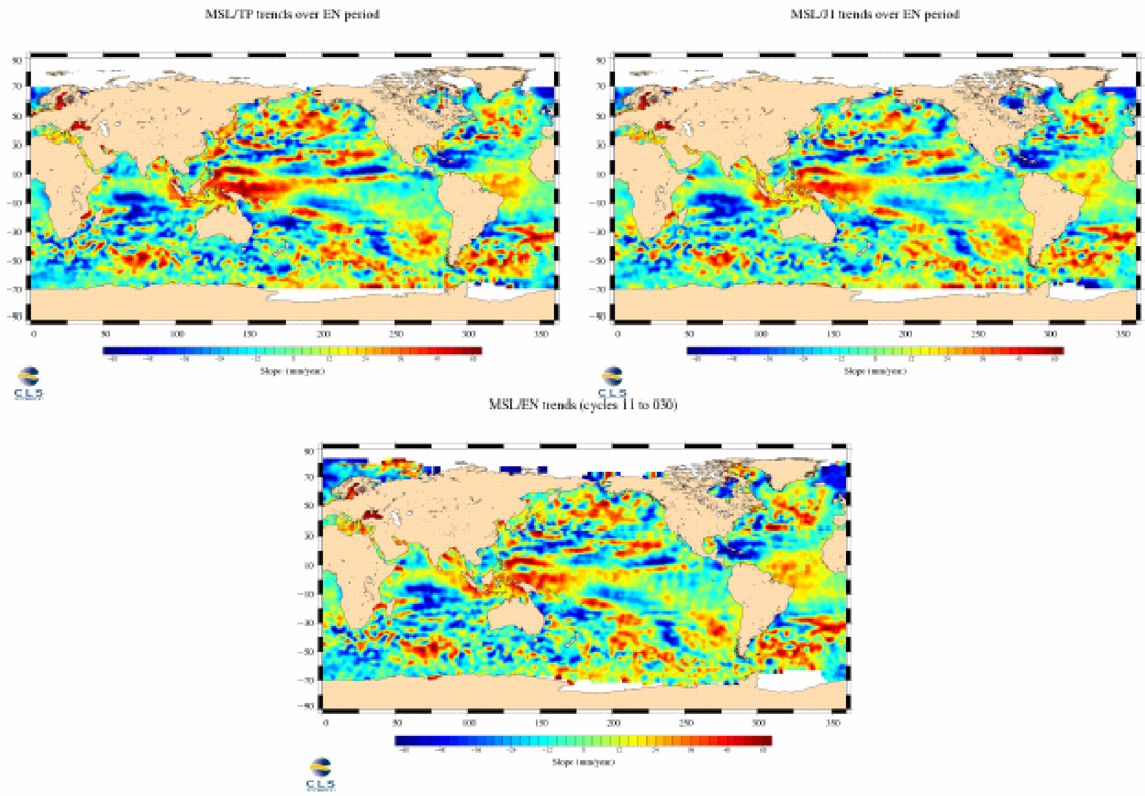

Figure 22: *MSL slopes over Envisat period for T/P (left), Jason-1 (right) and Envisat (bottom)*

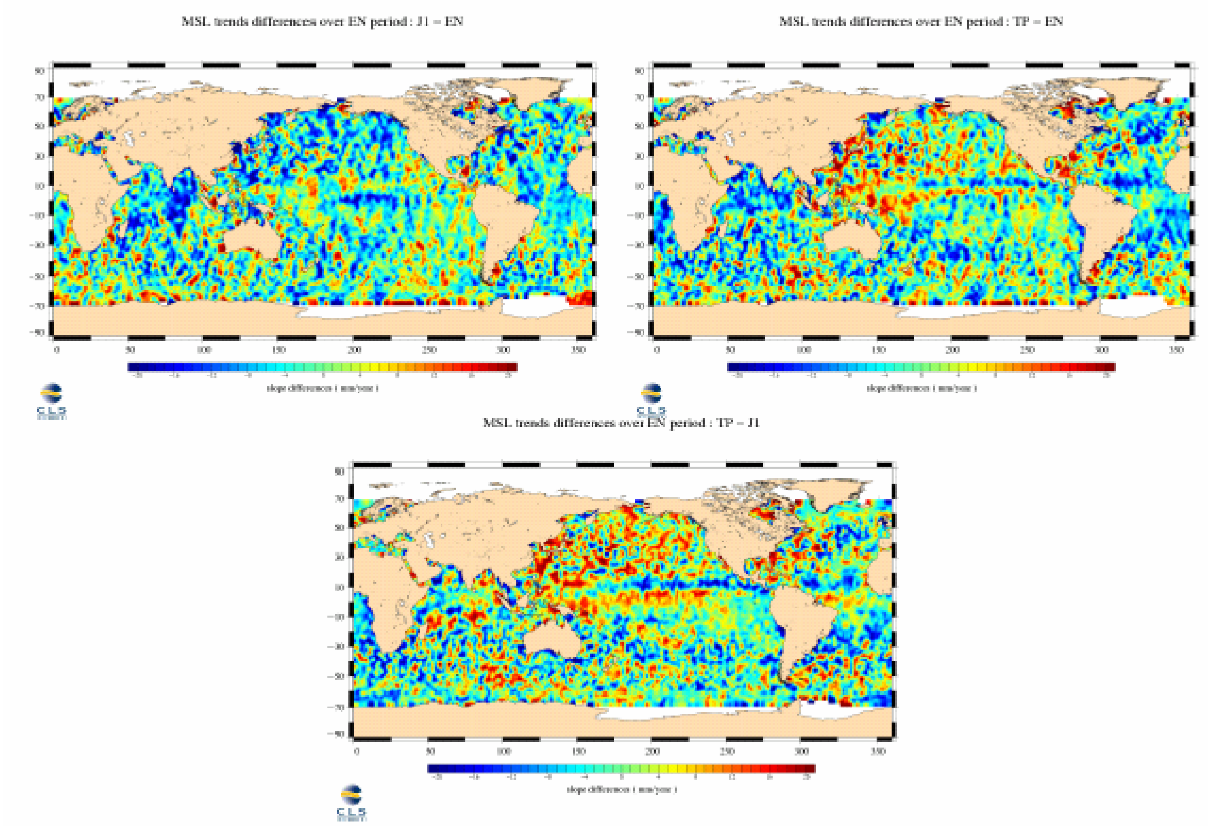

Figure 23: *MSL slopes differences over Envisat period between Jason-1 and Envisat (left), T/P and Envisat (right) and T/P and Jason-1 (bottom)*

1.3.4 Spatial SST and MSL slopes for T/P

The T/P MSL slopes have been mapped in figure 24 on the left. In order to correlate the MSL and the SST, the SST slopes have been plotted in the same figure on the right.
12 years of T/P data have been used to estimate the slopes; this allows us to have a good estimation of the local MSL trends. The adjustment errors of the MSL and the SST slopes are mapped in the figure 25.

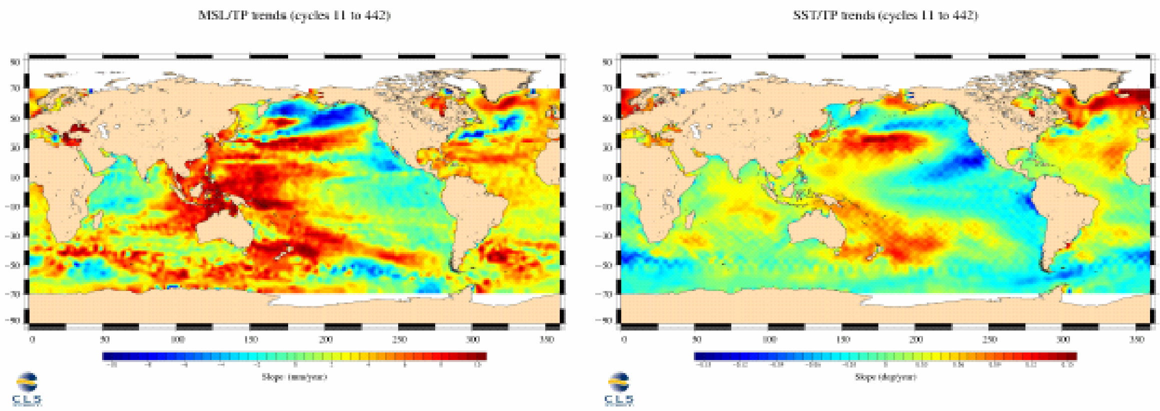

Figure 24: *T/P MSL and SST slopes over 12 years*

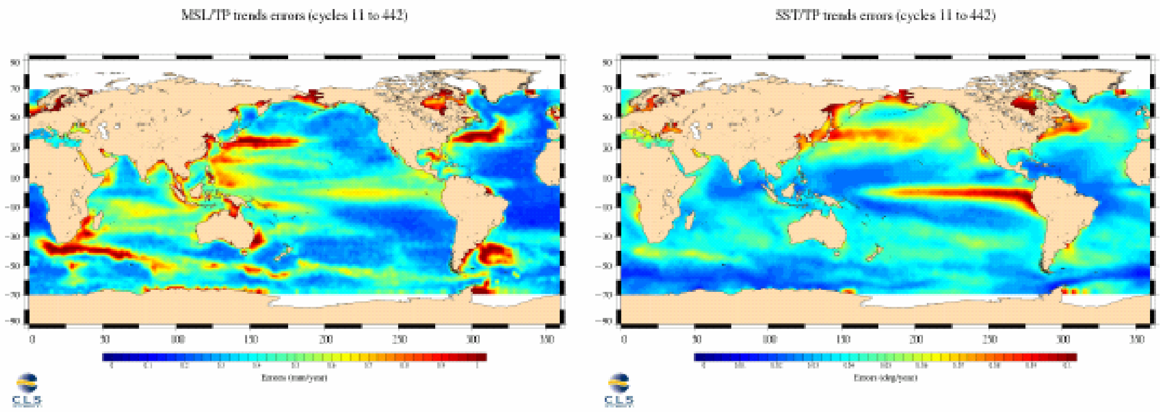

Figure 25: *Adjustment errors of T/P MSL and SST slopes over 12 years*